

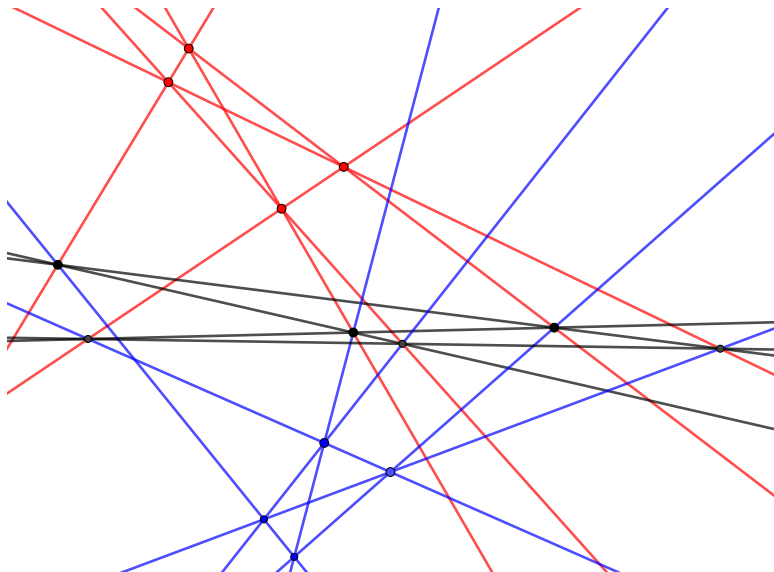
INCIDENCES AND TILINGS

SERGEY FOMIN AND PAVLO PYLYAVSKYY

ABSTRACT. We show that various classical theorems of real/complex linear incidence geometry, such as the theorems of Pappus, Desargues, Möbius, and so on, can be interpreted as special cases of a single “master theorem” that involves an arbitrary tiling of a closed oriented surface by quadrilateral tiles. This yields a general mechanism for producing new incidence theorems and generalizing the known ones.

*Science is what we understand well enough to explain to a computer.
Art is everything else we do.*

– D. E. Knuth [28]



1. INTRODUCTION

Linear incidence geometry studies configurations of points, lines, and (hyper)planes from the perspective of their relative position (e.g., whether a point lies on a line, whether two lines in 3-space intersect, etc.). This venerable subject goes back at least to the times of Euclid, with important contributions by Pappus, Desargues, Möbius, Hilbert, and many others; see, e.g., [5, 15, 34, 43, 62] for historical accounts.

Date: August 7, 2023.

2020 Mathematics Subject Classification. Primary 51A20, Secondary 05E14, 14N20, 51M15.

Key words and phrases. Linear incidence geometry, tiled surface, incidence theorem.

Partially supported by NSF grants DMS-2054231 (S. F.) and DMS-1949896 (P. P.).

A typical theorem of (real or complex) linear incidence geometry asserts that, given a finite configuration, say of points and lines in the projective plane, a particular collection of incidence constraints between these geometric objects implies another incidence constraint, under appropriate genericity assumptions. For compendiums of such incidence theorems, see for example [11, 32, 44, 46].

In recent decades, the advent of computational commutative algebra led to design and implementation of highly effective algorithmic approaches to automated proofs of incidence theorems, see, e.g., [11, 31, 32, 46, 47, 55]. Nowadays any such theorem can be proved by a computer, with minimal human input.

These developments, however, leave unanswered a key question: where do all these incidence theorems come from to begin with? That is, is there a systematic way to *generate* them? In this paper, we tackle this question by establishing a kind of “master theorem” of real/complex linear incidence geometry, from which various—perhaps all—incidence theorems can be obtained as special cases. As a result, we obtain a unifying perspective on *why* all of these incidence theorems hold.

To give the reader a quick taste of our master theorem (cf. Theorem 2.6), we formulate right away its simplified version for the case of the projective plane:

Theorem 1.1. *Consider a tiling of a closed oriented surface by quadrilateral tiles. Assume that the vertices of the tiling are colored black and white, so that every edge connects vertices of different color. Associate to each black (resp., white) vertex a point (resp., a line) in the real/complex projective plane, so that all these points and lines are distinct and no point lies on any of the lines associated with adjacent vertices. For each tile*

$$\begin{array}{ccc} A & \text{---} & \ell \\ | & & | \\ m & \text{---} & B \end{array}$$

(here A and B are points and ℓ and m are lines), consider the incidence condition

(*) *the points A , B , and $\ell \cap m$ are collinear.*

If condition () holds for all tiles but one, then it also holds for the remaining tile.*

Once this statement has been discovered, the proof is short and straightforward. Even so, the theorem turns out to be surprisingly powerful. As a proof-of-concept test, we consider various widely known theorems of classical real/complex two- and three-dimensional linear incidence geometry. In each case, we show how to interpret a given incidence theorem as a special case of Theorem 1.1 (resp., its 3D version). In particular, we present direct tiling-based proofs for the following classical theorems:

- in dimension two:
 - the Desargues theorem (Theorem 3.1);
 - the Pappus theorem (Theorem 3.2);
 - the complete quadrangle theorem (Theorems 3.3 and 3.6);
 - the permutation theorem (Theorem 3.11);
 - Saam’s theorems (Theorems 3.12 and 4.15);
 - the Goodman-Pollack theorem (Theorem 4.10);

- in dimension three:
 - the bundle theorem (Theorem 5.1);
 - the sixteen points theorem (Theorem 5.8);
 - the Möbius theorem and the octahedron theorem (Theorems 5.5 and 5.6).

To illustrate, Figure 1 shows two tilings (of the sphere and the torus, respectively) that yield the theorems of Desargues and Pappus. See Section 3 for detailed explanations.

It is possible to obtain a given incidence theorem from substantially different tilings. For example, the theorem of Pappus can be obtained from two non-isomorphic tilings of the torus, cf. Figures 9 and 13.

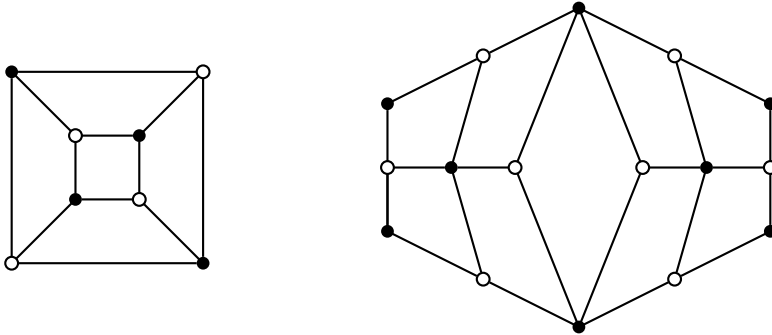


Figure 1: Tiled surfaces yielding the theorems of Desargues (left) and Pappus (right). Left: the tiling of the sphere that topologically corresponds to the surface of the cube. Right: glue the opposite sides of the shown hexagonal fundamental domain to obtain a tiling of the torus.

It is tempting, if perhaps too bold, to conjecture that *any* theorem of linear incidence geometry can be obtained as a special case of our master theorem. A result of this kind appears to be out of reach, due to the absence of any reasonable classification of incidence theorems, even in the case of the projective plane. Indeed, the universe of incidence theorems is too “wild” to be amenable to an explicit description, see [7, Sections 8.3–8.4], [35, Corollary 1.4], [36, 56, 61], [41, Theorem 6.5.17]. On the other hand, such complexity-theoretic results do not necessarily preclude the existence of a universal master theorem. That’s because the task of identifying a (possibly non-unique) instance of a master theorem that yields a given incidence theorem may not be easily accomplished. This is indeed the case for our master theorem: we do not know an algorithm that inputs an incidence theorem and outputs a tiled Riemann surface from which this theorem or its generalization (cf. Remark 3.7) can be obtained. Thus, finding a tiling-based proof for a given incidence theorem remains a form of art rather than science, by Knuth’s definition in the epigraph.

By design, our master theorem leads to the discovery of new (and generalizations of old) incidence theorems. See, in particular, Theorems 3.4, 3.8, 3.12, 3.15, 4.12, 5.11, 5.13, 7.11, and 7.15.

We refer the reader to [2, 3, 10, 12, 13, 23, 24, 38, 44, 49, 53] for general background in classical projective geometry.

To simplify exposition and curb the size of the paper, we restrict our treatment in several ways. First, while we realize the importance of more general frameworks of axiomatic projective geometry, we decided to focus in this paper on the classical setting of complex or real projective spaces. Many of our results can be generalized to geometries over other fields and even noncommutative skew fields. Second, we confine our treatment to configurations that consist exclusively of projective subspaces and do not involve conics/quadratics or varieties of higher degree. In future work, we plan to extend our framework to more general incidence theorems.

Third, we do not attempt to formulate the weakest genericity assumptions under which each of our theorems holds. This somewhat narrows, although not in an essential way, the class of incidence theorems under consideration. We habitually use the term “generic” to describe choices (of points, lines, planes, etc.) that belong to a Zariski dense subset of the appropriate configuration space.

The fact that we confine our treatment to “generic forms” of incidence theorems might provide another explanation for why Mnëv universality does not preclude the existence of a comprehensive master theorem of linear incidence geometry.

While we don’t make it explicit, our approach is rooted in *classical invariant theory*. From the perspective of this theory, incidence geometry can be viewed as a study of particular kinds of identities in certain rings of invariants. For example, collinearity of triples of points on the projective plane can be encoded by the vanishing of the corresponding Plücker coordinates (3×3 minors of a $3 \times n$ matrix). Various identities that Plücker coordinates satisfy lead to representability restrictions for the corresponding matroids. These identities and restrictions can be very complicated, as the aforementioned complexity/universality results attest. To bypass these difficulties, our approach implicitly relates to a different ring of invariants, namely the ring generated by pairings between vectors and covectors. In the case of SL_3 (i.e., the case of the projective plane), the ideal of relations among these pairings is generated by 4×4 Gramian determinants, each of which has 24 terms of degree 4. (By comparison, the Grassmann-Plücker relations for Plücker coordinates have degree 2 and involve just 3 terms.) It seems reasonable to ignore these Gramian relations and treat the pairings as if they were algebraically independent. Identity verification becomes easy, while the difficulty shifts towards reformulating incidence theorems in terms of such pairings.

The paper is organized as follows. Sections 2–5 constitute the core of the paper. In Section 2, we establish the general form of our master theorem (Theorem 2.6). In Sections 3–5, we demonstrate the power of this theorem by providing numerous applications to linear incidence geometry over the real or complex field, first in the plane (Sections 3–4) and then in 3-space (Section 5). We also provide (see Section 3) an interpretation of our approach in the more conventional language of Levi graphs.

Section 6 is devoted to combinatorial reformulations of our master theorem. The first reformulation uses nodal (multi-)curves on an oriented surface Σ ; such curves are in one-to-one correspondence with quadrilateral tilings of Σ . The second reformulation involves graphs properly embedded into Σ , so that each face is simply-connected. This generalizes a beautiful construction proposed by D. G. Glynn [17].

In Section 7, we discuss ways to obtain new incidence theorems from existing ones using the tiling technique. In particular, we show that *any* incidence theorem associated to a tiling \mathbf{T} can be generalized in multiple ways by inserting new tiles into \mathbf{T} .

Several geometric corollaries of the master theorem are presented in Section 8. We explain how an arbitrary triangulation of an oriented surface gives rise to an incidence theorem in the plane. Both Desargues' and Pappus' theorems can be obtained in this way. A three-dimensional analogue of this result yields the Möbius theorem. We also show that when the dual graph of a triangulation is Hamiltonian, the corresponding incidence theorem can be presented as a closure porism (Schließungssatz).

In Section 9, we prove that our tilings exhibit 3D/4D consistency in the sense of Bobenko-Suris [9] and provide solutions of Zamolodchikov's tetrahedron equation.

Variations of our main construction are discussed in Sections 10–11, where we in particular outline connections with Ceva's theorem, harmonic quadruples, basic Schubert Calculus, and circles on the Möbius plane.

ACKNOWLEDGMENTS

We took inspiration from the work of Jürgen Richter-Gebert [46, 48] and Bernd Sturmfels [55, 57] on invariant-theoretic approaches to incidence geometry and the work of Alexander Bobenko and Yuri Suris [8, 9] on integrable systems on quad-graphs.

We thank Alexander Barvinok and Michael Shapiro for enlightening discussions. We are grateful to Joe Buhler and Jeff Lagarias for their comments on the earlier version of the paper.

The main results of this paper were presented at the conference “Cluster algebras and Poisson geometry” (Levico Terme, Italy) in June 2023. We thank the organizers and participants of this conference for their substantive feedback.

We used `GeoGebra` for drawing point-and-line configurations.

2. THE MASTER THEOREM

Let \mathbb{P} be a real or complex finite-dimensional projective space of dimension ≥ 2 . (In this paper, we focus on applications where $\dim \mathbb{P} = 2$ or $\dim \mathbb{P} = 3$, i.e., \mathbb{P} is a plane or a 3-space.)

We denote by \mathbb{P}^* the set of hyperplanes in \mathbb{P} . In particular, when \mathbb{P} is a plane, the elements of \mathbb{P}^* are lines. A point $A \in \mathbb{P}$ and a hyperplane $\ell \in \mathbb{P}^*$ are called *incident* to each other if $A \in \ell$.

We denote by (AB) (resp., (ABC)) the line passing through two distinct points A and B (resp., the plane passing through distinct points A, B, C).

Definition 2.1. Throughout this paper, a *tile* is a topological quadrilateral (that is, a closed oriented disk with four marked points on its boundary) whose vertices are clockwise labeled A, ℓ, B, m , where $A, B \in \mathbb{P}$ are points and $\ell, m \in \mathbb{P}^*$ are hyperplanes:

$$(2.1) \quad \begin{array}{ccc} A & \text{---} & \ell \\ | & & | \\ m & \text{---} & B \end{array}$$

Such a tile is called *coherent* if

- neither A nor B is incident to either ℓ or m ; and
- either $A = B$ or $\ell = m$ or else the line (AB) and the codimension 2 subspace $\ell \cap m$ have a nonempty intersection.

Remark 2.2. In the case of the projective plane ($\dim \mathbb{P} = 2$), a coherent tile involves two points A, B and two lines ℓ, m not incident to them such that either $A = B$ or $\ell = m$ or else the line (AB) passes through the point $\ell \cap m$. See Figure 2.

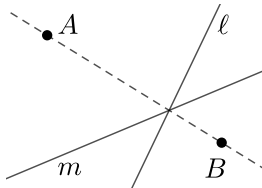


Figure 2: Definition of a coherent tile.

Remark 2.3. The notion of coherence introduced in Definition 2.1 does not depend on the (interlacing) linear order in which the points A, B and the lines ℓ, m are listed. That is, rotating or reflecting a tile does not affect its coherence.

The notion of coherence can be reformulated algebraically in terms of *cross-ratios*. This will require a bit of preparation. Assume that \mathbb{P} is the projectivization of a real or complex vector space \mathbb{V} , so that points in \mathbb{P} are identified with one-dimensional subspaces in \mathbb{V} . Hyperplanes in \mathbb{P} correspond to codimension 1 subspaces of \mathbb{V} , so they can be identified with one-dimensional subspaces in the dual space \mathbb{V}^* .

For a vector $\mathbf{V} \in \mathbb{V}$ and a covector $\mathbf{h} \in \mathbb{V}^*$, let $\langle \mathbf{V}, \mathbf{h} \rangle$ denote their pairing.

Definition 2.4. Let $\mathbf{A}, \mathbf{B} \in \mathbb{V}$ be vectors and let $A, B \in \mathbb{P}$ be the corresponding points. Let $\ell, \mathbf{m} \in \mathbb{V}^*$ be covectors and let $\ell, m \in \mathbb{P}^*$ be the corresponding hyperplanes. Assume that all four pairings $\langle \mathbf{A}, \ell \rangle$, $\langle \mathbf{A}, \mathbf{m} \rangle$, $\langle \mathbf{B}, \ell \rangle$, $\langle \mathbf{B}, \mathbf{m} \rangle$ are nonzero; equivalently, neither A nor B is incident to ℓ or m . The *mixed cross-ratio* $(A, B; \ell, m)$ is defined by

$$(2.2) \quad (A, B; \ell, m) = \frac{\langle \mathbf{A}, \ell \rangle \langle \mathbf{B}, \mathbf{m} \rangle}{\langle \mathbf{A}, \mathbf{m} \rangle \langle \mathbf{B}, \ell \rangle}.$$

We note that $(A, B; \ell, m)$ does not depend on the choice of vectors \mathbf{A}, \mathbf{B} and covectors ℓ, \mathbf{m} representing the points A, B and the hyperplanes ℓ, m , respectively. In fact,

$$(2.3) \quad (A, B; \ell, m) = (A, B; L, M),$$

the ordinary cross-ratio of four collinear points $A, B, L = (AB) \cap \ell$ and $M = (AB) \cap m$.

The instances $\dim \mathbb{P} = 2$ and $\dim \mathbb{P} = 3$ of the notion of mixed cross-ratio has been studied since at least early 20th century, see [12, (4.49), (4.71)] and references therein.

Proposition 2.5. *Let $A, B \in \mathbb{P}$ be points and $\ell, m \in \mathbb{P}^*$ be hyperplanes such that neither A nor B is incident to ℓ or m . The tile*

$$(2.4) \quad \begin{array}{ccc} A & \text{---} & \ell \\ | & & | \\ m & \text{---} & B \end{array}$$

(cf. (2.1)) is coherent if and only if

$$(2.5) \quad (A, B; \ell, m) = 1.$$

Proof. If the tile (2.4) is coherent, then the line (AB) passes through a point lying on $\ell \cap m$ (cf. Figure 2). This implies that $\frac{\langle \mathbf{A}, \ell \rangle}{\langle \mathbf{A}, \mathbf{m} \rangle} = \frac{\langle \mathbf{B}, \ell \rangle}{\langle \mathbf{B}, \mathbf{m} \rangle}$, and (2.5) follows, cf. (2.2).

On the other hand, if the tile (2.4) is not coherent, then the points $L = (AB) \cap \ell$ and $M = (AB) \cap m$ on the line (AB) are different from each other. Consequently $\frac{\langle \mathbf{A}, \ell \rangle}{\langle \mathbf{A}, \mathbf{m} \rangle} \neq \frac{\langle \mathbf{B}, \ell \rangle}{\langle \mathbf{B}, \mathbf{m} \rangle}$, contradicting (2.5). \square

We are now prepared to state and prove our master theorem.

Theorem 2.6. *Consider a tiling of a closed oriented surface by quadrilateral tiles. Assume that the vertices of the tiling are colored black and white, so that every edge connects vertices of different color. Associate to each black (resp., white) vertex a point (resp., a hyperplane) in the real/complex finite-dimensional projective space \mathbb{P} . Assume that for each edge $A - h$ of the tiling, the point A does not lie on the hyperplane h . If all tiles but one are coherent, then the remaining tile is coherent as well.*

Proof. The theorem follows by combining Proposition 2.5 with the observation that the product of mixed cross-ratios $(A, B; \ell, m)$ over all tiles (2.1)/(2.4) in the tiling is equal to 1. To see why the latter statement is true, replace each point $P \in \mathbb{P}$ (resp., hyperplane $h \in \mathbb{P}^*$) appearing in the tiling by an appropriate vector $\mathbf{p} \in \mathbb{V}$ (resp., covector $\mathbf{h} \in \mathbb{V}^*$). Then for each edge $P - h$ in the tiling, the pairing (\mathbf{P}, \mathbf{h}) appears in the numerator (resp., denominator) of the mixed cross-ratio for the unique tile in which P immediately precedes h in the clockwise (resp., counterclockwise) traversal of the boundary of the tile. \square

Remark 2.7. In the case $\dim \mathbb{P} = 2$ of Theorem 2.6, we recover Theorem 1.1.

Remark 2.8. There exist tilings of oriented surfaces by quadrilateral tiles whose vertices cannot be properly colored in two colors, as our construction demands. See Figure 3 for a (counter)example.

On the other hand, any tiling of a *sphere* by quadrilateral tiles necessarily has a requisite 2-coloring. Indeed, in the spherical case, every simple cycle in the 1-skeleton of the tiling can be paved by tiles, hence it cannot be odd.

When we want to emphasize that a given tiling \mathbf{T} of an oriented surface comes with a proper coloring of its vertices in two colors (as in Theorem 2.6), we say that \mathbf{T} is a *bicolored quadrilateral tiling*.

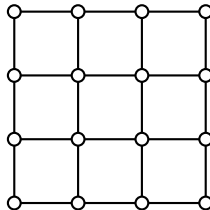


Figure 3: A tiling of the torus that does not yield an incidence theorem. (The opposite sides of the shown fundamental domain should be glued to each other.) The 1-skeleton of this tiling is not bipartite since it contains 3-cycles.

TRIVIAL INSTANCES OF THE MASTER THEOREM

A bicolored quadrilateral tiling of an oriented surface must be sufficiently “ample” in order for the associated incidence theorem to be nontrivial. We illustrate this by several examples of tilings whose associated theorems amount to tautologies.

Example 2.9. Tile a sphere S^2 by two quadrilateral tiles by drawing a circle on S^2 and splitting this circle into a 4-cycle. (That is, place four vertices onto the circle.) The resulting two tiles will be mirror images of each other:

$$(2.6) \quad \begin{array}{ccc} A & \text{---} & \ell \\ | & & | \\ m & \text{---} & B \end{array} \qquad \begin{array}{ccc} \ell & \text{---} & A \\ | & & | \\ B & \text{---} & m \end{array}$$

If one of these tiles is coherent, then so is the other—which is obvious because the two coherence statements coincide.

Example 2.10. Split a $2 \times 2k$ square into $4k$ unit squares and glue its opposite sides to each other to get a tiling of the torus by $4k$ tiles, shown below for $k = 1, 2$:

$$(2.7) \quad \begin{array}{ccc} A & \text{---} & \ell & \text{---} & A \\ | & & | & & | \\ m & \text{---} & B & \text{---} & m \\ | & & | & & | \\ A & \text{---} & \ell & \text{---} & A \end{array} \qquad \begin{array}{ccccccc} A & \text{---} & \ell & \text{---} & C & \text{---} & p & \text{---} & A \\ | & & | & & | & & | & & | \\ m & \text{---} & B & \text{---} & n & \text{---} & D & \text{---} & m \\ | & & | & & | & & | & & | \\ A & \text{---} & \ell & \text{---} & C & \text{---} & p & \text{---} & A \end{array}$$

The associated incidence theorem is vacuous since the coherence statements encoded by the tiles appearing in the same column are identical to each other. Thus, if all tiles but one are coherent, then the remaining tile is coherent just because the conclusion of this implication is contained among its conditions.

Example 2.11. The incidence theorem associated with the tiling of the torus

$$(2.8) \quad \begin{array}{ccccc} & a & \cdots & b & \cdots & a \\ & \diagdown & & \diagup & & \diagdown \\ & & C & & & D \\ & \diagup & & \diagdown & & \diagup \\ & a & \cdots & b & \cdots & a \end{array}$$

(as above, the opposite sides of the rectangular fundamental domain should be glued to each other) is trivial for a different reason: each of the four tiles has two vertices with the same label, so all four coherence statements are vacuous.

Example 2.12. The incidence theorem associated with the tiling of the sphere

$$(2.9) \quad \begin{array}{ccc} A & \text{---} & \ell \\ | & & / \\ & B & \\ | & & \\ m & \text{---} & C \end{array}$$

is rather shallow. If $\ell = m$ or the points A, B, C are not distinct, then the statement is vacuous. Otherwise, the theorem says that if $A, B, C \notin \ell$ and the point $D = \ell \cap m$ lies on the lines (AB) and (BC) , then $D \in (AC)$. This is clearly true because $B \neq D$ and therefore $(AB) = (BC) = (AC)$.

3. FIRST APPLICATIONS

In the words of S. A. Amitsur [1, Section A.2], *the three main theorems in (linear) projective geometry are the complete quadrilateral theorem, the Desargues theorem, and the Pappus theorem.* We begin by explaining how each of these three theorems can be obtained by direct application of our master theorem (Theorem 1.1/2.6).

THE DESARGUES THEOREM

Theorem 3.1 (G. Desargues, ca. 1639). *Let a, b, c be distinct concurrent lines on the complex/real projective plane. Pick generic points $A_1, A_2 \in a$, $B_1, B_2 \in b$, $C_1, C_2 \in c$. Then the points $A = (B_1C_1) \cap (B_2C_2)$, $B = (A_1C_1) \cap (A_2C_2)$, $C = (A_1B_1) \cap (A_2B_2)$ are collinear. See Figure 4.*

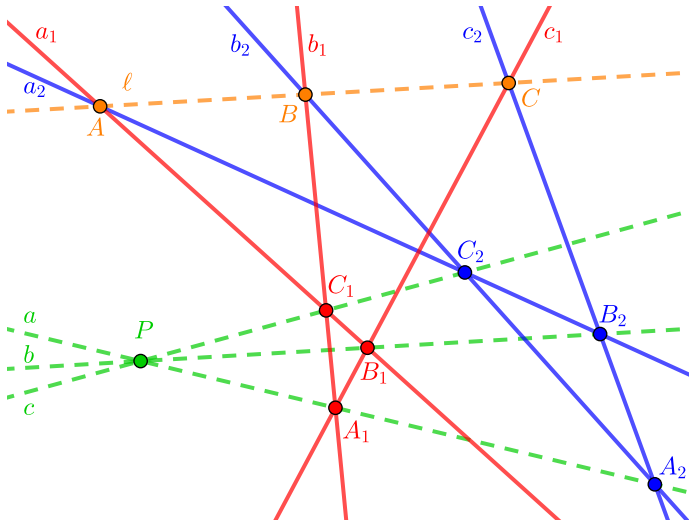


Figure 4: The Desargues theorem.

Proof. Denote

$$(3.1) \quad \begin{aligned} a &= (A_1A_2), & b &= (B_1B_2), & c &= (C_1C_2), \\ a_1 &= (B_1C_1), & b_1 &= (A_1C_1), & c_1 &= (A_1B_1), \end{aligned}$$

$$(3.2) \quad \begin{aligned} a_2 &= (B_2C_2), & b_2 &= (A_2C_2), & c_2 &= (A_2B_2), \end{aligned}$$

so that $A = a_1 \cap a_2$, $B = b_1 \cap b_2$, $C = c_1 \cap c_2$.

Let us formulate the pertinent conditions in terms of $a_1, a_2, A_1, A_2, b, c, B, C$:

- A_1, A_2 , and $b \cap c$ are collinear (given);
- A_1, B , and $a_1 \cap c$ are collinear (given);
- A_1, C , and $a_1 \cap b$ are collinear (given);
- A_2, B , and $a_2 \cap c$ are collinear (given);
- A_2, C , and $a_2 \cap b$ are collinear (given);
- B, C , and $a_1 \cap a_2$ are collinear (to be proved).

These six conditions correspond to the six tiles in the tiling of the sphere shown in Figure 5. The claim now follows by the master theorem. \square

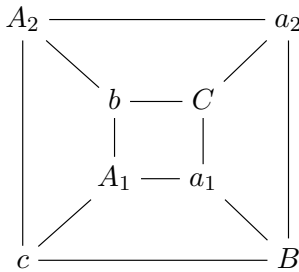


Figure 5: The tiling of the sphere used in the proof of the Desargues theorem.

For another version of essentially the same argument, see the proof of Corollary 4.4.

A more combinatorial viewpoint towards incidence geometry of point-and-line configurations in the projective plane, going back at least to the work of H. S. M. Coxeter, involves the notion of a Levi graph (or incidence graph); see, e.g., [45] for an excellent introduction to this approach. Let \mathcal{C} be a configuration of points and lines in the real/complex projective plane. (In this paper, we use the word *configuration* to describe a collection of geometric objects, with no *a priori* combinatorial constraints.) The *Levi graph* of \mathcal{C} is a bipartite graph whose vertices correspond to the points and lines of \mathcal{C} and whose edges record the incidences between them: whenever a point P lies on a line ℓ , the Levi graph includes the edge $P - \ell$. (We will use this notion a bit loosely, ignoring “accidental” incidences that do not affect the validity of the corresponding incidence theorems; these accidents can be eliminated by imposing appropriate genericity assumptions.)

Let us illustrate this viewpoint in the case of the Desargues theorem. In light of Definition 2.1/Remark 2.2, we replace each tile

$$\begin{array}{ccc} A & \text{---} & \ell \\ | & & | \\ m & \text{---} & B \end{array}$$

by the “quadripod”

$$(3.3) \quad \begin{array}{ccc} A & & \ell \\ & \searrow & \nearrow \\ & N & c \\ & \nearrow & \searrow \\ m & & B \end{array}$$

which encodes the coherence of the tile in terms of the Levi graph: we want the point $N = \ell \cap m$ to lie on the line $c = (AB)$. (Note that the edges $A - \ell - B - m - A$ from the boundary of the tile do not appear in the Levi graph, as they do not correspond to incidences in the configuration.)

Applying this procedure to the tiling in Figure 5, we obtain the Levi graph of the Desargues configuration, shown in Figure 6. An alternative rendering of this graph, matching the presentation given in [45, Fig. 5.25], is given in Figure 7.

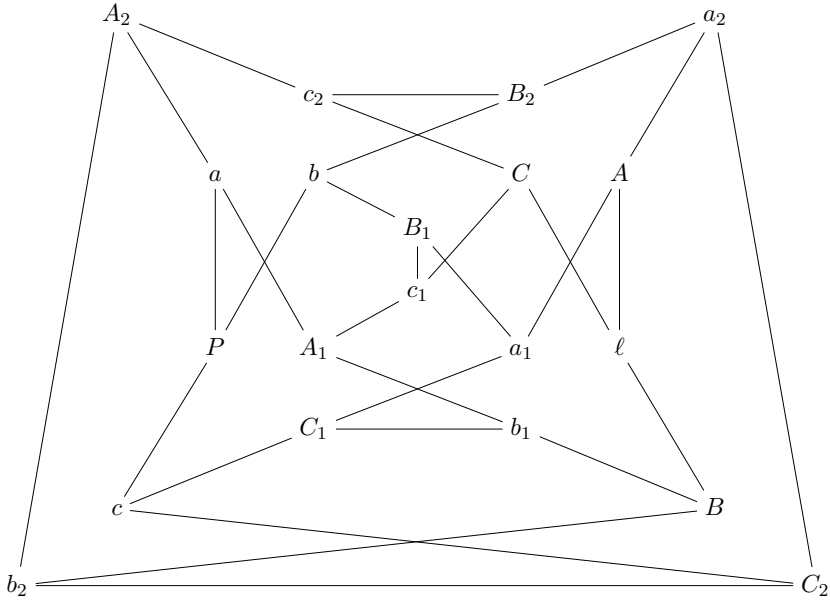


Figure 6: Obtaining the Levi graph of the Desargues configuration from the tiling in Figure 5. For example, at the top of the picture, the 5 edges incident to the vertices c_2 and/or B_2 come from the coherent tile with vertices A_2, a_2, C, b at the top of Figure 5.

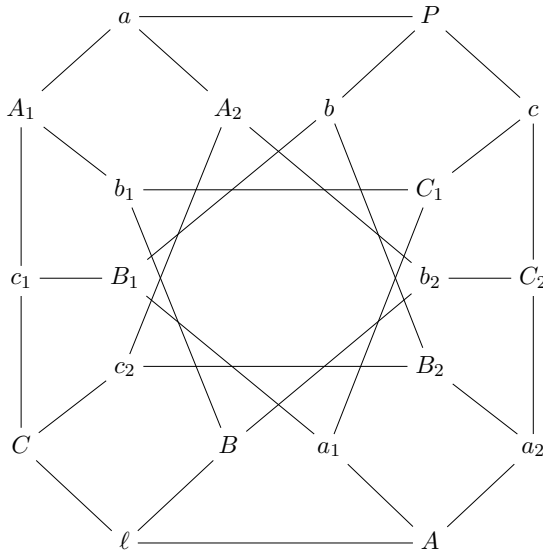


Figure 7: Alternative rendering of the Levi graph of the Desargues configuration.

We will soon see that, in general, additional steps may be required to get the Levi graph of an incidence theorem from the corresponding tiling. This can be seen from the simple fact that each tile gives rise to 5 edges whereas the number of edges in a Levi graph of an incidence theorem does not have to be divisible by 5.

THE PAPPUS THEOREM

We consider the following version of the classical Pappus theorem.

Theorem 3.2 (Pappus of Alexandria, around 340 CE). *Let $P_1, P_2, P_3, P_4, P_5, P_6$ be six generic points on the real/complex plane. Then any two of the following three conditions (cf. Figure 8) imply the third:*

- the lines (P_1P_2) , (P_3P_4) , (P_5P_6) intersect at a common point A ;
- the lines (P_2P_3) , (P_4P_5) , (P_6P_1) intersect at a common point B ;
- the lines (P_1P_4) , (P_2P_5) , (P_3P_6) intersect at a common point C .

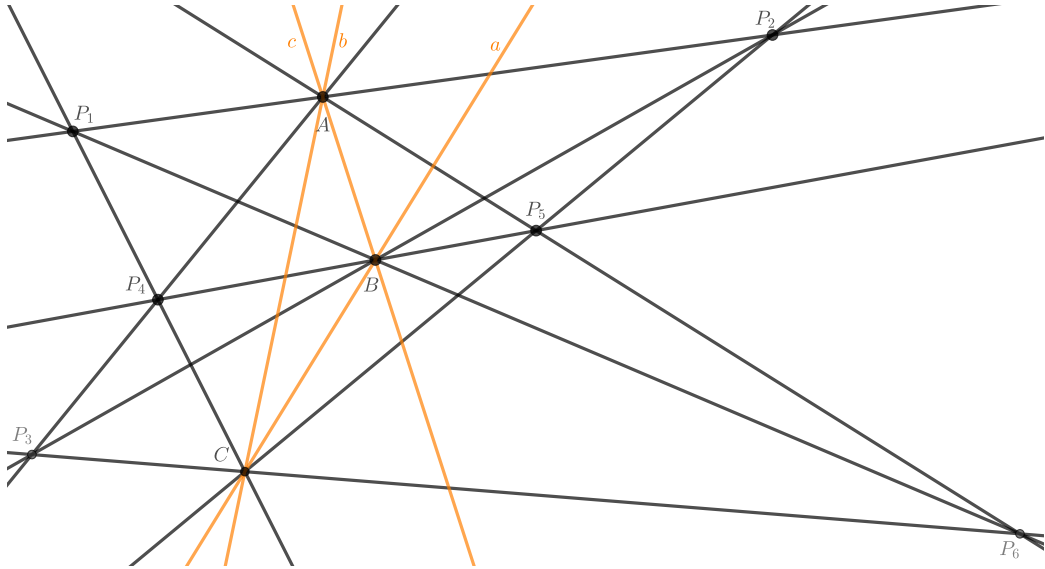


Figure 8: The Pappus theorem.

Proof. Define the points $A = (P_3P_4) \cap (P_5P_6)$, $B = (P_2P_3) \cap (P_1P_6)$, $C = (P_1P_4) \cap (P_2P_5)$ and the lines $a = (BC)$, $b = (AC)$, $c = (AB)$, so that $A = b \cap c$, $B = a \cap c$, $C = a \cap b$. By construction, we have:

- P_3, P_4 , and $b \cap c$ are collinear;
- P_5, P_6 , and $b \cap c$ are collinear;
- P_2, P_3 , and $a \cap c$ are collinear;
- P_6, P_1 , and $a \cap c$ are collinear;
- P_1, P_4 , and $a \cap b$ are collinear;
- P_2, P_5 , and $a \cap b$ are collinear.

The conditions appearing in the theorem become:

- P_1, P_2 , and $b \cap c$ are collinear;
- P_4, P_5 , and $a \cap c$ are collinear;
- P_3, P_6 , and $a \cap b$ are collinear.

These 9 conditions correspond to the 9 tiles in the tiling of the torus shown in Figure 9. The claim follows by the master theorem. \square

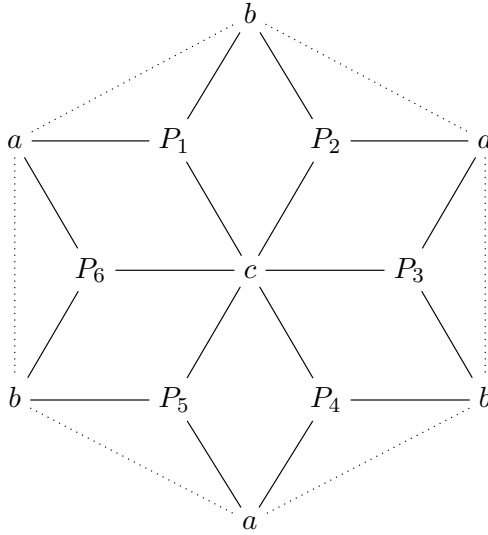


Figure 9: The tiling of the torus used in the proof of the Pappus theorem. Opposite sides of the shown hexagonal fundamental domain should be glued to each other. There are no edges between the vertices a and b .

To obtain the Levi graph of the Pappus configuration from the tiling in Figure 9, we need to perform the following steps:

- (1) insert the quadripod (3.3) into each tile, as before;
- (2) identify multiple occurrences of each of the points A, B, C to get Figure 10;
- (3) remove bivalent vertices a, b, c and the edges incident to them (bivalent vertices do not impose any restrictions on the rest of the configuration);
- (4) rearrange the drawing to get Figure 11. (Compare with [45, Fig. 5.23].)

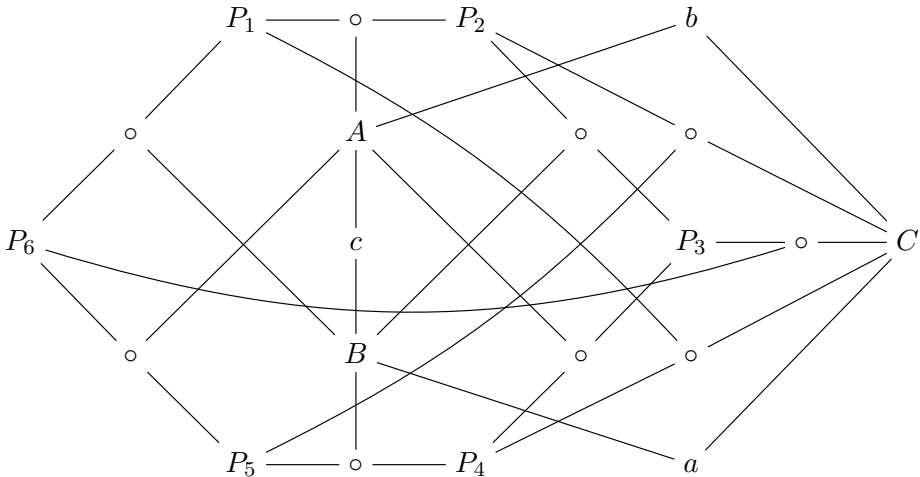


Figure 10: The intermediate Levi graph obtained from the tiling shown in Figure 9. Unlabeled vertices marked “ \circ ” correspond to lines.

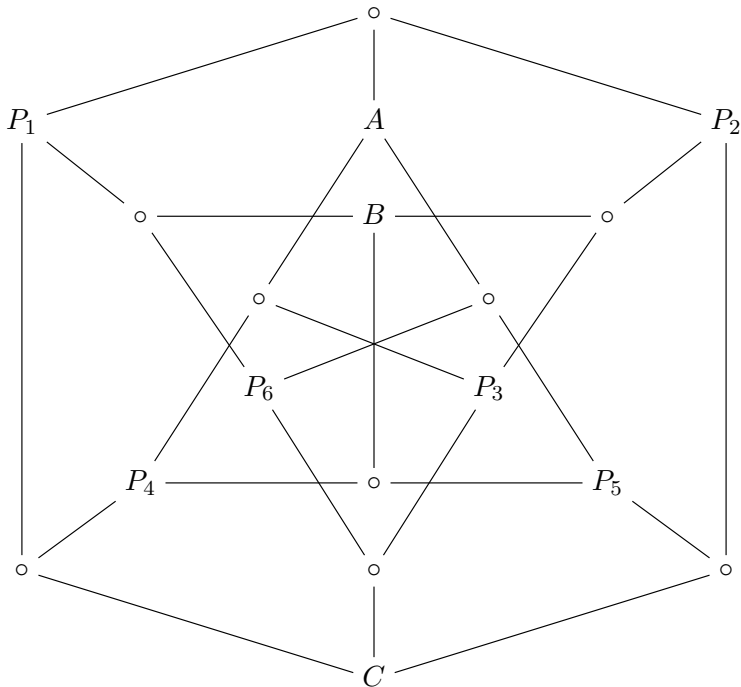


Figure 11: The Levi graph of the Pappus configuration. Each unlabeled vertex v corresponds to the line passing through the 3 points that label the vertices adjacent to v .

Surprisingly, there exists an alternative proof of the Pappus theorem, also based on our master theorem but utilizing a different tiling of the torus. This tiling, shown in Figure 13, involves 4 points and 5 lines (*vs.* 6 points and 3 lines in Figure 9).

Second proof of Theorem 3.2. As before, set $A = (P_3P_4) \cap (P_5P_6)$, $C = (P_1P_4) \cap (P_2P_5)$, and $b = AC$. Also define (cf. Figure 12):

$$\begin{aligned} q &= P_1P_6, & r &= P_1P_2, & s &= P_3P_6, & t &= P_2P_3, \\ D &= P_1P_4 \cap P_5P_6, & E &= P_2P_5 \cap P_3P_4. \end{aligned}$$

Reformulating the 9 collinearity conditions of the Pappus configuration in terms of the points P_4, P_5, D, E and the lines b, q, r, s, t , we obtain the following 9 conditions:

- P_4, D , and $b \cap s$ are collinear,
- P_4, D , and $q \cap r$ are collinear,
- P_4, E , and $b \cap r$ are collinear;
- P_4, E , and $s \cap t$ are collinear;
- P_5, D , and $b \cap r$ are collinear;
- P_5, D , and $s \cap q$ are collinear;
- P_5, E , and $b \cap s$ are collinear,
- P_5, E , and $r \cap t$ are collinear;
- P_4, P_5 , and $q \cap t$ are collinear.

These 9 conditions correspond to the 9 tiles in the tiling of the torus exhibited in Figure 13. The claim follows by the master theorem. \square

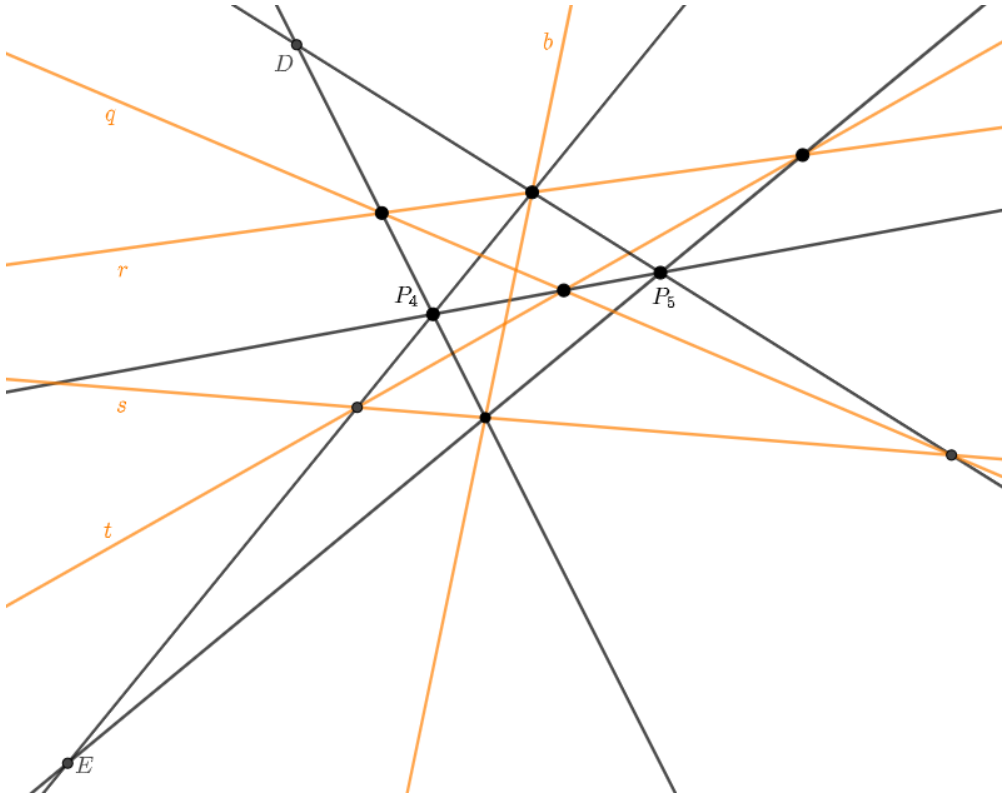


Figure 12: The Pappus theorem, second version.

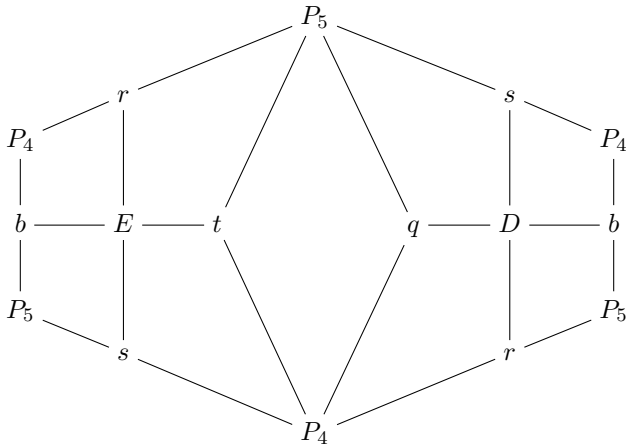


Figure 13: The tiling of the torus for the second proof of the Pappus theorem. Opposite sides of this hexagonal fundamental domain should be glued to each other.

To get the Levi graph of the Pappus configuration from the tiling in Figure 13, identify duplicate occurrences of (P_4E) , (P_5E) , (P_4D) , (P_5D) , $b \cap s$, $b \cap r$, then remove bivalent vertices b, D, E and the edges incident to them.

COMPLETE QUADRANGLES/QUADRILATERALS

Theorems 3.3 and 3.6 below are apparently due to G. Desargues, with precursors in the works of Euclid and Pappus of Alexandria, see [62, Chapter VIII, p. 288]. For other presentations and discussions, see, e.g., [46, Example 5], [49, Section 8.3], and/or [22, §2.4]. These results play an important role in R. Moufang's foundational work on axiomatization of projective geometry, cf. [38, p. 68].

Theorem 3.3. *Let A_1, A_2, A_3, A_4 be generic points on the real/complex projective plane. Draw six lines $\ell_{ij} = (A_i A_j)$, $1 \leq i < j \leq 4$, through various pairs of these points. Pick an arbitrary line and denote by P_{ij} the intersection of ℓ_{ij} with the chosen line. Now let us try to find another quadruple of points that would yield the same six points P_{ij} . To this end, take a generic point B_1 and draw the lines $m_{12} = (B_1 P_{12})$, $m_{13} = (B_1 P_{13})$, $m_{14} = (B_1 P_{14})$. Pick a generic point $B_2 \in m_{12}$ and draw the lines $m_{23} = (B_2 P_{23})$ and $m_{24} = (B_2 P_{24})$. Set $B_3 = m_{13} \cap m_{23}$ and $B_4 = m_{14} \cap m_{24}$. Then the line $m_{34} = (B_3 B_4)$ passes through P_{34} . See Figure 14.*

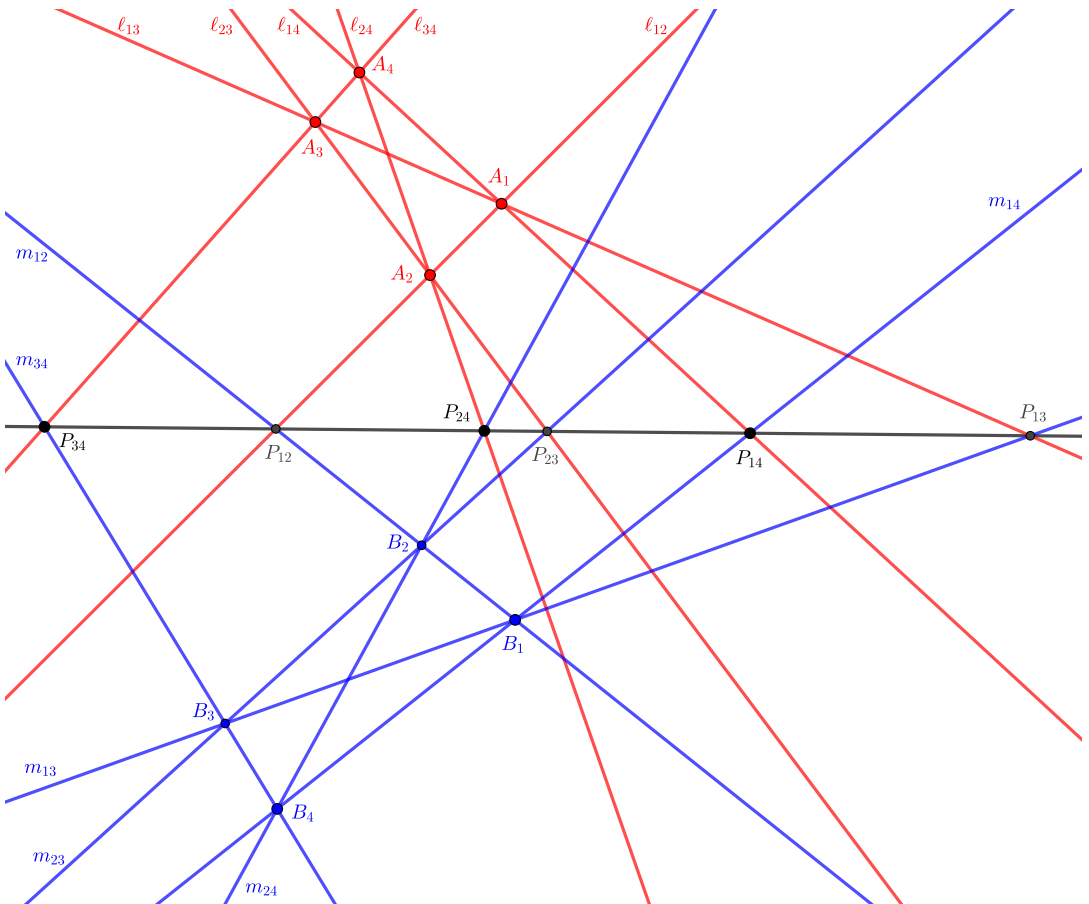


Figure 14: Theorem 3.3.

Proof. Apply the master theorem to the tiling in Figure 15. □

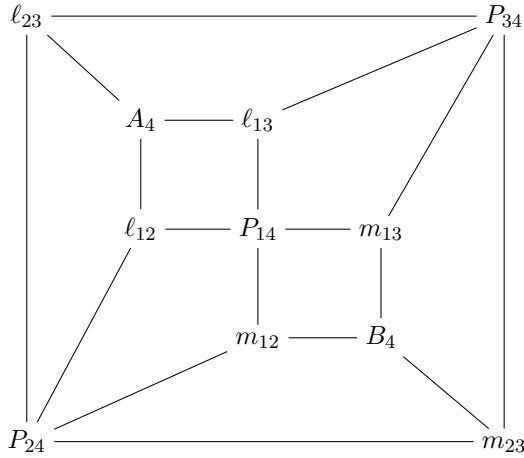


Figure 15: The tiling of the sphere used in the proofs of Theorems 3.3–3.4.

To obtain the Levi graph associated with the configuration in Figure 14, begin by inserting a quadripod (3.3) into each tile to obtain the graph shown in Figure 16. There, each of the three unlabeled vertices represents the line that passes through the six points P_{ij} . To get the Levi graph for Theorem 3.3, these three vertices must be identified (“glued”) into a single vertex.

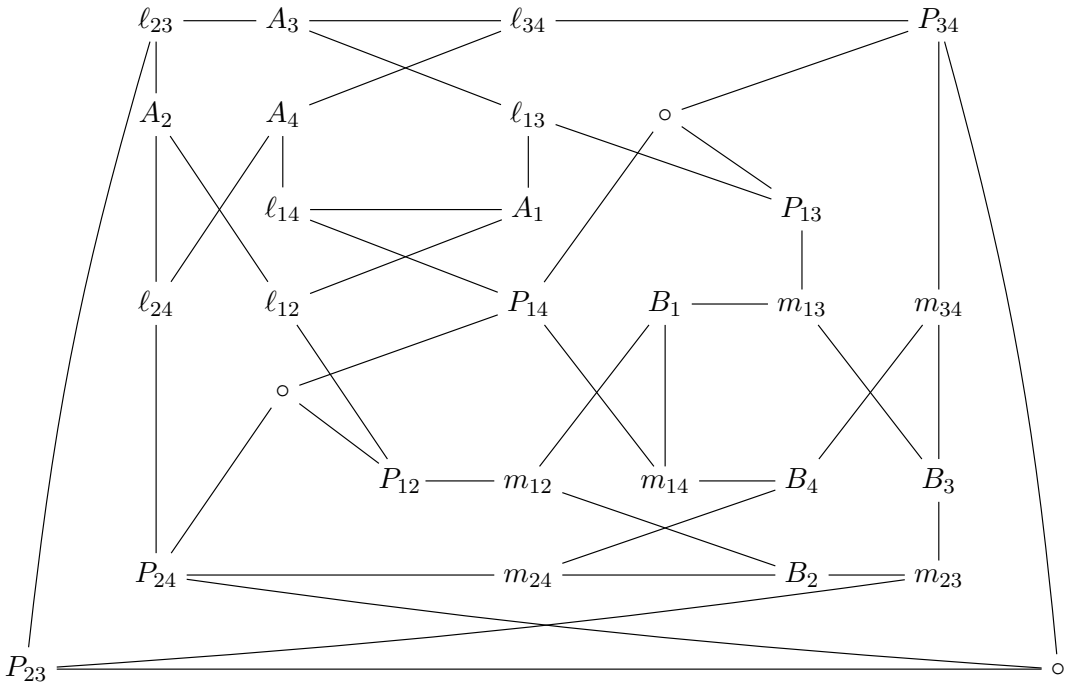


Figure 16: The Levi graph obtained from the tiling in Figure 15.

As the above proof suggests, Theorem 3.3 can be generalized. There is no need to require that the six points P_{ij} lie on the same line; it is enough to ask that the three triples $\{P_{13}, P_{14}, P_{34}\}$, $\{P_{12}, P_{14}, P_{24}\}$, and $\{P_{23}, P_{24}, P_{34}\}$ are collinear. The same proof still works, with the same tiling as before (see Figure 15). The key difference is that now, the graph in Figure 16 is the true Levi graph of the configuration, since the three unlabeled vertices no longer need to be glued together.

We thus obtain the following generalization of Theorem 3.3:

Theorem 3.4. *Let A_1, A_2, A_3, A_4 be four generic points on the real/complex projective plane. Draw six lines $\ell_{ij} = (A_i A_j)$, $1 \leq i < j \leq 4$, through pairs of these points. Pick three generic points $P_{14} \in \ell_{14}$, $P_{24} \in \ell_{24}$, $P_{34} \in \ell_{34}$, then set*

$$(3.4) \quad P_{12} = \ell_{12} \cap (P_{14}P_{24}), \quad P_{13} = \ell_{13} \cap (P_{14}P_{34}), \quad P_{23} = \ell_{23} \cap (P_{24}P_{34}).$$

Pick a generic point B_1 and define $m_{12} = (B_1 P_{12})$, $m_{13} = (B_1 P_{13})$, $m_{14} = (B_1 P_{14})$. Pick a generic point $B_2 \in m_{12}$ and draw the lines $m_{23} = (B_2 P_{23})$ and $m_{24} = (B_2 P_{24})$. Set $B_3 = m_{13} \cap m_{23}$ and $B_4 = m_{14} \cap m_{24}$. Then the line $m_{34} = (B_3 B_4)$ contains P_{34} . See Figure 17.

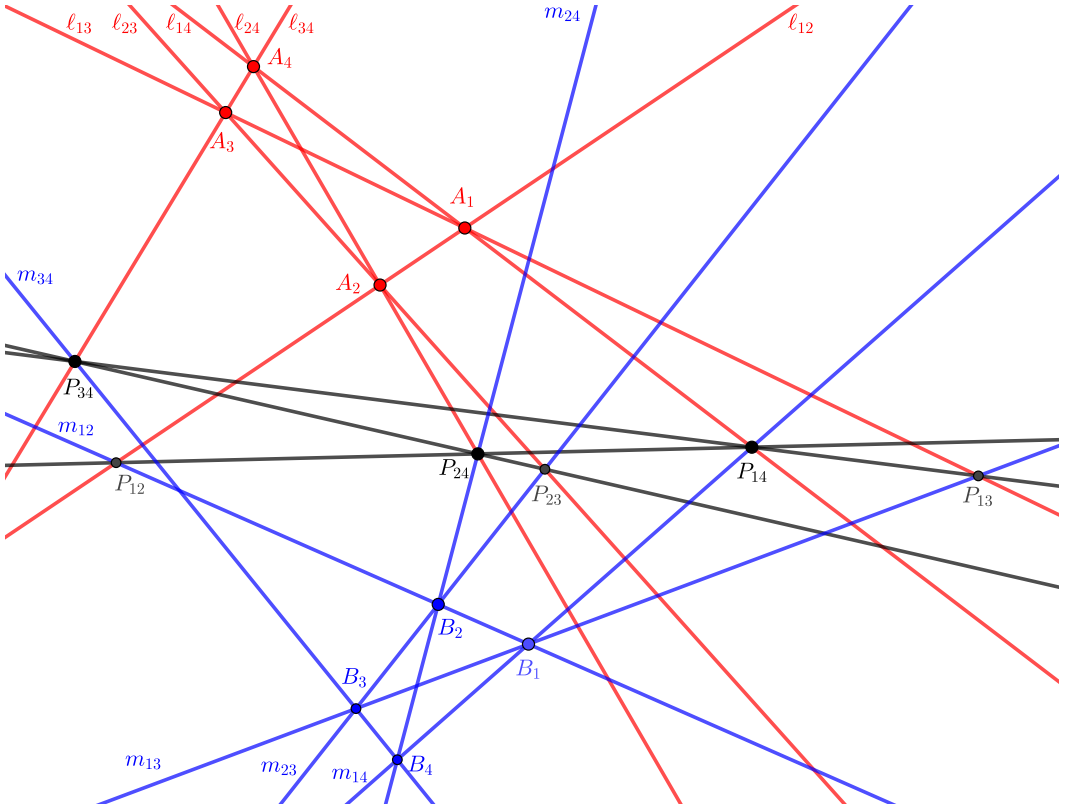


Figure 17: The configuration in Theorem 3.4.

Remark 3.5. The assumptions in Theorem 3.4 imply (right after (3.4)) that the points P_{12}, P_{13}, P_{23} are collinear, cf. the front page. Our proof does not rely on this observation.

Going in the opposite direction, we can further specialize Theorem 3.3 to obtain the following simplification (the “harmonic points theorem” [46, Example 4]):

Theorem 3.6. *Let A_1, A_2, A_3, A_4 be four generic points on the real/complex projective plane. Draw six lines $\ell_{ij} = (A_i A_j)$, $1 \leq i < j \leq 4$. Let $P_{12,34} = \ell_{12} \cap \ell_{34}$ and $P_{14,23} = \ell_{14} \cap \ell_{23}$. Draw the line $\ell_o = (P_{12,34} P_{14,23})$. Set $P_{13} = \ell_{13} \cap \ell_o$ and $P_{24} = \ell_{24} \cap \ell_o$. Take a generic point B_1 and set $m_{12} = (B_1 P_{12,34})$, $m_{13} = (B_1 P_{13})$, $m_{14} = (B_1 P_{14,23})$. Then pick a generic point $B_2 \in m_{12}$ and set $m_{23} = (B_2 P_{14,23})$, $m_{24} = (B_2 P_{24})$, $B_3 = m_{13} \cap m_{23}$, $B_4 = m_{14} \cap m_{24}$. Then the line $m_{34} = (B_3 B_4)$ passes through $P_{12,34}$. See Figure 18.*

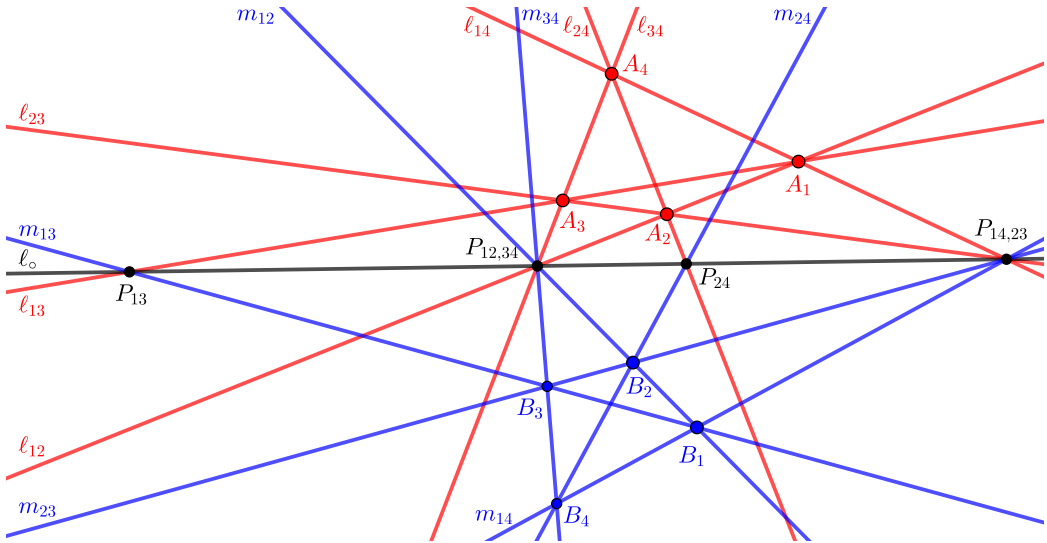


Figure 18: The configuration in Theorem 3.6.

Theorem 3.6 is immediate from Theorem 3.3: just make the additional (redundant) assumptions $P_{12} = P_{34}$ and $P_{14} = P_{23}$. The proof remains the same, except for the extra identifications in the Levi graph.

Remark 3.7. As explained above, the tiling in Figure 15 yields Theorem 3.4, from which Theorems 3.3 and 3.6 can be obtained by introducing additional—in point of fact, unnecessary—(co)incidence assumptions. These examples suggest that if we want our master theorem to potentially encompass all incidence theorems of plane projective geometry, then we need to allow, in addition to the choices embedded into the master theorem (i.e., the choices of a closed oriented surface and an arbitrary quadrilateral tiling of it), the ability to impose additional redundant constraints that may potentially simplify the statement of an incidence theorem.

From an algorithmic standpoint, this means that in order to exhibit an instance of the master theorem from which a given incidence theorem can be obtained, we may need to first identify and remove some redundant assumptions that do not affect the validity of the theorem. This could be a challenging algorithmic task in itself—but one that may have to be carried out in order to obtain (a generalization of) a given incidence theorem from a suitable tiled surface.

Adding the assumption $\ell_{12} = m_{12}$ to Theorem 3.4 and simplifying the ensuing statement, we obtain the following result.

Theorem 3.8. *Let A_1, A_2, A_3, A_4 be four generic points on the plane. Draw six lines $\ell_{ij} = (A_i A_j)$, $1 \leq i < j \leq 4$. Pick points $Q \in \ell_{34}$, $P_{13} \in \ell_{13}$, $P_{23} \in \ell_{23}$ and $B_1, B_2 \in \ell_{12}$. Construct $P_{14} = (QP_{13}) \cap \ell_{14}$, $P_{24} = (QP_{23}) \cap \ell_{24}$ and $B_3 = (B_1 P_{13}) \cap (B_2 P_{23})$, $B_4 = (B_1 P_{14}) \cap (B_2 P_{24})$. Then the points B_3, B_4, Q are collinear.*

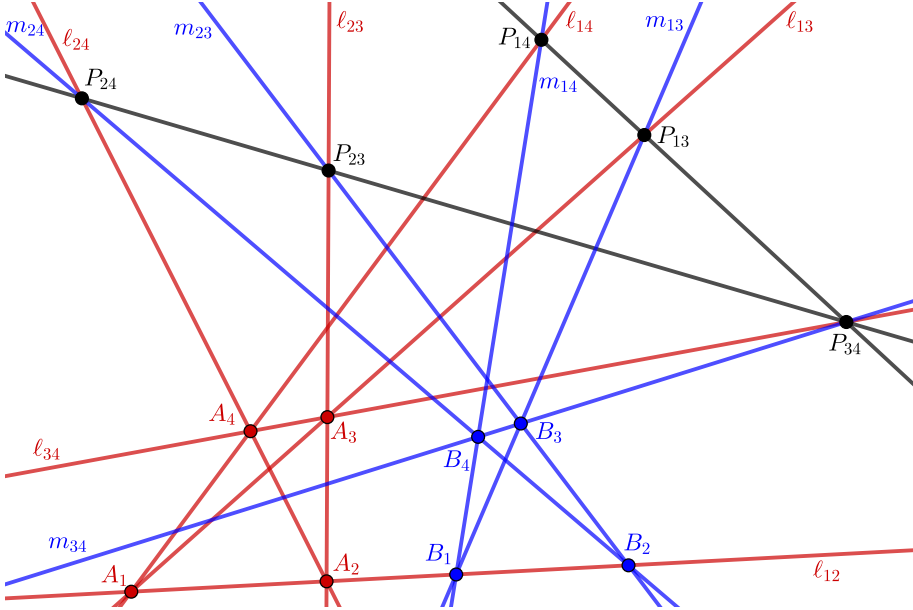


Figure 19: The configuration in Theorem 3.8.

Proof. Apply the master theorem to the tiling in Figure 20. (This tiling was obtained from the tiling in in Figure 15 by identifying the vertices ℓ_{12} and m_{12} .) \square

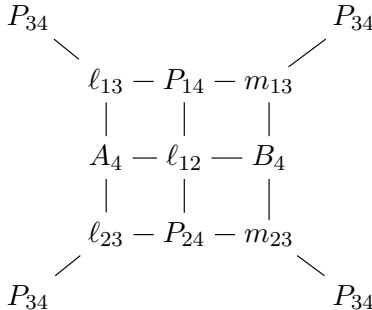


Figure 20: The tiling of the sphere used in the proof of Theorem 3.8.

Remark 3.9. Theorem 3.8 can be restated as follows. Consider two quadrilaterals that are in perspective. (In the above notation, take $A_3 P_{13} B_3 P_{23}$ and $A_4 P_{14} B_4 P_{24}$.) Construct the points where their corresponding sides meet. (These would be A_1, B_1, B_2, A_2 .) If three of these four points are collinear, then all four points are collinear.

Remark 3.10. Degenerating the above construction to the setting where both quadruples $\{A_3, A_4, B_3, B_4\}$ and $\{P_{13}, P_{14}, P_{23}, P_{24}\}$ are collinear, we obtain the *planar bundle theorem* [6, Theorem 2.5].

We conclude this section by a couple of additional applications of our master theorem in plane projective geometry.

THE PERMUTATION THEOREM

Theorem 3.11. *Take a generic quadruple p, q, r, s of concurrent lines on the real or complex projective plane. Let P_1, Q_1, R_1, S_1 and P_2, Q_2, R_2, S_2 denote the points of intersection of this quadruple with two generic lines ℓ_1 and ℓ_2 , see Figure 21. If three of the four lines (P_1Q_2) , (R_1S_2) , (R_2S_1) , (P_2Q_1) are concurrent, then all four of them are concurrent.*

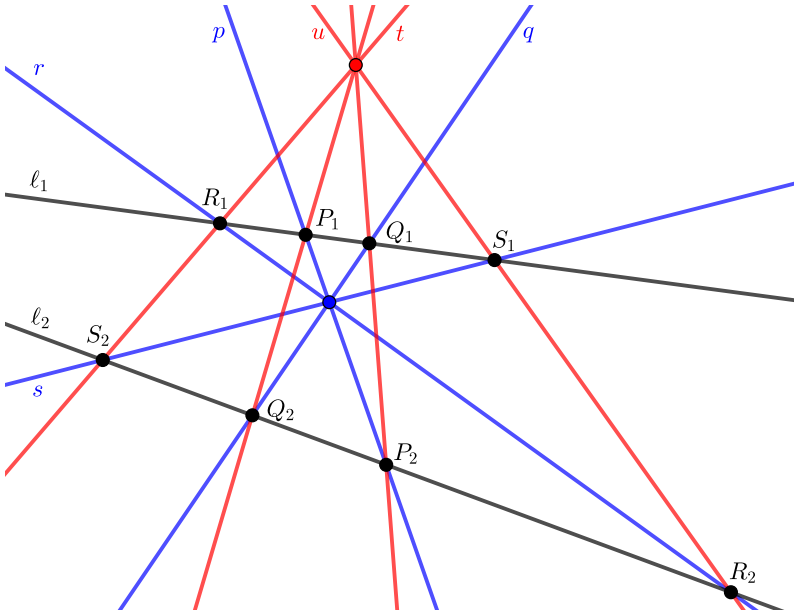


Figure 21: The permutation theorem.

Proof. Denote $t = (R_1S_2)$ and $u = (R_2S_1)$. Let us express the conditions appearing in the theorem in terms of the points P_1, P_2, Q_1, Q_2 and the lines r, s, t, u :

- P_1, Q_1 , and $r \cap t$ are collinear;
- P_1, Q_1 , and $s \cap u$ are collinear;
- P_2, Q_2 , and $r \cap u$ are collinear;
- P_2, Q_2 , and $s \cap t$ are collinear;
- $(P_1P_2), r, s$ are concurrent;
- $(Q_1Q_2), r, s$ are concurrent;
- $(P_1Q_2), t, u$ are concurrent;
- $(P_2Q_1), t, u$ are concurrent.

These 8 conditions correspond to 8 tiles in the tiling of the torus shown in Figure 22. The claim follows by the master theorem. \square

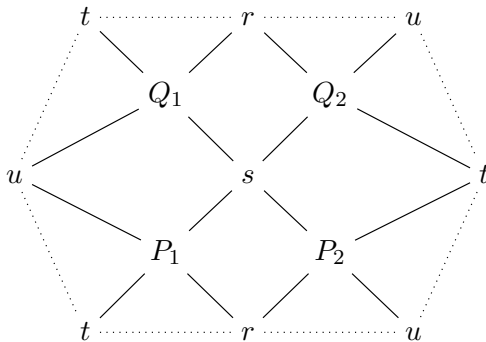


Figure 22: The tiling of the torus used in the proof of the permutation theorem. Opposite sides of the hexagonal fundamental domain should be glued to each other. There are no edges along the sides of the fundamental domain.

SAAM'S SEQUENCE OF PERSPECTIVITIES

The following theorem generalizes a result of A. Saam [51], reproduced in [46, Examples 7, 20].

Theorem 3.12. *Let $A, B, P_1, \dots, P_n, Q_1, \dots, Q_n, R_1, \dots, R_n, S_1, \dots, S_n$ be points on the real/complex projective plane. Consider the following conditions, where the indices are viewed modulo n :*

- *the lines $(Q_i S_i), (Q_{i-1} S_{i-1}), (AP_i)$ are concurrent;*
- *the lines $(Q_i S_{i-1}), (Q_{i+1} S_i), (BR_i)$ are concurrent;*
- *the points P_i, Q_i, R_i are collinear;*
- *the points R_i, S_i, P_{i+1} are collinear.*

If $4n - 1$ of these $4n$ conditions hold, then so does the remaining one.

Figure 23 illustrates Theorem 3.12 for $n = 4$.

Proof of Theorem 3.12. (For simplicity, we restrict the treatment to the case $n = 4$.) Apply the master theorem to the tiling of the sphere shown in Figure 24. \square

Remark 3.13. In the original formulation of Saam's theorem, the points A and B are assumed to coincide with each other. To use the notation from [46, Figure 7], there is no need to require that all eight radial lines pass through the same point H . It suffices to ask that the lines through 1, 5, 9, D pass through common point H , whereas the lines through 3, 7, B , and F pass through common point H' .

Remark 3.14. The special case $n = 3$ of Saam's sequence-of-perspectivities theorem (Theorem 3.12 with $A = B$), known as Nehring's theorem [39], can be seen to be a special case of the Pappus theorem. Using the notation from [11, Example 6.27], this can be explained as follows: remove the point O and the lines OA, OB, OC , then unmark the points A, B, C to get the Pappus configuration.

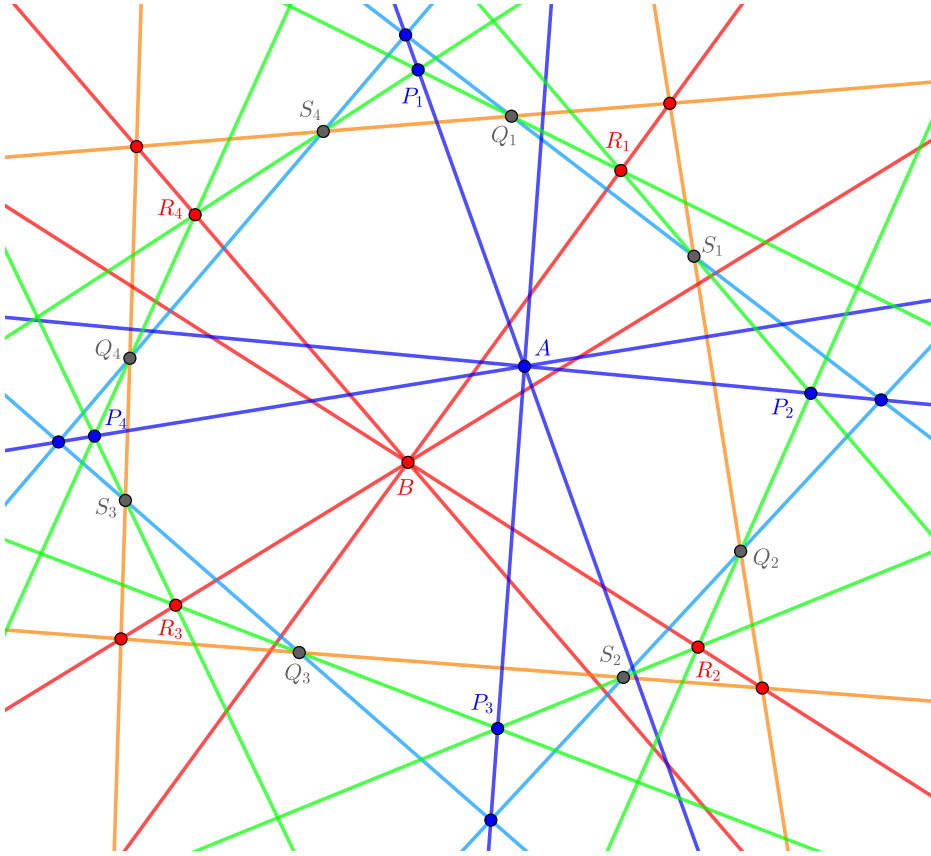


Figure 23: Generalization of Saam's sequence of perspectivities.

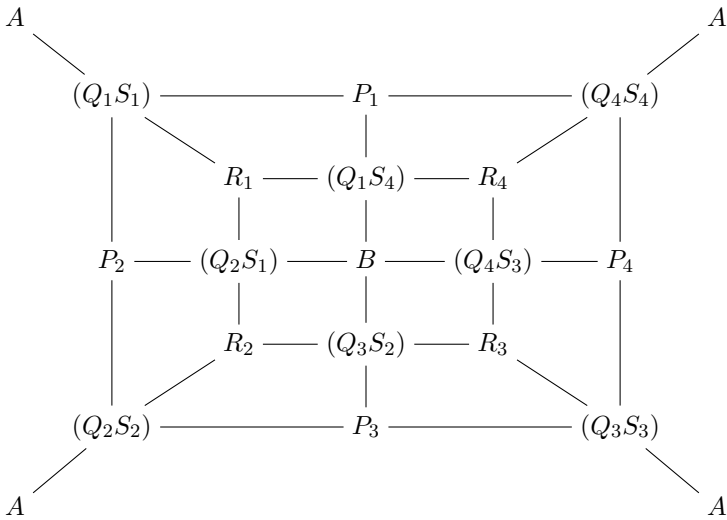


Figure 24: The proof of Theorem 3.12 for $n = 4$.

TWIN STARS OF DAVID

Theorem 3.15. *Let A, B, C, A', B', C' be six points on the real or complex plane. Let p, q, r, p', q', r' be six lines none of which passes through any of those six points. If eleven of the twelve triples of lines*

$$\{p, q, (A'C)\}, \{q, r, (BC')\}, \{p, r, (AB')\}, \{p', q', (AC')\}, \{q', r', (B'C)\}, \{p', r', (A'B)\}$$

$$\{p, q', (AC)\}, \{q, r', (BC)\}, \{p', r, (AB)\}, \{p', q, (A'C')\}, \{q', r, (B'C')\}, \{p, r', (A'B')\}$$

are concurrent, then the twelfth triple is concurrent as well. See Figure 25.

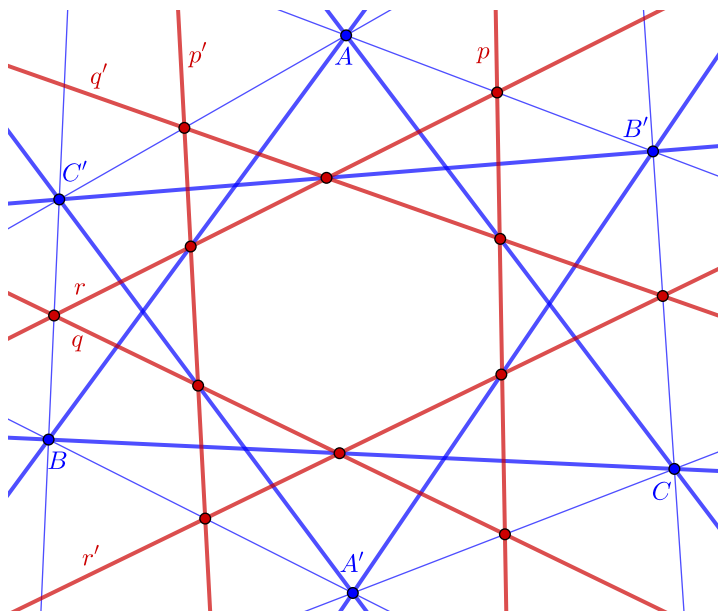


Figure 25: Twin stars of David.

Proof. Apply the master theorem to the tiling of the torus shown in Figure 26. □

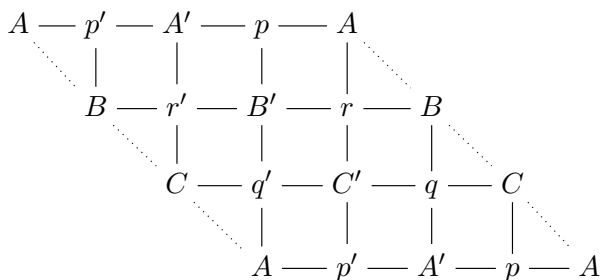


Figure 26: The proof of Theorem 3.15. The opposite sides of the fundamental domain should be glued to each other.

4. COHERENT POLYGONS

Definition 4.1. Let $n \geq 2$. Let A_1, \dots, A_n (resp., ℓ_1, \dots, ℓ_n) be an n -tuple of points (resp., lines) on the real/complex projective plane. Assume that each point A_i does not lie on either of the lines ℓ_i and ℓ_{i-1} (with the indexing understood modulo n). Consider a topological disk \mathbf{P} with $2n$ marked points on the boundary, labeled by $A_1, \ell_1, \dots, A_n, \ell_n$, in this order. (See Figure 27.) We call the $2n$ -gon \mathbf{P} *coherent* if the associated “generalized mixed cross ratio” $(A_1, \dots, A_n; \ell_1, \dots, \ell_n)$ is equal to 1:

$$(4.1) \quad (A_1, \dots, A_n; \ell_1, \dots, \ell_n) \stackrel{\text{def}}{=} \frac{\langle \mathbf{A}_1, \ell_1 \rangle \langle \mathbf{A}_2, \ell_2 \rangle \cdots \langle \mathbf{A}_n, \ell_n \rangle}{\langle \mathbf{A}_2, \ell_1 \rangle \langle \mathbf{A}_3, \ell_2 \rangle \cdots \langle \mathbf{A}_1, \ell_n \rangle} = 1,$$

where \mathbf{A}_i (resp., ℓ_i) is a vector (resp., covector) defining A_i (resp., ℓ_i).

We note that $(A_1, \dots, A_n; \ell_1, \dots, \ell_n)$ does not depend on the choice of vectors \mathbf{A}_i and covectors ℓ_i representing the points A_i and the hyperplanes ℓ_i , respectively.

In the case of a quadrilateral ($n = 2$), we recover the notion of coherence introduced in Definition 2.1, in light of Proposition 2.5.

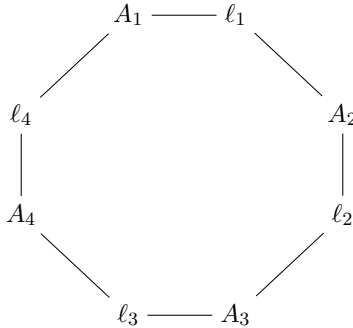


Figure 27: A coherent $2n$ -gon, for $n = 4$.

Proposition 4.2. Let $\mathbf{P} = A_1 \ell_1 \cdots A_n \ell_n$ be a $2n$ -gon with vertices labeled by n points A_1, \dots, A_n and n lines ℓ_1, \dots, ℓ_n on the real/complex projective plane. Assume that each point A_i does not lie on either of the lines ℓ_i and ℓ_{i-1} (with the indexing mod n). Suppose that no three of the points A_i are collinear. Then the following are equivalent:

- the polygon \mathbf{P} is coherent;
- the polygon \mathbf{P} can be tiled by coherent quadrilateral tiles.

In fact, a coherent polygon \mathbf{P} as above can always be tiled by $2n - 3$ coherent tiles all of whose vertices lying in the interior of \mathbf{P} are labeled by lines (and not by points).

Proof. Suppose that \mathbf{P} is tiled by coherent quadrilateral tiles. Multiplying equations (2.5) for all these tiles, we obtain equation (4.1). That is, \mathbf{P} is coherent.

We prove the reverse implication by induction on n . The base case $n = 2$ is trivial. Suppose that our $2n$ -gon \mathbf{P} is coherent. Define

$$B = (A_n A_1) \cap \ell_n, \quad C = (A_{n-1} A_n) \cap \ell_{n-1}, \quad \ell'_{n-1} = (BC).$$

Recall that A_{n-1}, A_n, A_1 are not collinear. Also, neither A_1 nor A_n lie on ℓ_n , hence the collinear points B, A_n, A_1 are distinct. Similarly, the collinear points C, A_{n-1}, A_n are distinct. Hence the line $\ell'_{n-1} = (BC)$ contains none of the points A_{n-1}, A_n, A_1 .

It is now straightforward to check that the two tiles shown below are coherent:

$$(4.2) \quad \begin{array}{ccccc} A_1 & \text{---} & \ell'_{n-1} & \text{---} & A_{n-1} \\ | & & | & & | \\ \ell_n & \text{---} & A_n & \text{---} & \ell_{n-1} \end{array}$$

Indeed, $(A_1A_n) \cap \ell'_{n-1} \cap \ell_n = B$ and $(A_{n-1}A_n) \cap \ell'_{n-1} \cap \ell_{n-1} = C$.

We now embed the tiles from (4.2) into the given $2n$ -gon \mathbf{P} , as shown in Figure 28. Since \mathbf{P} is coherent, as are these two quadrilateral tiles, it follows that the remaining $(2n - 2)$ -gon $\mathbf{P}' = A_1\ell_1 \cdots A_{n-1}\ell'_{n-1}$ is coherent as well. Moreover the noncollinearity condition for the points A_1, \dots, A_{n-1} still holds, so we can apply the induction assumption and obtain the desired tiling by $2 + 2(n - 1) - 3 = 2n - 3$ tiles. \square

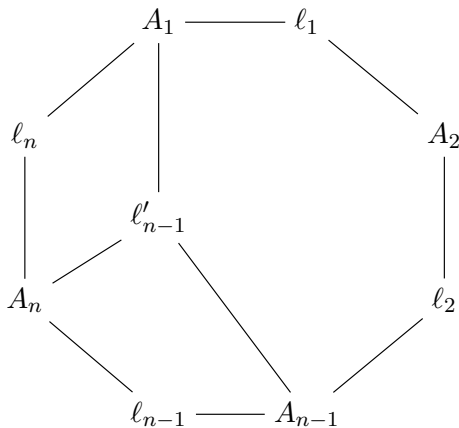


Figure 28: Proof of Proposition 4.2.

Corollary 4.3. *Let Σ be an oriented bordered surface whose boundary $\partial\Sigma$ is homeomorphic to a circle. Select $2n$ points on $\partial\Sigma$ and label them with n points and n lines $A_1, \ell_1, \dots, A_n, \ell_n$, in this order. Suppose that this labeling can be completed to a tiling of Σ by coherent quadrilateral tiles. Then the polygon $\mathbf{P} = A_1\ell_1 \cdots A_n\ell_n$ can be tiled by coherent tiles.*

To rephrase, adding handles to the surface does not expand the class of tileable polygons.

Proof. Multiplying the coherence conditions for all tiles in the tiling, we conclude that the polygon \mathbf{P} is coherent. By Proposition 4.2, this implies that \mathbf{P} can be tiled by coherent quadrilateral tiles. \square

While our arguments appearing below in this section utilize the notion of a coherent polygon, they do not really rely on Proposition 4.2. A combinatorially-minded reader can replace “coherent” by “tileable” throughout without any loss of content.

COHERENT HEXAGONS

The case $n = 3$ of Proposition 4.2 yields the following version of Desargues' theorem:

Corollary 4.4. *Let $A_1B_1C_1$ and $A_2B_2C_2$ be two generic triangles on the plane, with sides $a_1 = (B_1C_1)$, $b_1 = (A_1C_1)$, $c_1 = (A_1B_1)$ and $a_2 = (B_2C_2)$, $b_2 = (A_2C_2)$, $c_2 = (A_2B_2)$, respectively. The following are equivalent:*

- *the points $a_1 \cap a_2$, $b_1 \cap b_2$, $c_1 \cap c_2$ are collinear;*
- *the lines (A_1A_2) , (B_1B_2) , (C_1C_2) are concurrent;*
- *the hexagon shown in Figure 29(i) is coherent;*
- *this hexagon can be tiled as shown in Figure 29(ii);*
- *this hexagon can be tiled as shown in Figure 29(iii).*

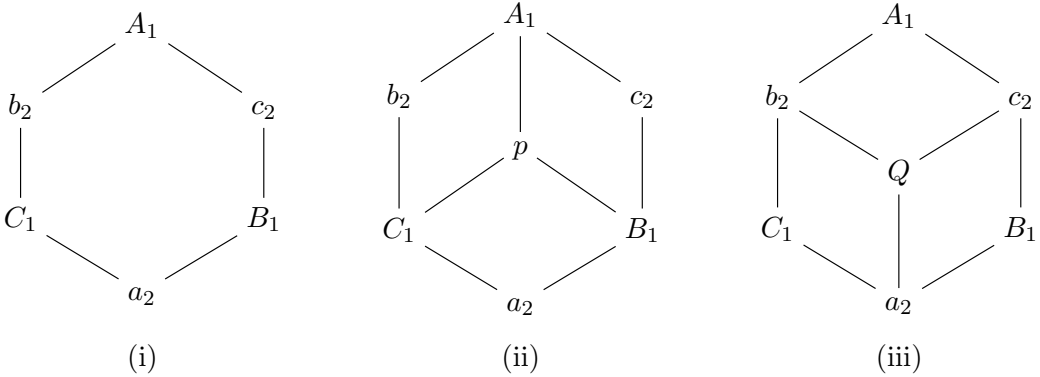


Figure 29: A hexagon and its two tilings.

Proof. The last three statements are equivalent to each other by Proposition 4.2. The existence of the tiling in Figure 29(ii) means that we can draw a line p through the points $a_1 \cap a_2$, $b_1 \cap b_2$, $c_1 \cap c_2$; likewise, the existence of the tiling in Figure 29(iii) means that we can find a point Q lying on the lines (A_1A_2) , (B_1B_2) , (C_1C_2) . \square

Remark 4.5. In Corollary 4.4, when we say that $A_1B_1C_1$ and $A_2B_2C_2$ are *triangles*, we implicitly require that

- the points A_1, B_1, C_1 are not collinear and
- the lines a_2, b_2, c_2 is not concurrent.

To illustrate the role of this requirement, let's assume, on the contrary, that A_1, B_1, C_1 are distinct *collinear* points. Let Q be a fourth generic point. Pick generic points $A_2 \in (A_1Q)$, $B_2 \in (B_1Q)$, $C_2 \in (C_1Q)$. Set $a_2 = (B_2C_2)$, $b_2 = (A_2C_2)$, $c_2 = (A_2B_2)$. Then the tiling in Figure 29(iii) is coherent by construction. However, there is no coherent tiling as in Figure 29(ii), since the line p would have to pass through the points $(A_1B_1) \cap c_2$, $(A_1C_1) \cap b_2$, $(B_1C_1) \cap a_2$, implying that p is the line through the three collinear points A_1, B_1, C_1 . But this would violate the condition that in a coherent tile, no two adjacent labels (a point and a line) are incident to each other.

COHERENT OCTAGONS

In this section, we discuss two kinds of coherent octagons (see Propositions 4.6 and 4.8), which come from special choices of vertex labels.

Proposition 4.6. *Let P_1, P_2, P_3, P_4 be four generic points on the plane. Let a and b be lines passing through $(P_1P_2) \cap (P_3P_4)$ and $(P_1P_4) \cap (P_2P_3)$, respectively. Then the octagon whose vertices are labeled by $P_1, a, P_2, b, P_3, a, P_4, b$ (see Figure 30) is coherent.*

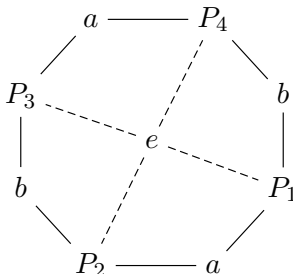


Figure 30: The octagon from Proposition 4.6 and its tiling. Note that each of the lines a and b appears twice along the boundary.

Proof. The proof is based on the tiling shown in Figure 30, where $e = (MN)$ is the line through the points $M = (P_1P_2) \cap (P_3P_4)$ and $N = (P_1P_4) \cap (P_2P_3)$. It is straightforward to check that the conditions for all four tiles are satisfied. \square

Remark 4.7. Our second proof of the Pappus theorem can be viewed as an application of Proposition 4.6: the octagons $P_4 r P_5 t P_4 s P_5 b$ and $P_5 s P_4 b P_5 r P_4 q$ in Figure 13 satisfy, up to projective duality, the conditions in Proposition 4.6.

Proposition 4.8. *Let P_1, P_2, P_3, P_4 be four generic points on the plane. Then the octagon $(P_1P_2)P_3(P_4P_1)P_2(P_3P_4)P_1(P_2P_3)P_4$ (see Figure 31) is coherent.*

Proof. The claim follows from the tiling shown in Figure 31, with $H = (P_1P_3) \cap (P_2P_4)$. It is easy to check that all four tiles are coherent. For example, the lines (P_1P_2) , (P_2P_3) , and $(P_4H) = (P_2P_4)$ intersect at P_2 . \square

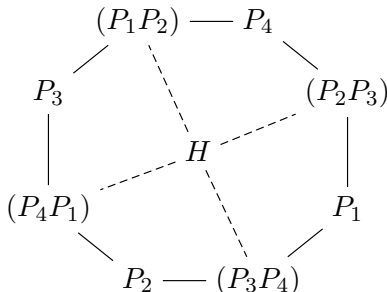


Figure 31: A coherent octagon obtained from a plane quadrilateral $P_1P_2P_3P_4$.

COHERENT DECAGONS

Proposition 4.8 straightforwardly generalizes to larger polygons with the number of sides not divisible by 3. The next interesting example is the decagon:

Proposition 4.9. *The decagon shown in Figure 32 is coherent.*

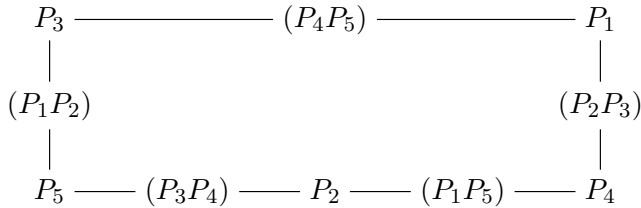


Figure 32: A coherent decagon.

Proof 1. The generalized mixed cross-ratio (cf. (4.1)) is equal to 1, as each of the five terms in the numerator cancels out a term in the denominator. \square

The above proof, while very simple, relies on algebraic calculation. Since our key goal is to show the universal applicability of tiling-based arguments, we provide two alternative proofs below. A fourth proof (which is simpler but relies on a modification of the tiling method) will be given in Section 10.

Proof 2. Denote

$$\begin{aligned} Q &= (P_1P_5) \cap (P_2P_3), & S &= (P_1P_2) \cap (P_3P_4), \\ M &= (P_1P_2) \cap (P_4Q), & N &= (P_2P_3) \cap (P_5S), & T &= (P_4Q) \cap (P_5S), \\ U &= (P_1N) \cap (P_3M), \end{aligned}$$

see Figure 33. The claim can now be obtained from the tiling shown in Figure 34. \square

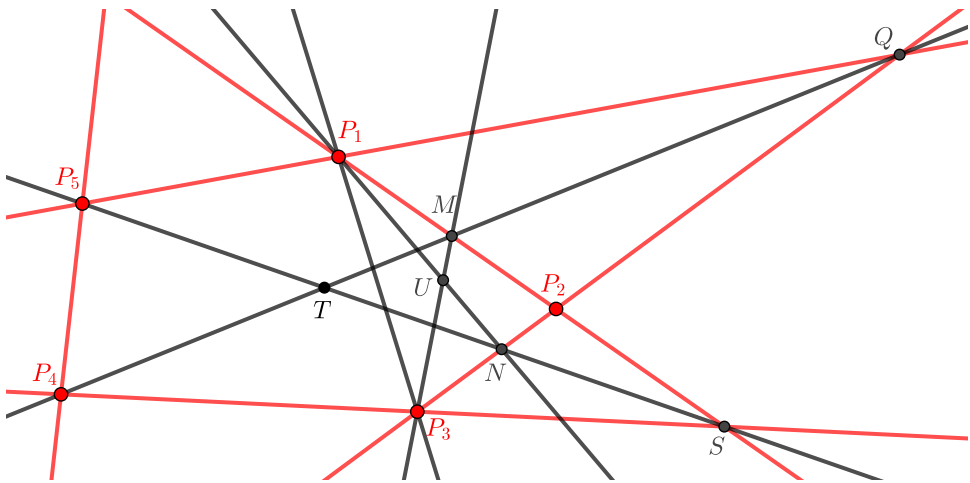


Figure 33: Notation used in the proof of Proposition 4.9.

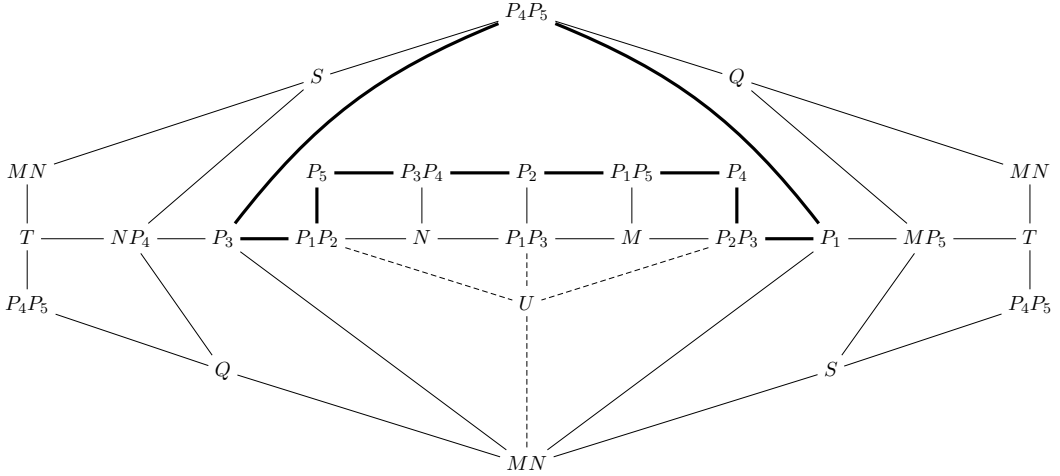


Figure 34: Tileability of the decagon from Figure 32 (shown in **bold**). Opposite sides of the shown hexagonal fundamental domain should be identified, yielding a torus. The tiling of the octagon $P_1P_2 - P_3 - MN - P_1 - P_2P_3 - M - P_1P_3 - N - P_1P_2$ around the vertex U follows the pattern of Figure 31. Here we use that $(P_1P_2) = (P_1M)$ and $(P_2P_3) = (P_3N)$. Furthermore, replacing the quadrilateral $P_1 - MN - P_3 - P_4P_5 - P_1$ by a single tile yields the tiling in Figure 13, so the tileability of this quadrilateral can be interpreted as an application of the Pappus theorem.

Proof 3. This proof utilizes the tiling of a genus 2 surface shown in Figure 35. □

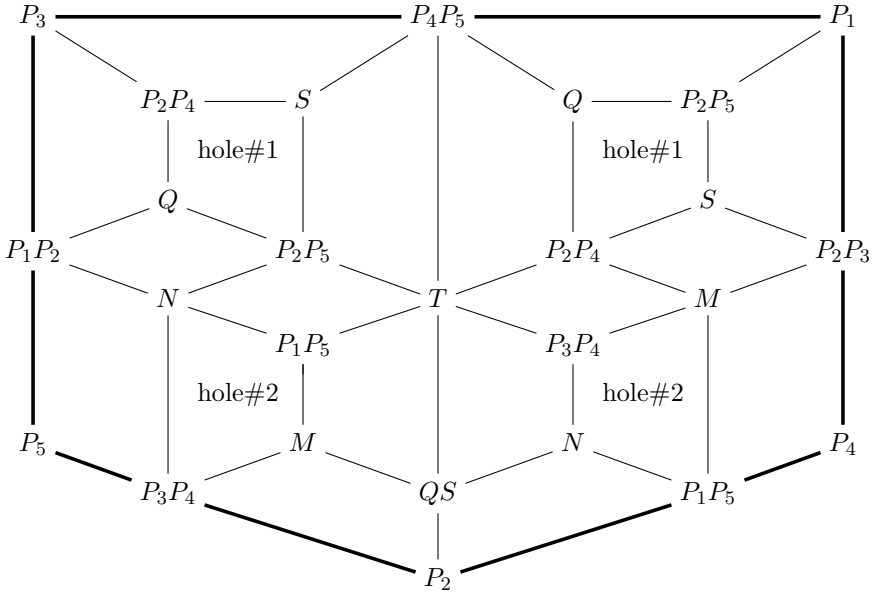


Figure 35: Another tiling of the decagon from Figure 32. The two holes in each pair (#1 and #2) should be glued to each other.

THE GOODMAN-POLLACK THEOREM

Coherent polygons of the kind shown in Figure 32 (cf. Proposition 4.8) appear in the proof of the “ n -star theorem” of J. Goodman and R. Pollack, see [20, Figure 3] and [46, Example 14]. Here is the statement for $n = 5$.

Theorem 4.10. *Let P_1, \dots, P_5 be five generic points on the plane. Denote*

$$\begin{aligned}
 Q_1 &= (P_3P_4) \cap (P_2P_5), \\
 Q_2 &= (P_4P_5) \cap (P_3P_1), \\
 Q_3 &= (P_5P_1) \cap (P_4P_2), \\
 Q_4 &= (P_1P_2) \cap (P_5P_3), \\
 Q_5 &= (P_2P_3) \cap (P_1P_4).
 \end{aligned}
 \tag{4.3}$$

If four of the points Q_1, \dots, Q_5 lie on a line, then the fifth point lies on the same line.

Proof. The conditions in Theorem 4.10 are encoded by the 5 tiles shown in Figure 36. The claim then follows by Proposition 4.9. \square

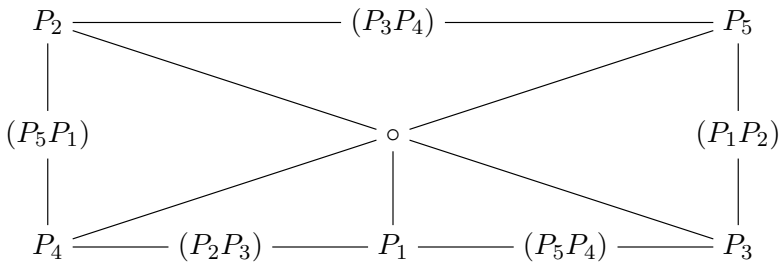


Figure 36: The proof of the Goodman-Pollack theorem. The line at the center passes through the points Q_1, \dots, Q_5 .

Remark 4.11. To get a self-contained tiling-based proof of Theorem 4.10, paste the tiling shown in Figure 36 into the decagonal region appearing in Figure 34. Alternatively, glue together the boundaries of the tilings shown in Figures 35 and 36.

Proposition 4.2 suggests the following generalization of Theorem 4.10.

Theorem 4.12. *Let P_1, \dots, P_5 be five generic points on the plane. Define Q_1, \dots, Q_5 as in (4.3). Then the points $(P_1P_2) \cap (Q_3Q_5)$, $(P_5P_1) \cap (Q_4Q_2)$, and Q_1 are collinear. See Figure 37.*

Before proving Theorem 4.12, let us explain why it can be viewed as a generalization of Theorem 4.10. If in Theorem 4.12, we make the additional (redundant) assumption that the points Q_2, Q_3, Q_4, Q_5 lie on a line ℓ , then $(Q_3Q_5) = (Q_4Q_2) = \ell$ and therefore Theorem 4.12 implies that $Q_1 \in \ell$.

Proof of Theorem 4.12. Combine Proposition 4.9 with the tiling shown in Figure 38. \square

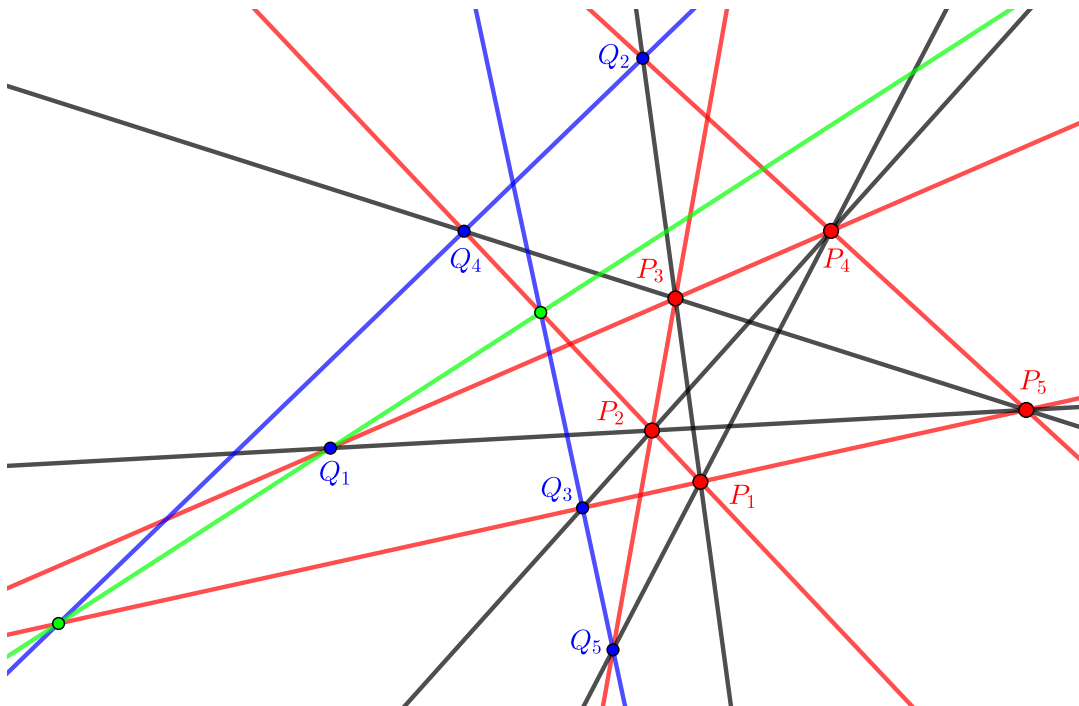


Figure 37: The configuration in Theorem 4.12.

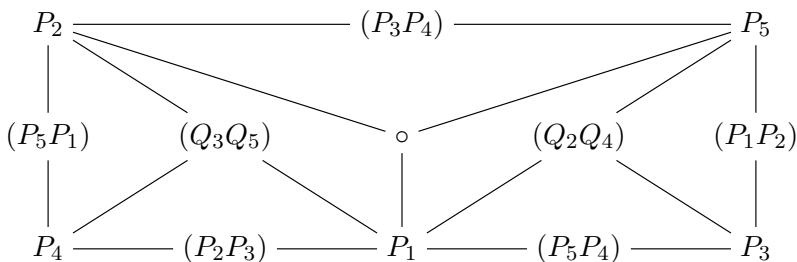


Figure 38: The proof of Theorem 4.12.

Remark 4.13. Propositions 4.8–4.9 generalize to larger $2n$ -gons (here $n \not\equiv 0 \pmod 3$) with boundary labels $P_1 - (P_2P_3) - P_4 - (P_6P_7) - \dots$. We provide hints for a tiling-based proof of this statement at the end of Section 10.

Remark 4.14. The proof of the general Goodman-Pollack theorem, for $n \geq 5$ points on the plane, breaks into two cases. If n is not divisible by 3, the proof is analogous to the one given above for $n = 5$, cf. Remark 4.13. If n is divisible by 3, then the statement becomes vacuous, since each concurrence condition is repeated more than once.

SAAM'S THEOREM

The following result is the $n = 5$ instance of Saam's theorem [50, 51], reproduced in [46, Example 6].

Theorem 4.15. *Let $B, P_1, P_2, P_3, P_4, P_5$ be six generic points on the plane. Pick a generic point $Q_1 \in (BP_1)$. Define (reading by columns):*

$$\begin{aligned} Q'_1 &= (Q_5P_3) \cap (BP_1), \\ Q'_2 &= (Q_1P_4) \cap (BP_2), & Q_2 &= (Q'_1P_4) \cap (BP_2), \\ Q_3 &= (Q'_2P_5) \cap (BP_3), & Q'_3 &= (Q'_2P_5) \cap (BP_3), \\ Q'_4 &= (Q_3P_1) \cap (BP_4), & Q'_4 &= (Q'_3P_1) \cap (BP_4), \\ Q_5 &= (Q'_4P_2) \cap (BP_5), & Q'_5 &= (Q'_4P_2) \cap (BP_5). \end{aligned}$$

Then the points Q'_5, P_3, Q_1 are collinear. See Figure 39.

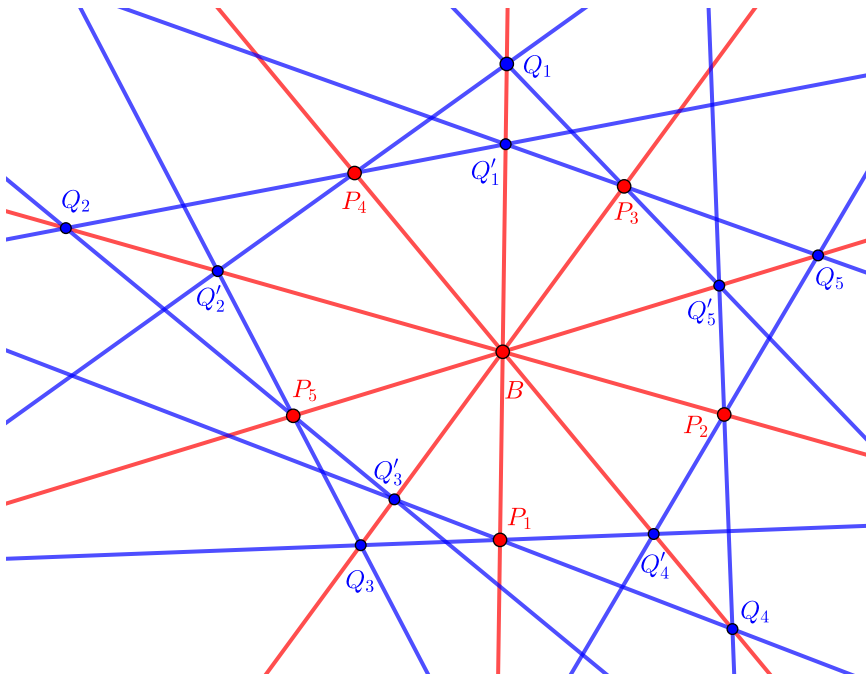


Figure 39: The configuration in Theorem 4.15.

Proof. The claim follows from the tiling shown in Figure 40, once we observe that for the 20-gon on the perimeter of this tiling, the generalized mixed ratio is equal to 1 for trivial algebraic reasons. (All factors cancel each other out in pairs.)

To get an entirely tiling-based proof, we need to tile the aforementioned 20-gon. One possible tiling is shown in Figure 41. There, each octagonal ‘‘petal’’ is an 8-cycle from Proposition 4.8, so it can be tiled as in Figure 31. In the interior 20-gon, the 10 sides involving the vertices labeled B can be glued in 5 pairs, respecting both the labeling and the orientation. The remaining 10 sides form the (properly oriented) 10-gon $Q_1 - (Q_2Q_4) - Q_5 - (Q_1Q_3) - Q_4 - (Q_2Q_5) - Q_3 - (Q_1Q_4) - Q_2 - (Q_3Q_5) - Q_1$.

This is a 10-gon from Figure 32, with respect to the cyclic ordering $Q_1Q_4Q_2Q_5Q_3$; so it can be tiled as shown in Figure 34 or Figure 35. \square

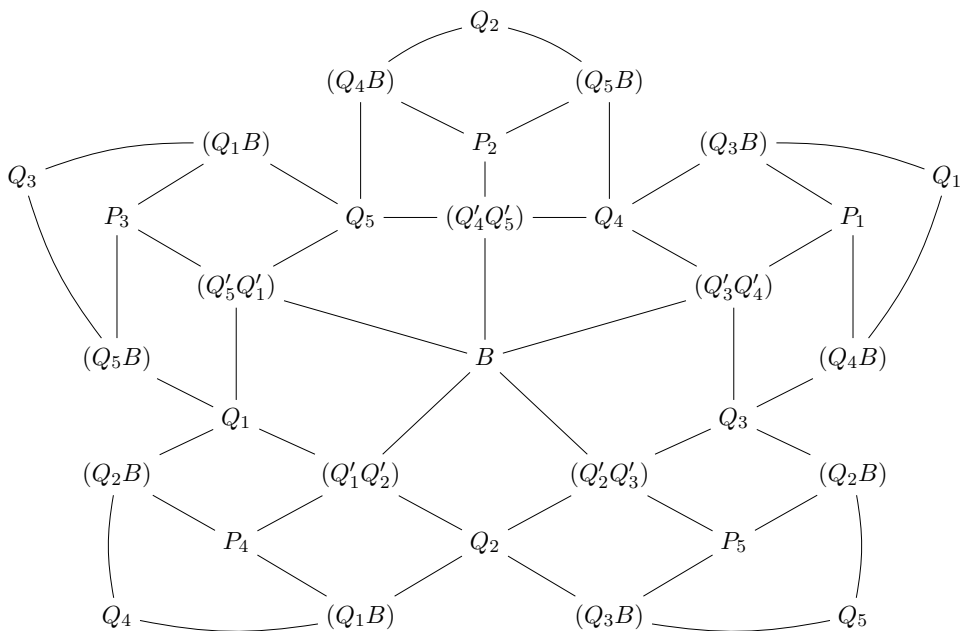


Figure 40: The tiling used in the proof of Theorem 4.15.

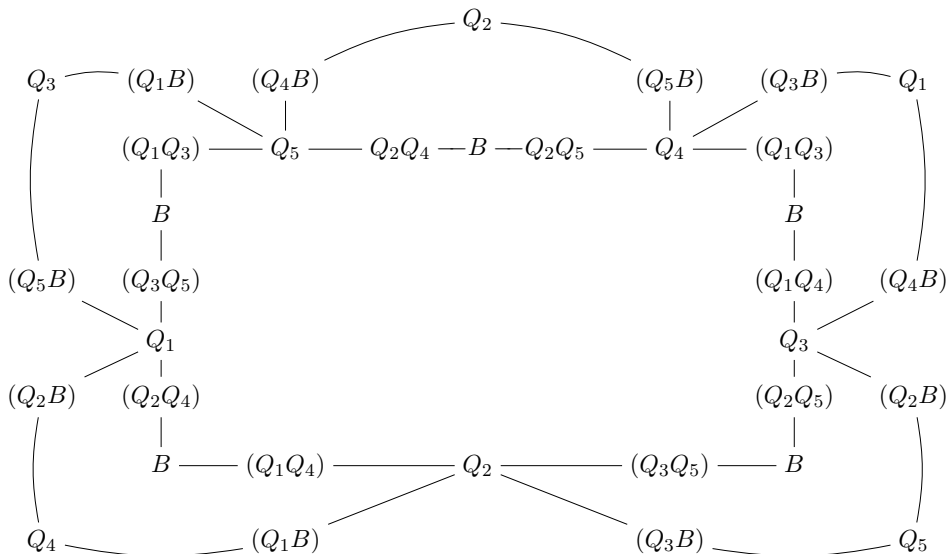


Figure 41: Tiling the 20-gon appearing along the perimeter of Figure 40.

5. APPLICATIONS IN THREE-DIMENSIONAL GEOMETRY

THE BUNDLE THEOREM

The *bundle theorem* (see, e.g., [6,27] and references therein) is the following result.

Theorem 5.1. *Let $\ell_1, \ell_2, \ell_3, \ell_4$ be four lines in the real/complex projective 3-space, no three of them coplanar. If five of the pairs (ℓ_i, ℓ_j) ($i \neq j$) are coplanar, then the sixth pair is also coplanar.*

Proof. Choose two generic points P_i and Q_i on each of the four lines ℓ_i . In the tiling of the sphere shown in Figure 42, the six tiles correspond to the six coplanarities for the pairs (ℓ_i, ℓ_j) . The claim follows. \square

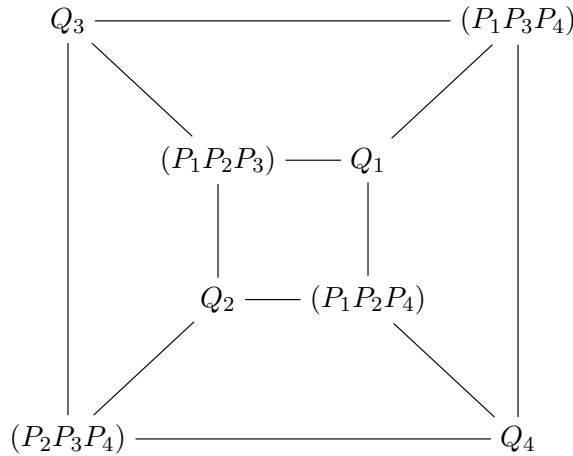


Figure 42: The tiling of the sphere used in the proof of the bundle theorem. Each tile (a face of the cube) corresponds to a coplanarity condition. For example, the coherence of the outer face means that the points P_3, P_4, Q_3, Q_4 (equivalently, the lines ℓ_3 and ℓ_4) are coplanar.

Remark 5.2. If three lines do not lie in a plane but are pairwise coplanar, then these three lines intersect at a common point. So the four lines $\ell_1, \ell_2, \ell_3, \ell_4$ in Theorem 5.1 do, in fact, intersect at a single point, thus forming a “bundle” (hence the name).

Remark 5.3. The above proof of Theorem 5.1 implicitly relies on the non-coplanarity condition on the triples of lines ℓ_i . Indeed, the coherence of the tiles shown in Figure 42 requires each point Q_i to lie outside the planes of the form $(P_i P_j P_k)$, which is ensured by the fact that the lines ℓ_i, ℓ_j, ℓ_k are non-coplanar.

Remark 5.4. Ignoring the labels, the tiling in Figure 42 coincides with the tiling in Figure 5. Thus, the bundle theorem can be viewed as the 3-dimensional counterpart of Desargues’ theorem.

A 3-dimensional counterpart of the Pappus theorem will be presented later in this section, see Theorem 5.13.

THE CUBE THEOREM

The *cube theorem* below is due to A. F. Möbius [37], cf. [3, vol. 1, Exercise I.II.10] or [46, Example 11].

Theorem 5.5. *Let P_1, \dots, P_8 be points in the 3-space such that none of the quadruples $\{P_i, P_j, P_k, P_\ell\}$ ($1 \leq i < j < k \leq 4 < \ell$) are coplanar. If seven of the eight quadruples*

$$(5.1) \quad \begin{aligned} & \{P_1, P_2, P_7, P_8\}, \{P_1, P_2, P_5, P_6\}, \{P_1, P_4, P_5, P_8\}, \{P_1, P_4, P_6, P_7\}, \\ & \{P_2, P_3, P_5, P_8\}, \{P_2, P_3, P_6, P_7\}, \{P_3, P_4, P_7, P_8\}, \{P_3, P_4, P_5, P_6\} \end{aligned}$$

are coplanar, then the remaining quadruple is also coplanar. See Figure 43.

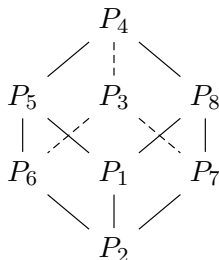


Figure 43: The cube theorem. Given eight points P_i associated with the vertices of the cube as shown in the picture, the theorem asserts that if the four points associated with each face of the cube are coplanar, as is the quadruple $\{P_1, P_4, P_6, P_7\}$, then the quadruple $\{P_2, P_3, P_5, P_8\}$ is coplanar as well.

Proof. Apply the master theorem to the tiling of the torus shown in Figure 44. □

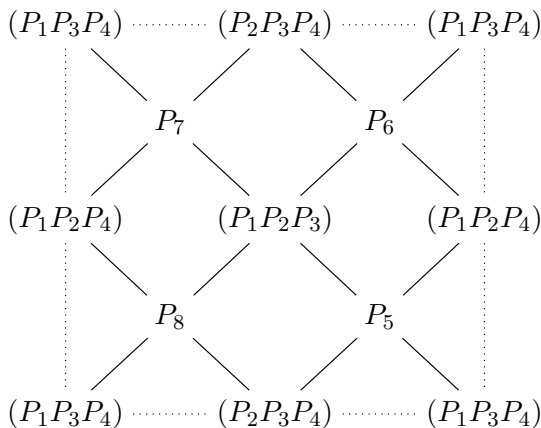


Figure 44: The tiling of the torus that yields the cube theorem. Opposite sides of the rectangular fundamental domain should be glued to each other. There are no edges between the vertices connected by dotted lines. The eight coplanarity conditions (5.1) are encoded by the eight tiles. For example, the tile at the center-top with the vertices P_7 , $(P_2P_3P_4)$, P_6 and $(P_1P_2P_3)$ encodes the coplanarity of the lines (P_6P_7) and $(P_2P_3P_4) \cap (P_1P_2P_3) = (P_2P_3)$, i.e., the coplanarity of the quadruple $\{P_2, P_3, P_6, P_7\}$.

THE OCTAHEDRON THEOREM

In the forthcoming treatment of 4D consistency (see Section 9), we will utilize a version of Theorem 5.5 known as the *octahedron theorem* (see, e.g., [40, Example 11] and references therein).

Theorem 5.6. *Let $f_{12}, f_{13}, f_{14}, f_{23}, f_{24}, f_{34}$ be six points in 3-space. Assume that the planes $(f_{12}f_{13}f_{14}), (f_{12}f_{23}f_{24}), (f_{13}f_{23}f_{34}), (f_{14}f_{24}f_{34})$ have a common point and the six given points are otherwise generic. Then the planes $(f_{12}f_{13}f_{23}), (f_{12}f_{14}f_{24}), (f_{13}f_{14}f_{34}), (f_{23}f_{24}f_{34})$ have a common point.*

Theorem 5.6 can be visually presented as follows, cf. Figure 45. Given an (irregular) octahedron in the real 3-space, color its eight faces in two colors, red and blue, so that adjacent faces are colored in different colors. Then the four red faces intersect at a point if and only if the four blue faces intersect at a point.

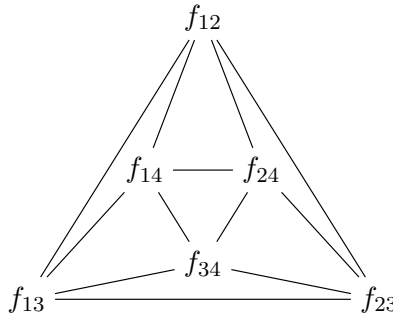


Figure 45: The octahedron theorem (Theorem 5.6).

Proof. The octahedron theorem is obtained from the cube theorem (Theorem 5.5) under the following change of notation:

$$\begin{aligned}
 P_1 &= (f_{12}f_{13}f_{14}) \cap (f_{12}f_{23}f_{24}) \cap (f_{13}f_{23}f_{34}) \cap (f_{14}f_{24}f_{34}), \\
 P_2 &= f_{12}, \\
 P_3 &= (f_{12}f_{13}f_{23}) \cap (f_{12}f_{14}f_{24}) \cap (f_{13}f_{14}f_{34}) \cap (f_{23}f_{24}f_{34}), \\
 P_4 &= f_{34}, \\
 P_5 &= f_{13}, \\
 P_6 &= f_{14}, \\
 P_7 &= f_{24}, \\
 P_8 &= f_{23}.
 \end{aligned}$$

To be a bit more precise, set $P_3 = (f_{12}f_{13}f_{23}) \cap (f_{12}f_{14}f_{24}) \cap (f_{13}f_{14}f_{34})$. Then all quadruples in (5.1) except for $\{P_3, P_4, P_7, P_8\}$ are coplanar, hence the latter quadruple is coplanar as well. \square

Remark 5.7. Cox’s first theorem [9, Exercise 2.28] is essentially a reformulation of the octahedron theorem.

THE SIXTEEN POINTS THEOREM

The sixteen points theorem is the following classical result in 3-dimensional projective geometry, see, e.g., [3, p. 46], [22, §4.2] or [46, Example 11].

Theorem 5.8 (The sixteen points theorem). *Let $a_1, a_2, a_3, a_4, b_1, b_2, b_3, b_4$ be a generic collection of eight lines in 3-space such that fifteen of the pairs (a_i, b_j) are coplanar. Then the remaining pair is also coplanar.*

Proof 1. Let the eight given lines be

$$\begin{aligned} a_1 &= (P_1Q_1), & a_2 &= (P_2Q_2), & a_3 &= (P_3Q_3), & a_4 &= (P_4Q_4), \\ b_1 &= (P_1R_1), & b_2 &= (P_2R_2), & b_3 &= (P_3R_3), & b_4 &= (P_4R_4). \end{aligned}$$

Then the four conditions $a_i \cap b_i \neq \emptyset$ are automatic, while the remaining 12 conditions $a_i \cap b_j \neq \emptyset$ ($i \neq j$) are encoded by the 12 tiles of the tiling of the torus shown in Figure 46. The claim follows. \square

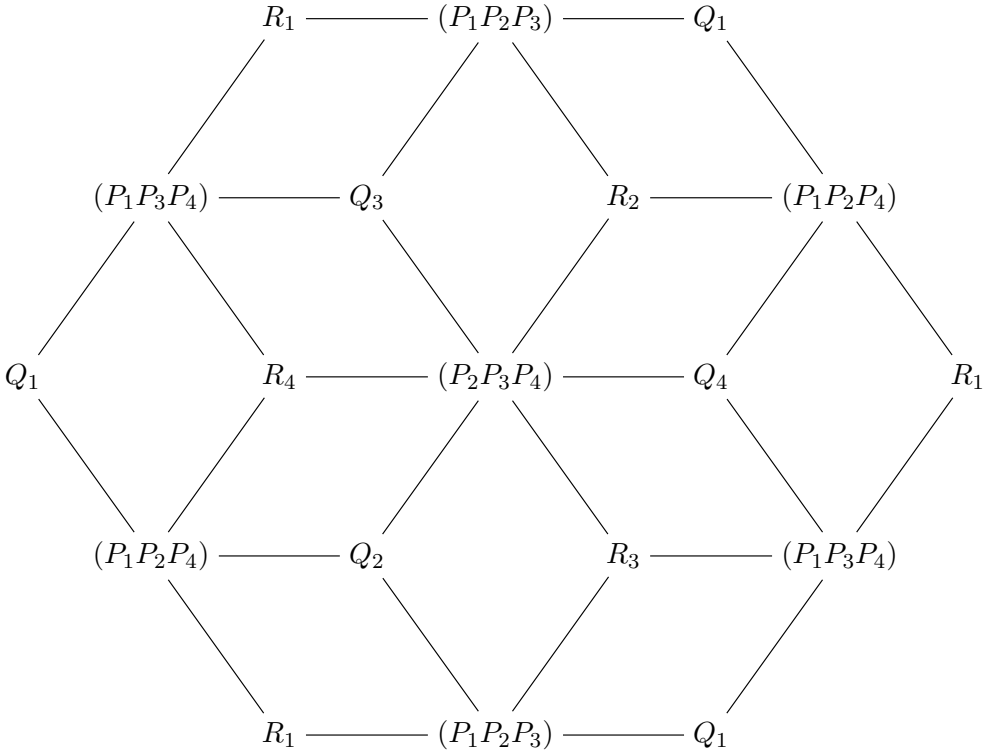


Figure 46: The tiling of the torus used in the proof of the sixteen points theorem. Opposite sides of the hexagonal fundamental domain should be glued to each other. The coherence of each tile can be interpreted as coplanarity of two lines a_i and b_j with $i \neq j$. For example, the tile at the center-top with the vertices $Q_3, (P_1P_2P_3), R_2,$ and $(P_2P_3P_4)$ encodes the coplanarity of the points P_2, P_3, Q_3, R_2 or, equivalently, the coplanarity of the lines $a_3 = (P_3Q_3)$ and $b_2 = (P_2R_2)$.

Proof 2. The sixteen points theorem can be viewed as the cube theorem in disguise, as we shall now explain. Assume that the pairs (a_i, b_j) , for $i, j \in \{1, 2\}$ are coplanar, as are the pairs (a_i, b_j) , for $i, j \in \{3, 4\}$. Denote

$$\begin{aligned} P_1 &= a_1 \cap b_2, & P_3 &= a_2 \cap b_1, & P_5 &= a_3 \cap b_4, & P_7 &= a_4 \cap b_3, \\ P_2 &= a_1 \cap b_1, & P_4 &= a_2 \cap b_2, & P_6 &= a_4 \cap b_4, & P_8 &= a_3 \cap b_3, \end{aligned}$$

so that

$$(5.2) \quad \begin{aligned} a_1 &= (P_1 P_2), & a_2 &= (P_3 P_4), & a_3 &= (P_5 P_8), & a_4 &= (P_6 P_7), \\ b_1 &= (P_2 P_3), & b_2 &= (P_1 P_4), & b_3 &= (P_7 P_8), & b_4 &= (P_5 P_6). \end{aligned}$$

Let us now express the sixteen coplanarity conditions in Theorem 5.8 in terms of the eight points $P_1, P_2, P_3, P_4, P_5, P_6, P_7, P_8$. Eight of these sixteen coplanarity conditions have already been assumed (and are automatic from (5.2)). The remaining eight conditions concern the coplanarity of the pairs of lines

$$\begin{aligned} (a_1, b_3), (a_1, b_4), (a_2, b_3), (a_2, b_4), \\ (a_3, b_1), (a_4, b_1), (a_3, b_2), (a_4, b_2), \end{aligned}$$

or equivalently the coplanarity of the quadruples of points

$$\begin{aligned} \{P_1, P_2, P_7, P_8\}, \{P_1, P_2, P_5, P_6\}, \{P_3, P_4, P_7, P_8\}, \{P_3, P_4, P_5, P_6\}, \\ \{P_2, P_3, P_5, P_8\}, \{P_2, P_3, P_6, P_7\}, \{P_1, P_4, P_5, P_8\}, \{P_1, P_4, P_6, P_7\}. \end{aligned}$$

Note that these are precisely the quadruples appearing in (5.1) (in different order). Thus, the statement that the coplanarity of seven of these eight quadruples implies the coplanarity of the remaining one is precisely Theorem 5.5. \square

Remark 5.9. The sixteen points theorem has the following interpretation rooted in classical Schubert Calculus. Consider three generic lines a_1, a_2, a_3 in $\mathbb{C}\mathbb{P}^3$. The lines b piercing each of a_1, a_2, a_3 form a one-parameter family, a ruling \mathcal{B} of a hyperboloid \mathbf{H} . The original lines a_1, a_2, a_3 belong to the other ruling of \mathbf{H} , which we denote by \mathcal{A} ; see, e.g., [30, Section 1]. Now consider a fourth line a_4 . If a_4 is also generic, then the one-parameter family \mathcal{B} contains precisely two lines b_1 and b_2 that pierce all four lines a_1, a_2, a_3, a_4 . Namely, locate the two intersection points of a_4 with the hyperboloid \mathbf{H} and take the lines in \mathcal{B} that pass through either of these two points. If, on the other hand, a_4 is not generic, so that there exist at least three lines $b_1, b_2, b_3 \in \mathcal{B}$ that pierce a_1, a_2, a_3, a_4 (as in the sixteen points theorem), then a_4 intersects \mathbf{H} in three points and therefore a_4 must lie on \mathbf{H} . More concretely, a_4 must belong to the same ruling \mathcal{A} of \mathbf{H} that contains a_1, a_2, a_3 . In that case, *any* line b_4 that pierces a_1, a_2, a_3 (that is, any line $b_4 \in \mathcal{B}$) also pierces a_4 , and we recover the assertion of the sixteen points theorem.

Put differently, we know from Schubert Calculus that given four generic lines a_1, a_2, a_3, a_4 , there exist exactly two lines b_1 and b_2 that pierce each of a_1, a_2, a_3, a_4 . (This classical fact is a special case of Lemma 11.3 below.) The sixteen points theorem says that if four lines a_1, a_2, a_3, a_4 can be pierced by three lines b_1, b_2, b_3 (thus a_1, a_2, a_3, a_4 are not generic), then there must exist infinitely many lines piercing a_1, a_2, a_3, a_4 , so that any line b_4 that pierces a_1, a_2, a_3 will pierce a_4 as well.

THE GLYNN CONFIGURATION

The following “sibling” of the Möbius configuration from Theorem 5.5 was discovered by D. G. Glynn [19, Section 4.1]:

Theorem 5.10. *Let P_1, \dots, P_8 be points in the 3-space such that none of the quadruples $\{P_i, P_j, P_k, P_\ell\}$ ($1 \leq i < j < k \leq 4 < \ell$) is coplanar. If seven of the eight quadruples*

$$(5.3) \quad \begin{aligned} & \{P_1, P_2, P_5, P_7\}, \{P_1, P_3, P_5, P_8\}, \{P_1, P_3, P_6, P_7\}, \{P_1, P_4, P_6, P_8\}, \\ & \{P_2, P_3, P_6, P_8\}, \{P_2, P_4, P_5, P_6\}, \{P_2, P_4, P_7, P_8\}, \{P_3, P_4, P_5, P_7\} \end{aligned}$$

are coplanar, then the remaining quadruple is also coplanar. See Figure 47.

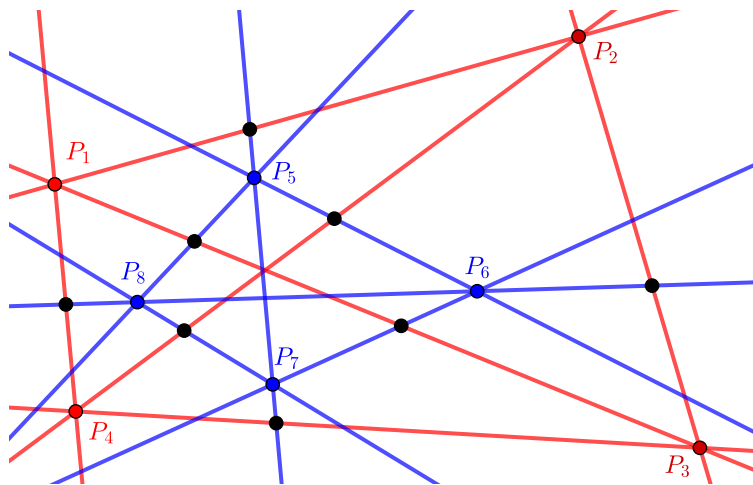


Figure 47: The Glynn configuration.

Proof. Apply the master theorem to the tiling of the torus shown in Figure 48. □

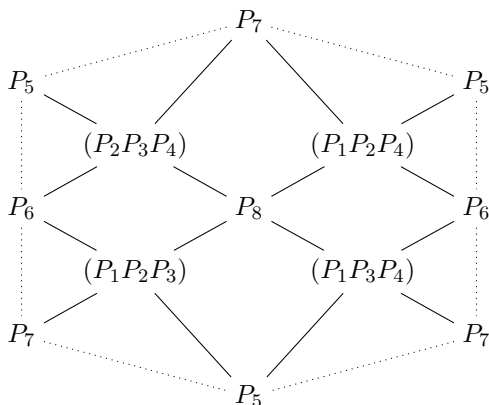


Figure 48: The tiling yielding Theorem 5.10. Opposite sides of the hexagonal fundamental domain should be glued to each other. There are no edges between P_5, P_6, P_7 .

TWO LINES PIERCING FIVE LINES

Theorem 5.11. *Let ℓ_1, ℓ_2 be a generic pair of lines and let m_1, m_2, m_3, m_4, m_5 be five lines each of which pierces both ℓ_1 and ℓ_2 . Pick a generic point P_1 on the line m_3 . Find $P_2 \in m_4$ such that (P_1P_2) pierces m_1 . Find $P_3 \in m_5$ such that (P_2P_3) pierces m_2 . Find $P_4 \in m_3$ such that (P_3P_4) pierces m_1 . Find $P_5 \in m_4$ such that (P_4P_5) pierces m_2 . Find $P_6 \in m_5$ such that (P_5P_6) pierces m_1 . Then (P_6P_1) pierces m_2 . See Figure 49.*

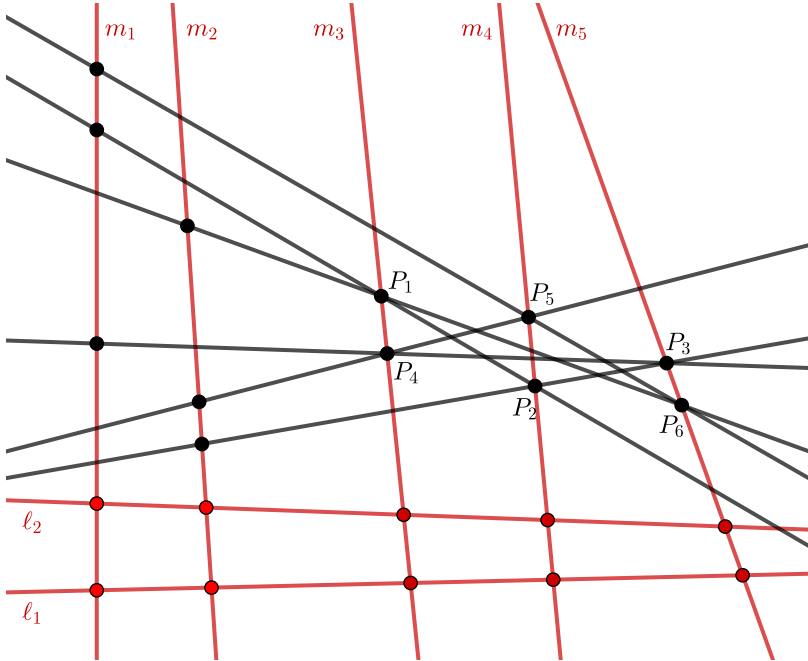


Figure 49: The 3-dimensional configuration in Theorem 5.11.

Proof. Let h_{ij} be the plane containing the lines ℓ_i and m_j , for $i, j \in \{1, 2\}$. Then

$$\begin{aligned} h_{11} \cap h_{12} &= \ell_1, & h_{21} \cap h_{22} &= \ell_2, \\ h_{11} \cap h_{21} &= m_1, & h_{12} \cap h_{22} &= m_2. \end{aligned}$$

Also, $(P_1P_4) = m_3$, $(P_2P_5) = m_4$, $(P_3P_6) = m_5$. It is then easy to check that the piercing conditions in the theorem are encoded by the tiles of the tiling shown in Figure 50. The claim follows by the master theorem. \square

Remark 5.12. As mentioned in Remark 5.9, four generic lines in 3-space can be pierced, in two different ways, by a fifth line. When *five* lines m_1, \dots, m_5 can be pierced in this way, they are in special position: as Theorem 5.11 shows, the existence of two piercing lines ℓ_1 and ℓ_2 forces the hexagon $P_1P_2P_3P_4P_5P_6$ inscribed in the triple of lines (m_3, m_4, m_5) to close up. Note that instead of (m_3, m_4, m_5) , we could have chosen any sub-triple of the 5-tuple (m_1, \dots, m_5) .

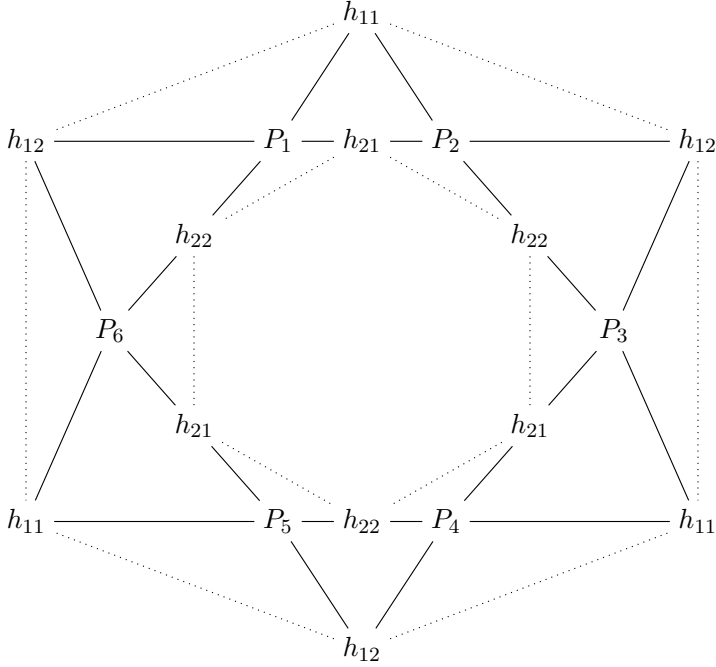


Figure 50: The tiling of the genus 2 surface used in the proof of Theorem 5.11. The opposite sides of each of the two dotted hexagons should be glued to each other.

THREE-DIMENSIONAL COUNTERPART OF THE PAPPUS THEOREM

Consider the tiling in Figure 9, which was used in the proof of the Pappus theorem. As before, let P_1, \dots, P_6 be points—but this time, let a, b, c be planes in 3-space. As a result, we obtain the following “three-dimensional Pappus theorem.”

Theorem 5.13. *Let P_1, \dots, P_6 be six generic points in 3-space. Take a generic line m_1 that pierces the lines (P_1P_2) , (P_3P_4) , (P_5P_6) . Find a line m_2 that pierces m_1 together with (P_2P_3) , (P_4P_5) , (P_6P_1) . Let $O = m_1 \cap m_2$. Then the line ℓ_1 that passes through O and pierces (P_1P_4) and (P_2P_5) will also pierce (P_3P_6) .*

Proof. Let a, b , and c be the planes spanned by the pairs of lines (m_2, ℓ_1) , (m_1, ℓ_1) , and (m_1, m_2) , respectively. The claim can now be obtained by applying the master theorem to the tiling in Figure 9. \square

Remark 5.14. Theorem 5.13 can be illustrated using Figure 49. Just remove line ℓ_2 and make the three lines m_1, m_2, ℓ_1 intersect at a point O .

Remark 5.15. As noted in Remark 5.9, the lines that pierce a given triple of generic lines $\{a_1, a_2, a_3\}$ form a ruling of a hyperboloid $\mathbf{H} = \mathbf{H}(a_1, a_2, a_3)$. With this notation, line m_1 in Theorem 5.13 lies on the hyperboloid $\mathbf{H}_1 = \mathbf{H}((P_1P_2), (P_3P_4), (P_5P_6))$. Similarly, line m_2 lies on $\mathbf{H}_2 = \mathbf{H}((P_2P_3), (P_4P_5), (P_6P_1))$. Theorem 5.13 says that any point $O \in \mathbf{H}_1 \cap \mathbf{H}_2$ lies on $\mathbf{H}_3 = \mathbf{H}((P_1P_4), (P_2P_5), (P_3P_6))$. Thus, the intersection $\mathbf{H}_1 \cap \mathbf{H}_2 \cap \mathbf{H}_3$ is 1-dimensional rather than 0-dimensional, as one would expect.

INCIDENCE THEOREMS IN CHANGING DIMENSIONS

Remark 5.16. For a given a bicolored quadrilateral tiling \mathbf{T} , our master theorem (Theorem 2.6) yields an incidence theorem associated to \mathbf{T} , for an arbitrary choice of dimension $d = \dim \mathbb{P} \geq 2$ of the ambient real/complex projective space \mathbb{P} . It is then natural to wonder: what happens to the resulting incidence theorem as d varies? Thus far, we have seen two examples of this kind:

- the tiling in Figures 5 and 42 (the surface of a cube) yields the Desargues theorem (Theorem 3.1) for $d = 2$ and the bundle theorem (Theorem 5.1) for $d = 3$;
- the tiling in Figure 9 yields the Pappus theorem (Theorem 3.2) for $d = 2$ and Theorem 5.13 for $d = 3$.

Speaking in general, we have not observed a transparent direct relationship between the 2-dimensional and 3-dimensional statements coming from the same tiling, short of their common generalization in the form of Theorem 2.6.

In most cases, an incidence theorem becomes simpler (and sometimes trivial) when the ambient dimension d decreases. One notable exception to this rule is Desargues' theorem, which is ostensibly more substantial than its 3-dimensional counterpart.

There are many examples where a tiling yields a trivial incidence theorem for $d = 2$ but not for $d = 3$. We next discuss one common mechanism behind such occurrences.

Lemma 5.17. *Let Q_1, Q_2, Q_3, Q_4 be four distinct points on the real/complex projective plane and let $\ell_1, \ell_2, \ell_3, \ell_4$ be four distinct lines. Suppose that the tiles*

$$(5.4) \quad \begin{array}{cccc} Q_1 - \ell_1 & Q_1 - \ell_3 & Q_3 - \ell_1 & Q_3 - \ell_3 \\ | & | & | & | \\ \ell_2 - Q_2 & \ell_4 - Q_2 & \ell_2 - Q_4 & \ell_4 - Q_4 \end{array}$$

are coherent. Then one of the following two statements holds:

- (i) the six lines $\ell_1, \ell_2, \ell_3, \ell_4, (Q_1Q_2), (Q_3Q_4)$ are concurrent;
- (ii) the six points $Q_1, Q_2, Q_3, Q_4, \ell_1 \cap \ell_2, \ell_3 \cap \ell_4$ are collinear.

Proof. The coherence of the tiles (5.4) means that each of the points $\ell_1 \cap \ell_2$ and $\ell_3 \cap \ell_4$ lies on each of the lines (Q_1Q_2) and (Q_3Q_4) . If the latter two lines are distinct, then their intersection must coincide with both $\ell_1 \cap \ell_2$ and $\ell_3 \cap \ell_4$, yielding (i). Otherwise, the points Q_1, Q_2, Q_3, Q_4 lie on the same line that moreover contains $\ell_1 \cap \ell_2$ and $\ell_3 \cap \ell_4$, yielding (ii). \square

Lemma 5.17 shows that whenever a tiling contains four tiles as in (5.4), the $d=2$ case of the corresponding incidence theorem involves a rather degenerate point-and-line configuration that includes either six concurrent lines or six collinear points. As a result, the final statement may end up collapsing to a trivial one.

Example 5.18. Figure 44 contains two instances of Lemma 5.17. Because of that, the 2-dimensional counterpart of the Möbius theorem (Theorem 5.5) turns out to be trivial. For another example of a similar kind, see Theorem 5.11/Figure 50.

Remark 5.19. In Section 2 (see Examples 2.9–2.12), we discussed several situations wherein an incidence theorem associated with a given tiling is trivial regardless of dimension. The phenomena discussed in Example 5.18 are more subtle than those.

6. COMBINATORIAL REFORMULATIONS OF THE MASTER THEOREM

Fix a finite-dimensional real/complex projective space \mathbb{P} . For any bicolored quadrilateral tiling of an oriented closed surface Σ (of arbitrary genus), Theorem 2.6 yields an incidence theorem in \mathbb{P} . In this section, we discuss a couple of alternative ways to describe such tilings. In each case, we obtain reformulations of the master theorem (or its individual instances) in a new combinatorial language.

GRAPHS EMBEDDED INTO SURFACES

Definition 6.1. Consider a tiling \mathbf{T} of an oriented closed surface Σ by quadrilateral tiles. (Each pair of tiles are either disjoint, or share a side, or share a vertex.) Assume that the vertices of the tiling are colored black and white, so that each edge connects vertices of different color. Construct a graph $\mathbf{G} = \mathbf{G}(\mathbf{T})$ embedded in Σ as follows. The vertices of \mathbf{G} are the white vertices of the tiling \mathbf{T} . Each tile in \mathbf{T} gives rise to an edge in \mathbf{G} that connects the two white vertices of the tile.

We note that the *faces* of \mathbf{G} (i.e., connected components of the complement of \mathbf{G} inside Σ) correspond to the black vertices of the tiling.

A couple of examples of the above construction are given in Figure 51.

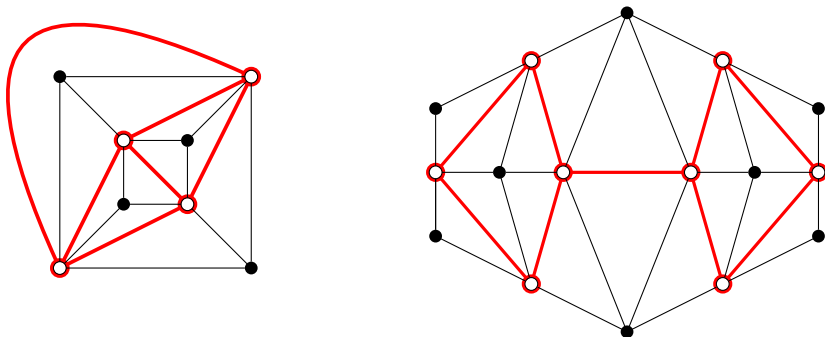


Figure 51: The correspondence $\mathbf{T} \mapsto \mathbf{G} = \mathbf{G}(\mathbf{T})$ for the tilings from Figure 1, cf. also Figures 5 and 13. On the right, the opposite sides of the hexagonal fundamental domain should be glued to each other, producing a graph \mathbf{G} embedded in the torus. This graph has 5 vertices (corresponding to the hyperplanes b, r, s, q, t in Figure 13), 9 edges (shown in the figure above) and 4 faces (2 pentagons and 2 quadrilaterals).

Proposition 6.2. *The map $\mathbf{T} \mapsto \mathbf{G}$ described in Definition 6.1 is a bijection between*

- *bicolored quadrilateral tilings \mathbf{T} of a Riemann surface Σ (viewed up to isotopy of the surface Σ) and*
- *graphs \mathbf{G} embedded in Σ (and viewed up to isotopy of Σ) in which every vertex has degree ≥ 2 , every face has ≥ 2 sides, and each face is homeomorphic to a disk.*

Proof. The properties of \mathbf{G} listed above are readily checked for any graph $\mathbf{G}(\mathbf{T})$ obtained from a triangulation \mathbf{T} . Conversely, given such an embedded graph \mathbf{G} , we can recover the corresponding triangulation \mathbf{T} by placing a black vertex inside each face of \mathbf{G} and connecting each of these black vertices, inside the corresponding face, to the (white) vertices of \mathbf{G} lying on the boundary of that face. \square

Remark 6.3. Interchanging the black and white colors in a triangulation \mathbf{T} results in replacing the embedded graph $\mathbf{G}(\mathbf{T})$ by its (Poincaré) dual graph. The corresponding incidence theorems are projectively dual to each other.

Remark 6.4. Graphs embedded into surfaces so that every face is a topological disk are sometimes called (topological) *maps* (on surfaces); see, e.g., [29, Section 1.3.2].

Remark 6.5. The above correspondence becomes especially transparent when the surface Σ is a sphere while the graph \mathbf{G} comes from the 1-skeleton of a convex 3-dimensional polytope \mathbf{P} (whose boundary can be identified with the sphere Σ). Thus, every 3-dimensional polytope \mathbf{P} gives rise to an incidence theorem. Dual polytopes produce projectively dual theorems (which we view as equivalent). Several specific instances of this construction are listed in Figure 52.

Desargues theorem, the bundle theorem	tetrahedron
complete quadrilateral theorem	triangular prism
Theorem 3.8	square pyramid
Saam's sequence of perspectivities	square antiprism

Figure 52: Incidence theorems coming from 3-dimensional convex polytopes. Each polytope can be replaced by its dual.

Remark 6.6. Denote $d = \dim \mathbb{P}$. In the special case when the number of vertices in the graph \mathbf{G} (equivalently, the number of white vertices in the corresponding tiling \mathbf{T}) is equal to $d + 1$, we recover the ingenious construction of D. G. Glynn [17]. Let us explain.

Let \mathbf{G} be a graph embedded into a closed oriented surface as in Proposition 6.2, with vertex set V of cardinality $d + 1$ and a set of faces F of arbitrary cardinality. Associate with each vertex $v \in V$ (resp., a face $f \in F$) a point P_v (resp., P_f). For each $v \in V$, let $h_v \subset \mathbb{P}$ be the hyperplane spanned by the set $\{P_u \mid u \in V, u \neq v\}$. We thus obtain a labeling of the vertices v (resp., faces f) of \mathbf{G} by the hyperplanes h_v (resp., points P_f). Equivalently, we get a labeling of the white (resp., black) vertices of the corresponding tiling \mathbf{T} by hyperplanes (resp., points) in \mathbb{P} . The corresponding instance of our master theorem is a restatement of the main result of [17].

A particularly nice feature of the special case $|V| = d + 1$ treated in [17] is that the resulting incidence theorems are immediately stated in “matroidal” terms, i.e., in terms of a finite collection of points in \mathbb{P} and dependency relations among them. It is also shown in [17] that in the genus 0 case (i.e., when Σ is a sphere), the ensuing incidence theorems hold over arbitrary skew fields (such as the quaternions).

On the other hand, the restriction $|V| = d + 1$ substantially limits the range of potential applications. For example, in the case of the projective plane ($d = 2$), this restriction would limit us to tilings with three white (or three black) vertices. It appears that most incidence theorems discussed in this paper cannot be directly obtained from such tilings.

NODAL CURVES ON A SURFACE

We next discuss, somewhat informally, another “cryptomorphic” version of the combinatorial construction underlying our master theorem.

Definition 6.7. Given a tiling \mathbf{T} of a surface Σ , construct a nodal curve $\mathbf{C} = \mathbf{C}(\mathbf{T})$ on Σ as follows. Choose a “midpoint” inside each edge of the tiling. For each tile, connect both pairs of opposite midpoints to each other. If you like, smoothen the resulting curve. (Everything is viewed up to isotopy.) Examples related to Desargues, Pappus, and permutation theorems are shown in Figures 53–54.

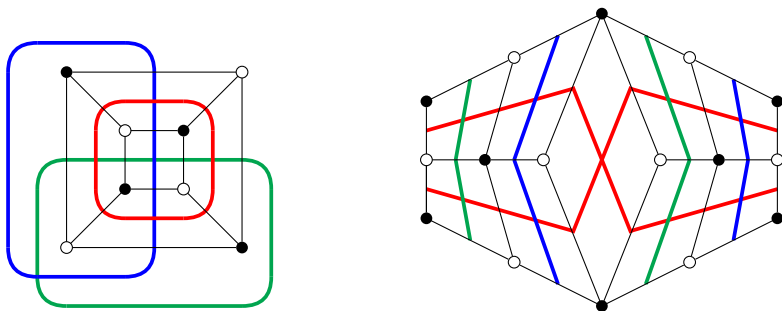


Figure 53: Nodal curves corresponding to the tilings in Figure 1 (or Figures 5 and 13). Each component of a nodal curve is shown in different color.

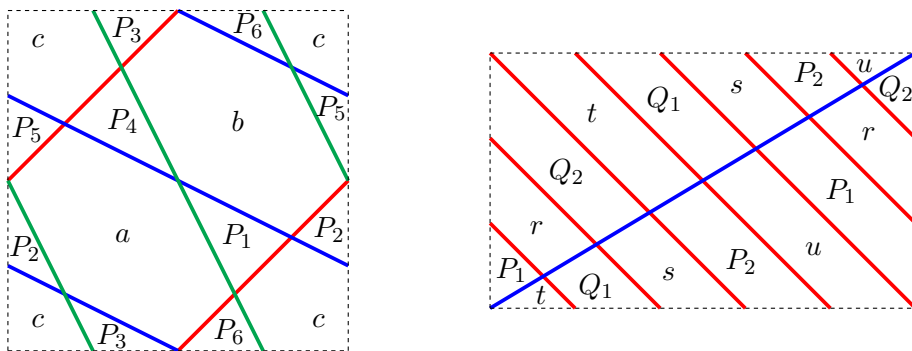


Figure 54: Nodal curves on the torus corresponding to the tilings in Figures 9 and 22. Region labels match the vertex labels of the tiling.

Remark 6.8. Let \mathbf{T} be a bicolored quadrilateral tiling of a surface Σ . Let $\mathbf{C} = \mathbf{C}(\mathbf{T})$ be the associated curve on Σ . A *region* of \mathbf{C} is a connected component of the complement $\Sigma - \mathbf{C}$. We then have:

- every region of \mathbf{C} is homeomorphic to a disk;
- every region of \mathbf{C} is not a monogon (i.e., has at least two nodes on its boundary);
- each region is colored black or white, so that adjacent regions have different colors.

To recover the tiling from a nodal curve \mathbf{C} satisfying these conditions, place a black (resp., white) vertex inside each black (resp., white) region and connect these vertices across curve segments separating neighboring regions.

7. DEDUCING INCIDENCE THEOREMS FROM EACH OTHER

The study of logical dependencies among various incidence theorems has been an important research direction within incidence geometry since its inception in ancient Greece. Some of these dependencies can be naturally interpreted in terms of associated tilings. In this section, we discuss several settings in which this phenomenon occurs.

We begin by examining several combinatorial constructions that yield material equivalences between incidence theorems, i.e., instances where two incidence theorems are equivalent to each other, for some transparent reason.

PROJECTIVE DUALITY

Projective duality between points and hyperplanes implies that each incidence theorem has a dual counterpart in which the points of the original theorem are replaced by hyperplanes, and vice versa. This is readily seen at the level of tilings: simply swap the black and white colors of the vertices to get a tiling for the dual theorem.

To illustrate, dualizing Proposition 4.6 yields the following statement.

Proposition 7.1. *Let p_1, p_2, p_3, p_4 be four generic lines on the plane. Suppose that*

- (a) *A is a generic point on the line passing through $p_1 \cap p_2$ and $p_3 \cap p_4$;*
- (b) *B is a generic point on the line passing through $p_1 \cap p_4$ and $p_2 \cap p_3$.*

Then

- (c) *the octagon with vertex labels $p_1, A, p_2, B, p_3, A, p_4, B$ (see Figure 55) is coherent.*
- Conversely, (a) and (c) imply (b).*

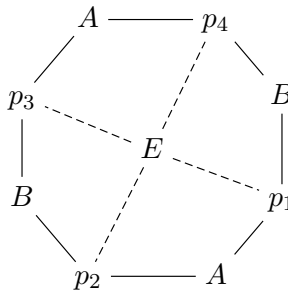


Figure 55: The octagon from Proposition 7.1 and its tiling.

Dualizing the second proof of Theorem 3.2 (cf. Figure 13), we obtain the following version of the Pappus theorem.

Theorem 7.2 (Pappus). *Let Q, S, R, T be four points on the real/complex plane and let d, e, p_4, p_5 be four lines. Consider the six tiles appearing in Figure 56 (including the octagonal tile in the middle). If five of these six tiles are coherent, then the remaining tile is coherent as well. Cf. Figure 57.*

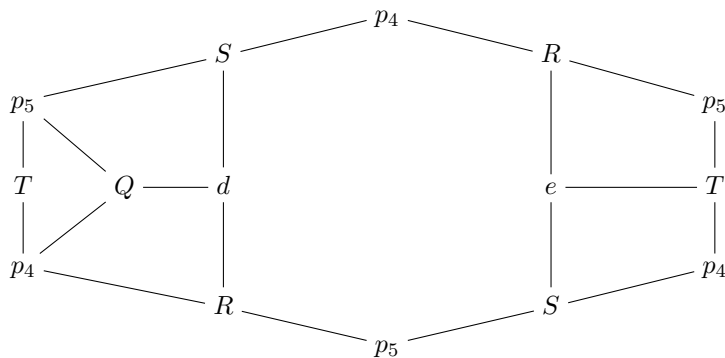


Figure 56: The tiling of the torus for the dual version of the Pappus theorem. Opposite sides of the shown hexagonal fundamental domain should be glued to each other.

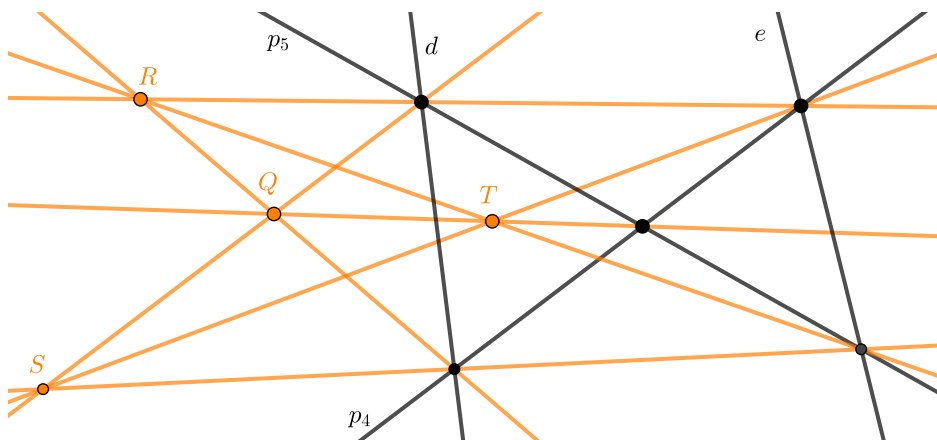


Figure 57: The dual version of the Pappus theorem.

LOCAL MOVES ON TILINGS

We next discuss several types of *local moves* (that is, local transformations of tilings of an oriented surface) that translate into equivalences between the corresponding incidence theorems.

Definition 7.3 (*Fusion of adjacent tiles*). Suppose that a tiling \mathbf{T} of an oriented surface by quadrilateral tiles contains a vertex v of degree 2. Remove v together with the two edges incident to it to obtain a new tiling \mathbf{T}' in which the two tiles surrounding v have been *fused* into a single quadrilateral tile. It is not hard to see that the incidence theorems associated to \mathbf{T} and \mathbf{T}' are closely related; in fact, each of them immediately implies the other. See Figure 58.

The removal of v from \mathbf{T} can potentially produce a tiling \mathbf{T}' that contains a “self-folded” quadrilateral tile in which two adjacent sides have been glued to each other, cf. the bottom row of Figure 58. Although thus far in the paper, we did not allow such tiles, they may appear as a result of fusion moves. This is not going to create problems since self-folded tiles can be easily eliminated, see Definition 7.4 below.

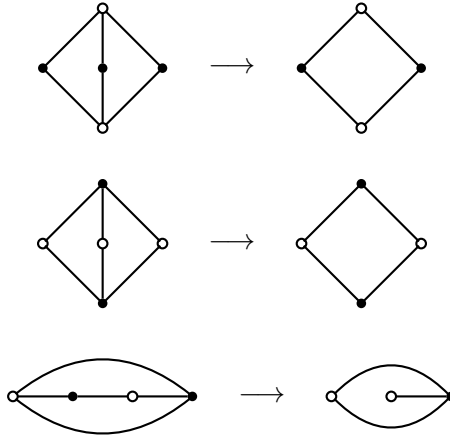


Figure 58: Fusion of tiles.

Definition 7.4 (*Getting rid of self-folded tiles*). For a self-folded tile, the coherence condition is always vacuous. Consequently, such tiles can be removed (collapsed), as shown in Figure 59, without affecting the content of the associated incidence theorem.

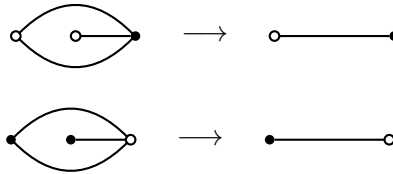


Figure 59: Removal of self-folded tiles.

Definition 7.5 (*Desargues moves*). The most interesting type of local move is a *Desargues move* shown in Figure 60, corresponds to applying the Desargues theorem, see Corollary 4.4. If two tilings differ by a Desargues move, then the corresponding incidence theorems can be obtained from each other via a single application of Desargues' theorem.

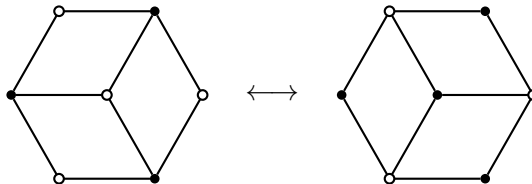


Figure 60: A Desargues move shown above can be performed left-to-right or right-to-left. The six vertices of the ambient hexagon do not have to be distinct.

Problem 7.6. If two tilings can be obtained from each other by a sequence of local moves described in Definitions 7.3–7.5 (see Figures 58–60), then the corresponding incidence theorems are equivalent modulo Desargues' theorem. Therefore it would be interesting to effectively describe the equivalence classes of tilings with respect to these local moves.

LOCAL MOVES ON NODAL CURVES

Remark 7.7. The construction described in Definition 6.7 associates a nodal curve to a tiled surface, and vice versa (cf. Remark 6.8). Accordingly, the local moves discussed above can be translated into the language of curves on a surface. To be specific, local moves on tilings shown in Figures 58–60 correspond, under the construction from Definition 6.7, to local moves on nodal curves that are shown in Figure 61. In particular, the *braid move* in the bottom row of Figure 61 corresponds to a Desargues move from Definition 7.5/Figure 60. Note that a braid move may create a monogon even if the original curve did not have such regions, see Figure 62.

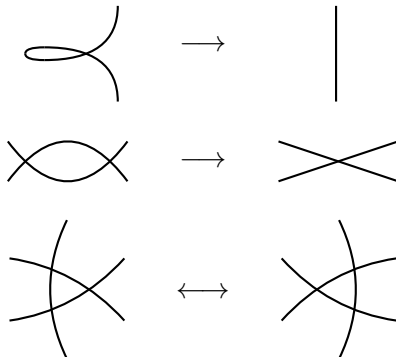


Figure 61: Local moves on nodal curves. The moves in the top and bottom rows are similar to Reidemeister moves of types I and III, respectively. The move in the middle (which corresponds to fusion moves on tilings, see Definition 7.3/Figure 58) is however different from Reidemeister II.

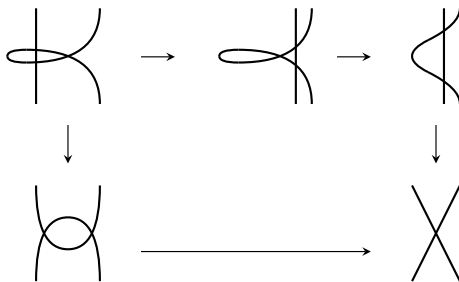


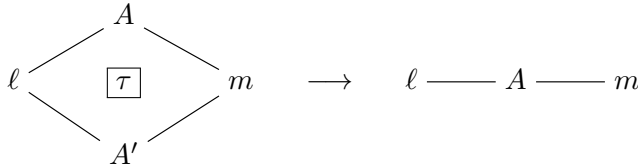
Figure 62: The phenomenon of confluence of local moves on nodal curves.

Problem 7.8. Reformulating Problem 7.6, it would be interesting to classify the equivalence classes of nodal curves on closed oriented surfaces with respect to the local moves in Figure 61. As in Remark 6.8, we assume that each region (a connected component of the complement of a curve) is homeomorphic to a disk and that these regions are properly colored in two colors. It is natural to ask whether all such curves within a given move-equivalence class that have the smallest number of nodes are braid-equivalent to each other, cf. Figure 62. (Incidence theorems associated with curves that differ by a braid move are equivalent modulo Desargues' theorem.)

COLLAPSE AND INSERTION OF TILES

We next discuss several combinatorial transformations of tiled surfaces that yield logical implications between incidence theorems, that is, instances where one such theorem directly follows from some other theorem(s). The simplest, yet nontrivial, example of such combinatorial transformations involves a single tile:

Definition 7.9. Let \mathbf{T} be a bicolored quadrilateral tiling of an oriented surface Σ . Pick a tile τ in \mathbf{T} and construct a new tiling \mathbf{T}' by removing the interior of τ and gluing its four edges in pairs, as shown below:



We say that the resulting tiling \mathbf{T}' is obtained from \mathbf{T} by *collapsing* the tile τ . Going in the opposite direction, we say that \mathbf{T} is obtained from \mathbf{T}' by *inserting* the tile τ into the length-2 path $l - A - m$ in \mathbf{T}' .

The incidence theorem associated with \mathbf{T}' is obtained from the one associated with \mathbf{T} by making the additional assumption $A = A'$.

Tile insertion can be used to produce nontrivial generalizations of existing incidence theorems. Several examples illustrating this technique are given below.

Example 7.10. Recall that the permutation theorem (Theorem 3.11) can be obtained from the tiling in Figure 22. Insert two tiles into the latter tiling to obtain the tiling shown in Figure 63. The latter tiling yields a generalization of the permutation theorem stated below in Theorem 7.11.

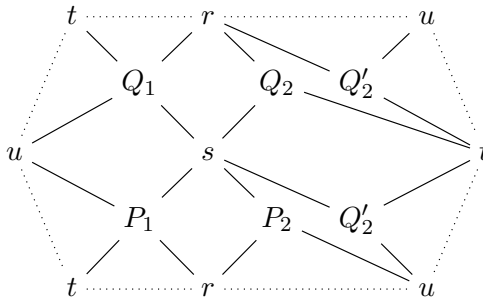


Figure 63: The tiling of the torus obtained by inserting two tiles into the tiling in Figure 22.

Theorem 7.11. Let P_1, Q_1, R_1, S_1 be four distinct collinear points in the real/complex projective plane. Let R_2, S_2 be two generic points in the plane. Define $r = (R_1R_2)$, $s = (S_1S_2)$, $t = (R_1S_2)$, $u = (R_2S_1)$, $A = r \cap s$, $B = t \cap u$. Pick a point $P_2 \in (AP_1)$. Set $P'_2 = (S_1P_2) \cap (BQ_1)$, $Q_2 = (S_2P'_2) \cap (AQ_1)$, $Q'_2 = (R_1Q_2) \cap (BP_1)$. Then the points Q'_2, P_2, R_2 are collinear. See Figure 64.

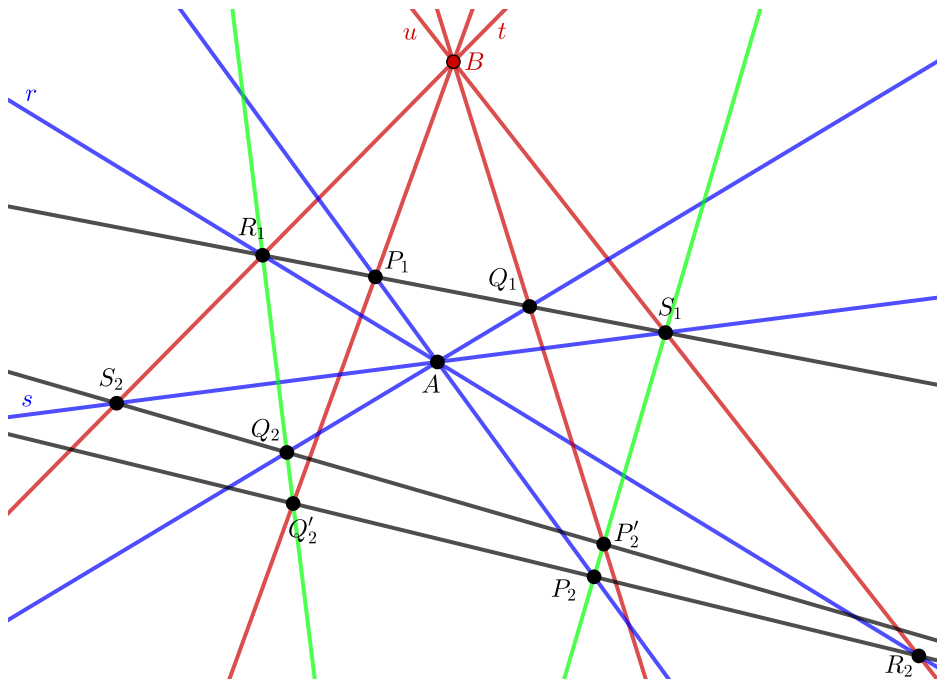


Figure 64: Generalization of the permutation theorem.

Remark 7.12. Theorem 7.11 has a basic property that the original permutation theorem (Theorem 3.11) lacks: configurations appearing in Theorem 7.11 can be constructed, step by step, using a straightedge alone. By contrast, Theorem 3.11 assumes a certain condition (*viz.*, that three of the four lines (P_1Q_2) , (R_1S_2) , (R_2S_1) , (P_2Q_1) are concurrent) that cannot be guaranteed by a straightedge-only construction.

Example 7.13. A further generalization of the permutation theorem can be obtained by inserting two additional tiles into the tiling in Figure 63 (thus, inserting four tiles into the tiling in Figure 22), as shown in Figure 65. The resulting generalization of the permutation theorem is illustrated in Figure 66. We omit a formal statement of this generalization, which can be recovered from the figure.

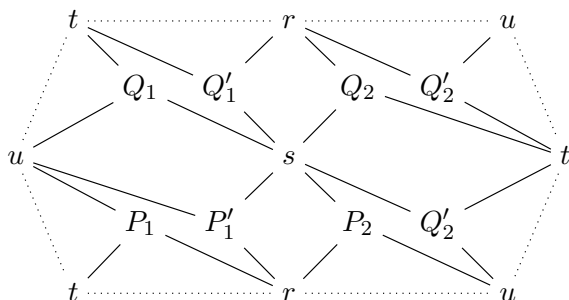


Figure 65: The tiling of the torus obtained by inserting four tiles into the tiling in Figure 22.

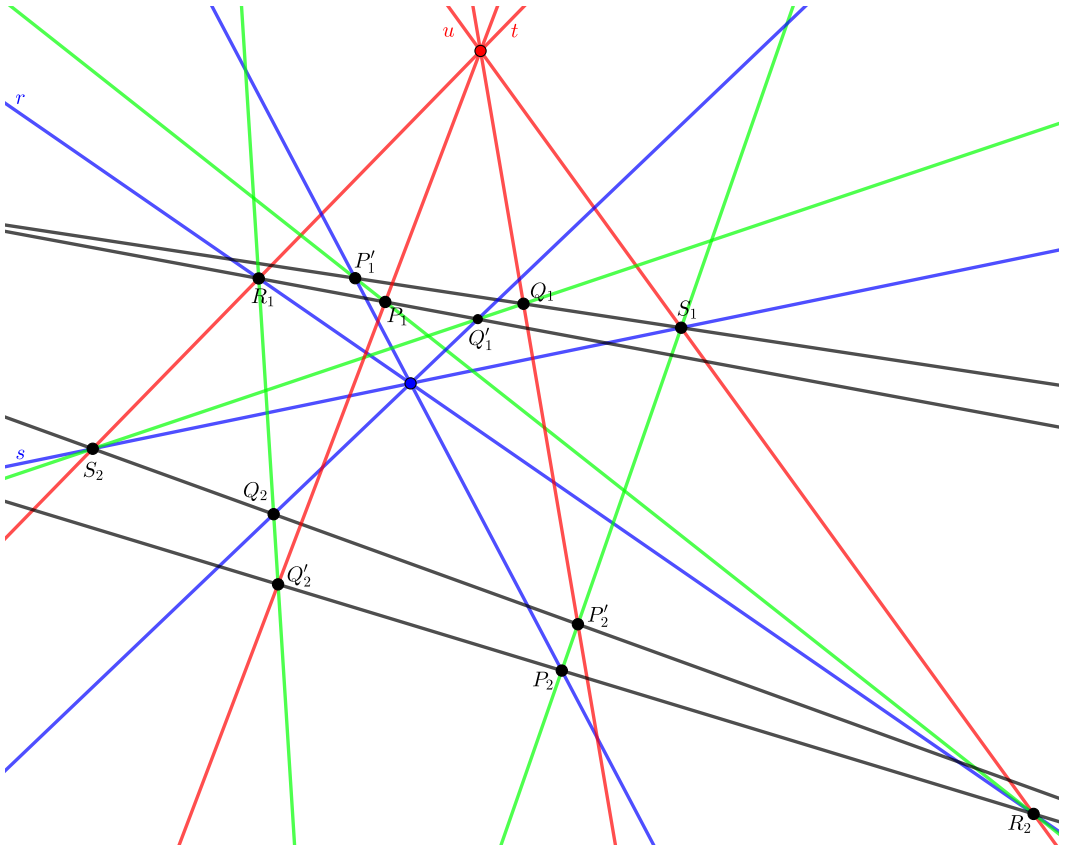


Figure 66: Further generalization of the permutation theorem.

Example 7.14. Recall that the Pappus theorem can be obtained from the tiling in Figure 9. Insert a tile in the middle of the latter tiling to obtain the tiling shown in Figure 67. The latter tiling yields a generalization of the Pappus theorem stated below in Theorem 7.15.

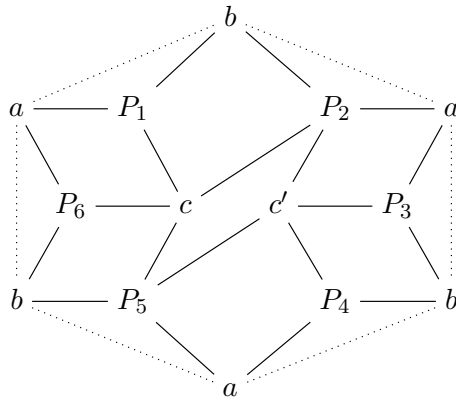


Figure 67: The tiling of the torus obtained by inserting a tile into the tiling in Figure 9.

Theorem 7.15. Consider three distinct lines (P_1P_4) , (P_2P_5) , (P_3P_6) on the real or complex plane that intersect at a common point C . (The points P_i are generically chosen on the corresponding lines.) Set $A = (P_1P_2) \cap (P_5P_6)$, $B = (P_2P_3) \cap (P_4P_5)$, $A' = (AC) \cap (P_3P_4)$, $B' = (BC) \cap (P_1P_6)$. Then the lines (AB') , $(A'B)$, (P_2P_5) are concurrent. See Figure 68.

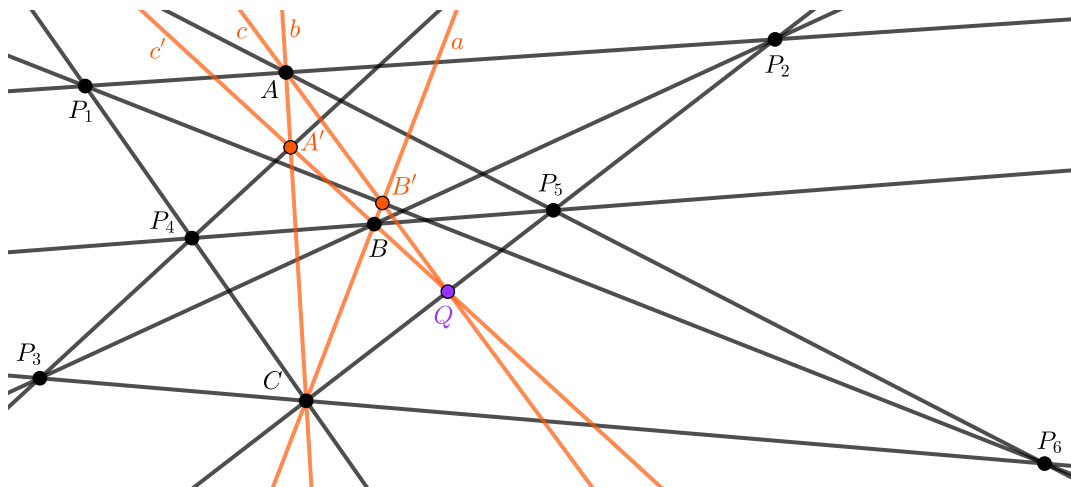


Figure 68: Generalization of the Pappus theorem.

Example 7.16. A further generalization of the Pappus theorem can be obtained by inserting two additional tiles into the tiling in Figure 67 (thus, inserting three tiles into the tiling in Figure 9), as shown in Figure 69. The resulting generalization of the Pappus theorem is illustrated in Figure 70. We omit a formal statement of this generalization, which can be recovered from the figure.

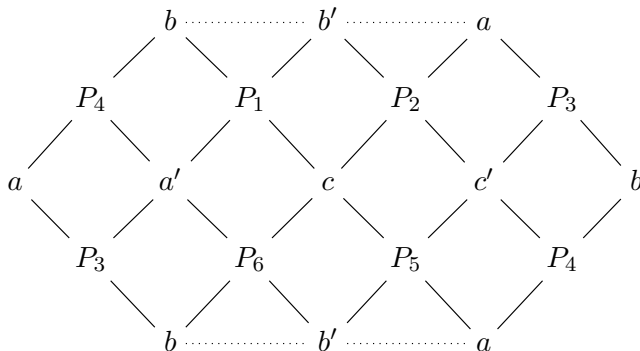


Figure 69: The tiling of the torus obtained by inserting three tiles into the tiling in Figure 9.

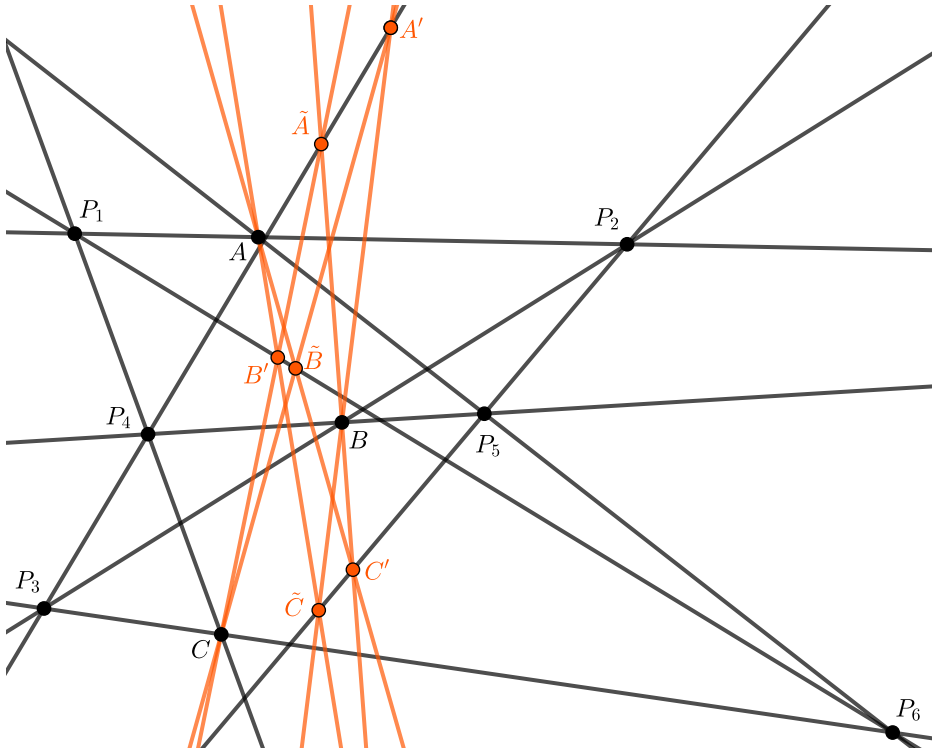


Figure 70: Further generalization of the Pappus theorem.

Remark 7.17. The tile insertion construction of Definition 7.9 can be used to “lift” an arbitrary bicolored quadrilateral tiling \mathbf{T} of an oriented surface Σ to a tiling \mathbf{T}' of Σ in which every black vertex is trivalent, see Figure 71. (If \mathbf{T} contains bivalent vertices, remove them first, as explained in Definition 7.3.) Translating this into the language of graphs properly embedded into the surface (see Definition 6.1), we conclude that each face of the graph $\mathbf{G}(\mathbf{T}')$ is a triangle, i.e., $\mathbf{G}(\mathbf{T}')$ describes a *triangulation* of the surface Σ . Thus, any incidence theorem associated to a tiled surface can be generalized to an incidence theorem associated to a triangulated surface. We will make the latter statement explicit in Corollary 8.3, cf. also Remark 8.6.

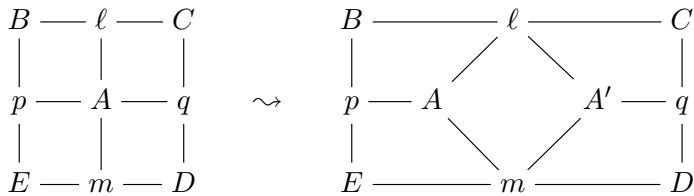


Figure 71: Splitting a four-valent vertex A into two, by inserting a tile. Iterating this operation, we can get rid of all black vertices of degree ≥ 4 . Indeed, a black vertex of degree $d \geq 4$ can be split into two black vertices of degrees 3 and $d - 1$, respectively.

COLLAPSING AROUND A FOUR-VALENT VERTEX

Remark 7.18. Another situation in which assigning identical labels to different vertices of a tiling gives rise to a “collapsing” transformation is shown in Figure 72. Let \mathbf{T} be a tiling that contains a vertex A of degree 4, as shown in Figure 72 on the left. Removing the four tiles surrounding A from \mathbf{T} and replacing them by the two tiles shown in Figure 72 on the right produces a tiling \mathbf{T}' . We claim that the incidence theorem associated with \mathbf{T}' is immediate from the incidence theorem associated with \mathbf{T} , and moreover this implication does not rely on the master theorem. Suppose that all tiles in \mathbf{T}' , with the exception of one tile τ , are known to be coherent. There are two possible cases, depending on whether τ is one of the two tiles shown in Figure 72 on the right, or not. In each case, the claim follows from the special case $p = p'$ of the incidence theorem associated with \mathbf{T} by setting $A = (BC) \cap (DE)$.

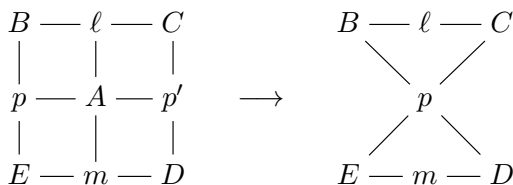


Figure 72: Tile collapse around a four-valent vertex.

Example 7.19. Both the complete quad theorem (Theorem 3.3) and its generalization given in Theorem 3.4 can be deduced from Desargues’ theorem, as follows. Consider the tiling in Figure 73, which can be viewed as invoking Desargues’ theorem twice (cf. Remark 7.20 below). Apply the collapsing transformation from Remark 7.18 around vertex ℓ to obtain the tiling in Figure 15, which was used to establish Theorem 3.4.

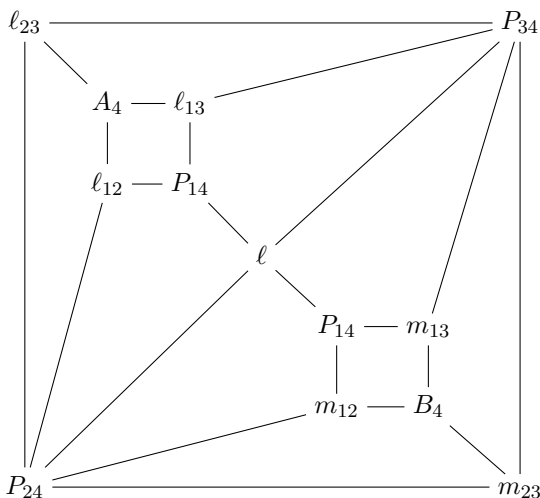


Figure 73: Deducing the complete quad theorem from the Desargues theorem.

GLUING OF TILINGS

Remark 7.20 (*Gluing of tilings*). Given a pair of tilings of closed surfaces, we can get a new tiling by gluing the given tilings along disks. The theorems associated to the two original tilings will accordingly imply the theorem associated to the third.

The simplest version of this procedure glues two tilings along an arbitrary pair of quadrilateral tiles (one in each tiling). To give an example, start with a tiling of the sphere into three tiles, see (2.9), and glue in two cubes (each corresponding to an instance of Desargues' theorem) to obtain the tiling in Figure 73.

A bit more complicated version of gluing involves locating, in each of the two input tilings, a hexagon tiled by three tiles. We can then glue the two tilings along these hexagons, potentially using Corollary 4.4 (Desargues' theorem) in between. A further generalization of this construction involves gluing along $2n$ -gons bounding a disk.

PAPPUS IMPLIES DESARGUES

It is well known that Pappus' theorem implies Desargues'; the first proof of this fact was given by G. Hessenberg [21]. It was later discovered that his proof had gaps. In particular, it only established a "generic" version of the statement (which is sufficient for our purposes). For the history of this result and its proofs, see [42, 52]. As pointed out in [42], all known arguments require (at least) three applications of Pappus to get Desargues.

We next provide a tiling-based proof of Hessenberg's theorem. It is inspired by A. Seidenberg's presentation in [53, pp. 92–94]. We will invoke, three times in a row, the version of the Pappus theorem given in Theorem 7.2/Figures 56–57. As a result, we will obtain Desargues' theorem, in the formulation given in Theorem 3.1.

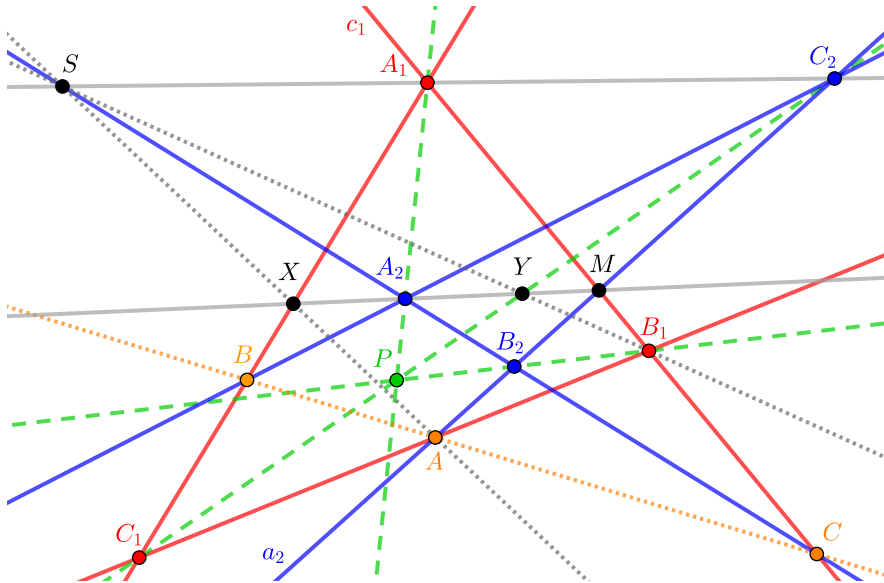


Figure 74: Pappus implies Desargues: the points-and-lines configuration.

We refer the reader to Figure 74. Let $A_1B_1C_1$ and $A_2B_2C_2$ be triangles perspective from a point P . As before (cf. Theorem 3.1 and (3.1)–(3.2)), denote

$$a_i = (B_iC_i), \quad b_i = (A_iC_i), \quad c_i = (A_iB_i),$$

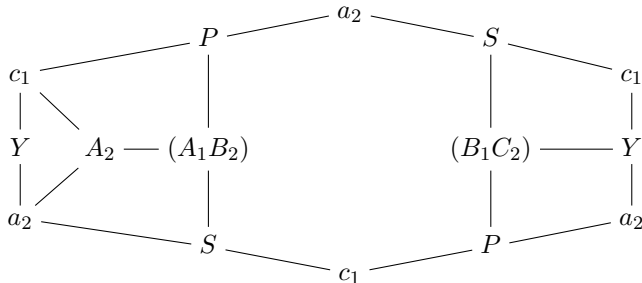
$$A = a_1 \cap a_2, \quad B = b_1 \cap b_2, \quad C = c_1 \cap c_2.$$

Our goal is to prove that the points A, B, C are collinear.

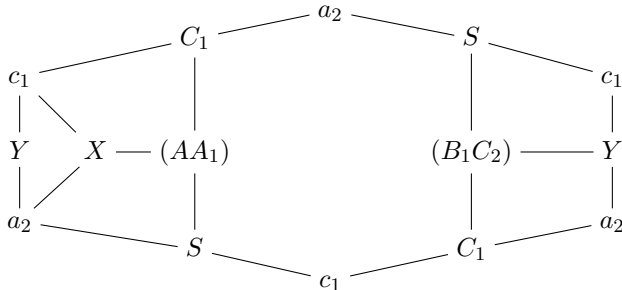
We set

$$S = c_2 \cap (A_1C_2), \quad M = c_1 \cap a_2, \quad X = b_1 \cap (A_2M), \quad Y = (A_2M) \cap (C_1C_2).$$

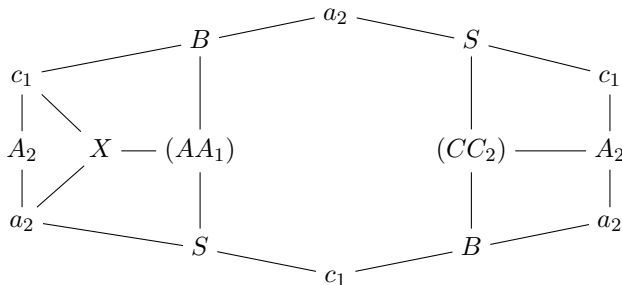
We begin by applying the tiling version of the Pappus theorem (more specifically, Theorem 7.2) to the following tiling of the torus:



It is straightforward to check that all tiles except for the one in the upper-right corner are coherent. (For the octagonal tile, use Proposition 7.1.) It follows that the latter tile is coherent as well. Again invoking Theorem 7.2 and Proposition 7.1 for the tiling



we conclude that the tile with vertices $a_2, X, (AA_1), S$ is coherent. We then verify that all five quadrilateral tiles appearing in the tiling



are coherent, so the octagonal tile is coherent as well. Applying Proposition 7.1 to the latter tile, we conclude that the points A, B, C are collinear. \square

8. GEOMETRIC RAMIFICATIONS OF THE MASTER THEOREM

In this section, we discuss various geometric interpretations and corollaries of our master theorem.

THE POLYGON TRICK

On a plane, the vertices of a polygon encode as much information as its sides. This simple observation can be used to reformulate incidence theorems:

Remark 8.1. Any theorem stated in terms of m points P_1, \dots, P_m and $n \geq 3$ generic lines ℓ_1, \dots, ℓ_n in the plane can be restated entirely in terms of points by replacing the lines ℓ_1, \dots, ℓ_n by the points Q_1, \dots, Q_n defined by $Q_i = \ell_i \cap \ell_{i+1}$, where the subscripts are taken modulo n . Put differently, we set $\ell_i = (Q_{i-1}Q_i)$ —again, with subscripts viewed modulo n .

To illustrate, Figure 8 yields an incidence theorem stated in terms of the points P_1, \dots, P_6 and the lines a, b, c . The above observation allows us to restate this theorem in terms of the nine points $P_1, \dots, P_6, A = c \cap b, B = a \cap c, C = a \cap b$, resulting in the traditional version of the Pappus theorem.

For $n \geq 4$, the above reformulation depends on the choice of a cyclic ordering among the lines ℓ_1, \dots, ℓ_n (more precisely, cyclic ordering viewed up to global reversal).

For $n \geq 6$, we may alternatively split the lines into collections of size ≥ 3 and apply the above substitution procedure to each of these collections.

The construction in Remark 8.1 straightforwardly extends to higher dimensions. In particular, in 3-space we get the following:

Remark 8.2. Any theorem stated in terms of m points P_1, \dots, P_m and $n \geq 3$ generic planes h_1, \dots, h_n in 3-space can be restated entirely in terms of points by replacing the planes h_1, \dots, h_n by the points Q_1, \dots, Q_n defined by $Q_i = h_i \cap h_{i+1} \cap h_{i+2}$, where the subscripts are taken modulo n . Equivalently, set $h_i = (Q_{i-2}Q_{i-1}Q_i)$ —again, with subscripts viewed modulo n .

To illustrate, the tiling in Figure 44 yields an incidence theorem stated in terms of four points and four planes. Replacing the four planes by four points defined as above yields the cube theorem of Möbius (Theorem 5.5).

As in Remark 8.1, the construction depends on the choice of a cyclic ordering (indexing) of the n given planes h_1, \dots, h_n . It can also be generalized by utilizing a grouping of these n planes into n overlapping blocks of size 3 such that each plane appears in exactly 3 blocks. The points Q_i are then defined by taking intersections of the planes that make up each block. To illustrate, we can use the Fano block design to replace 7 generic planes h_1, \dots, h_7 by 7 generic points Q_1, \dots, Q_7 as follows:

$$\begin{aligned} Q_i &= h_i \cap h_{i-1} \cap h_{i-3} & (i = 1, \dots, 7, \text{ all indices viewed mod } 7); \\ h_i &= (Q_i Q_{i+1} Q_{i+3}) & (i = 1, \dots, 7, \text{ all indices viewed mod } 7). \end{aligned}$$

We note that in the particular case when $n = \dim \mathbb{P} + 1$, the reformulation described in Remarks 8.1–8.2 yields D. G. Glynn’s construction [17] discussed in Remark 6.6.

TRIANGULATED SURFACES AND 2D INCIDENCE THEOREMS

Returning to the construction of Definition 6.1 and assuming that all faces of an embedded graph are triangles (cf. Remark 7.17), we arrive at the following corollary of our master theorem.

Corollary 8.3. *Let T be a triangulation of a closed oriented surface. For each vertex v in T , choose a different point P_v on the real/complex plane. For each edge $u \xrightarrow{e} v$ in T , choose a point P_e on the line $(P_u P_v)$. Assume that all these points are distinct. For each triangle in T with sides a, b, c , consider the condition*

$$(8.1) \quad \text{the points } P_a, P_b, \text{ and } P_c \text{ are collinear.}$$

If (8.1) holds for all triangles in T except one, then it holds for the remaining triangle.

Figure 75 illustrates condition (8.1) for two adjacent triangles in a triangulation.

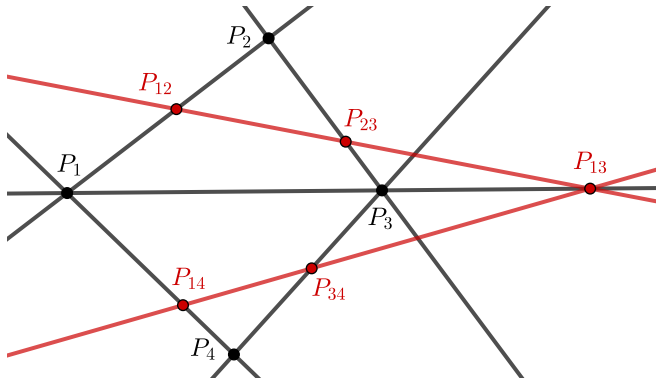


Figure 75: Condition (8.1) for two adjacent triangles. The points P_{ij}, P_{ik}, P_{jk} chosen on the sides of each triangle must be collinear.

Proof. Construct a tiling of the surface as explained in the proof of Proposition 6.2, but with points and lines interchanged:

- color the vertices of T black;
- place a white vertex inside each triangle of T ;
- connect this vertex to the three vertices of the triangle;
- remove the edges of T from the resulting graph.

The tiles \square_e of the resulting tiling are in bijection with the edges e of the original triangulation T . We then label the vertices of the tiling:

- to each black vertex v of the tiling, we associate the point P_v ;
- to each white vertex of the tiling corresponding to a triangle in T satisfying (8.1), we assign the line passing through the points P_a, P_b , and P_c ;
- to the remaining triangle, say with sides a_o, b_o, c_o , we assign the line $(P_{a_o} P_{b_o})$.

For each edge $u \xrightarrow{e} v$ in T different from c_o , the coherence of the corresponding tile \square_e follows from the above definitions: the lines associated to the two white vertices of the tile intersect at the point P_e , which lies on the line $(P_u P_v)$. The master theorem implies that the remaining tile is coherent, implying that the line $(P_{a_o} P_{b_o})$ passes through P_{c_o} , as desired. \square

Example 8.4 (*Desargues' Theorem*). Triangulate the sphere into four triangles, as in a tetrahedron. Corresponding to the four vertices of this triangulation, pick four points P_1, P_2, P_3, P_4 on the plane. Corresponding to the six edges of the triangulation, pick six points P_{ij} , each lying on its respective line $(P_i P_j)$. Corresponding to the four faces of the triangulation, we have four instances of condition (8.1), shown as red lines in Figure 76. If three of these instances hold, then the fourth one holds as well. This statement is a reformulation of the Desargues theorem.

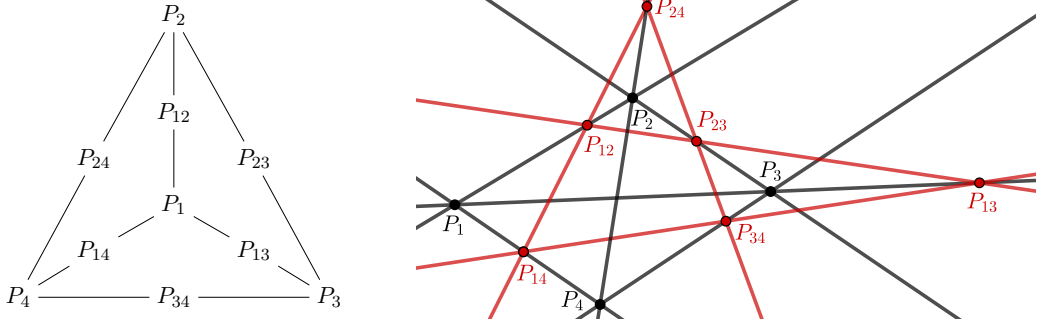


Figure 76: Obtaining the Desargues configuration from a triangulation of the sphere.

Example 8.5 (*Pappus' Theorem*). Triangulate the torus into six triangles as shown in Figure 77. Corresponding to the three vertices of this triangulation, pick three points A, B, C on the plane. Draw the lines $(AB), (AC), (BC)$. Corresponding to the nine edges of the triangulation, place nine points $A_i \in (BC), B_i \in (AC), C_i \in (AB)$. Corresponding to the six faces of the triangulation, we have six instances of condition (8.1), shown as red lines in Figure 77. If five of these instances hold, then the sixth one holds as well. This statement is a reformulation of the Pappus theorem.

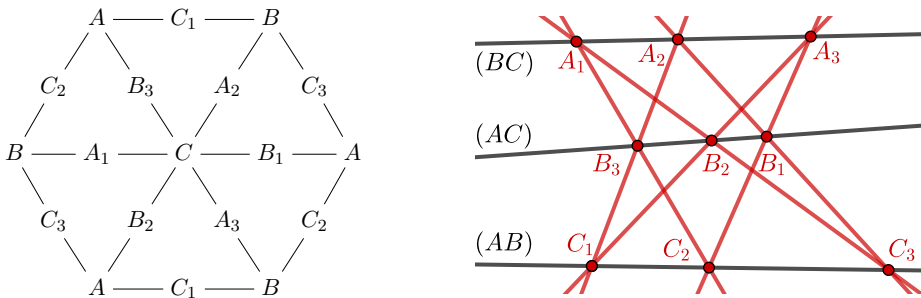


Figure 77: Obtaining the Pappus configuration from a triangulation of the torus. The opposite sides of the hexagonal fundamental domain should be glued to each other.

Remark 8.6. Corollary 8.3 generalizes from triangulations to arbitrary polygonal subdivisions of a surface. (The proof remains essentially the same.) On the other hand, the resulting theorem follows from Corollary 8.3 by considering a triangulation obtained by subdividing the polygonal faces into triangles. (Here we assume that the conclusion of the theorem refers to a triangular face.)

HAMILTONIAN CYCLES AND CLOSURE THEOREMS

Most theorems of classical planar linear incidence geometry can be presented in the form of a *closure theorem* (Schließungssatz), an assertion that a particular straightedge-only construction closes up, producing a periodic sequence of points. (Cf. Remark 7.12.) We next describe a combinatorial technique that can be used to interpret individual instances of Corollary 8.3 as closure theorems. This technique applies whenever the dual graph of a triangulation satisfies the relatively mild combinatorial condition of *Hamiltonicity*. (For simplicial polyhedra, this condition features in a famous conjecture of P. G. Tait, disproved by W. Tutte, see, e.g., [4, Section 18.2].)

Theorem 8.7. *Let T be a triangulation of a closed oriented surface. Assume that each pair of triangles in T have at most one side in common. Let G be the dual trivalent graph of T . Suppose that G has a Hamiltonian cycle. Let $\Delta_1, \dots, \Delta_N$ be the corresponding sequence of triangles in T . In other words, consecutive triangles Δ_i and Δ_{i+1} (all our indexing is modulo N) are adjacent for every i , and each triangle in T appears exactly once in the sequence (Δ_i) . Then the following closure theorem holds:*

For each vertex v in T , choose a different point P_v on the real/complex plane. For each edge $u \xrightarrow{e} v$ in T shared by two consecutive triangles Δ_i and Δ_{i+1} , denote $\ell_i = (P_u P_v)$. For each of the remaining edges $u \xrightarrow{e} v$ in T , choose a point $P_e \in (P_u P_v)$.

Pick a point $Q_1 \in \ell_1$. Assume that all the chosen points are distinct. Recursively define the points $Q_i \in \ell_i$, $i \geq 2$, by $Q_i = \ell_i \cap (Q_{i-1} P_e)$, where e is the unique side of the triangle Δ_i not shared with the triangles $\Delta_{i\pm 1}$. Then $Q_{N+1} = Q_1$.

Example 8.8. In the case of Desargues’ theorem (cf. Example 8.4), one choice of a Hamiltonian cycle is shown in Figure 78 on the left. Then Theorem 8.7 asserts the following. Pick generic points P_1, P_2, P_3, P_4 on the plane. Set $\ell_1 = (P_1 P_3)$, $\ell_2 = (P_1 P_4)$, $\ell_3 = (P_2 P_4)$, $\ell_4 = (P_2 P_3)$. Choose $P_{12} \in (P_1 P_2)$ and $P_{34} \in (P_3 P_4)$. Pick $P_{13} \in \ell_1$. Set $P_{14} = \ell_2 \cap (P_{13} P_{34})$, $P_{24} = \ell_3 \cap (P_{12} P_{14})$, $P_{23} = \ell_4 \cap (P_{24} P_{34})$. Then $P_{13} = \ell_1 \cap (P_{12} P_{23})$.

Example 8.9. For the Pappus theorem (cf. Example 8.5), we can choose a Hamiltonian cycle as shown in Figure 78 on the right. Set $Q_1 = A_1$, so that $\ell_1 = (BC)$, $\ell_2 = (AC)$, $\ell_3 = (AB)$, $\ell_4 = (BC)$, $\ell_5 = (AC)$, $\ell_6 = (AB)$. Theorem 8.7 asserts that, given $A_2 \in (BC)$, $B_2 \in (AC)$, $C_2 \in (AC)$, the recursively defined sequence $A_1, B_3, C_1, A_3, B_1, C_3, \dots$ (cf. Figure 77) is 6-periodic. The details are left to the reader.

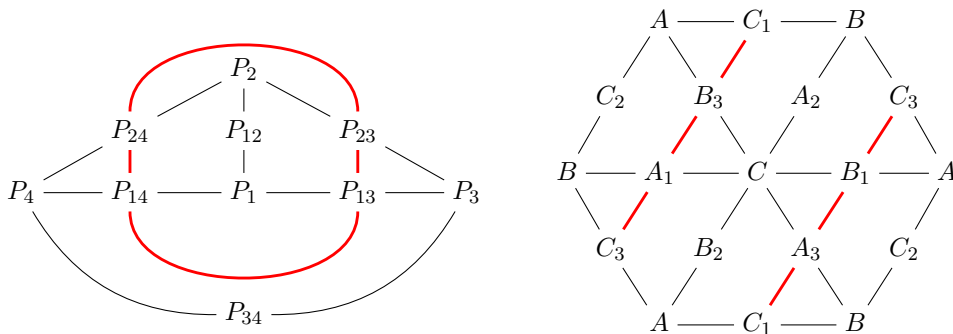


Figure 78: Left: A triangulation from Figure 76 and a closed curve through it that corresponds to a Hamiltonian cycle in the dual trivalent graph. Right: a similar closed curve through the triangulation from Figure 77.

QUADRANGULATED SURFACES AND 3D INCIDENCE THEOREMS

The construction of Corollary 8.3 extends to 3D, with essentially the same proof:

Corollary 8.10. *Let T be a tiling of a closed oriented surface by quadrilateral tiles. For each vertex v in T , choose a different point P_v in the real/complex 3-space. For each edge $u \xrightarrow{e} v$ in T , choose a point P_e on the line $(P_u P_v)$. Assume that all these points are distinct. For each quadrilateral tile in T with sides a, b, c, d (listed consecutively), consider the condition*

$$(8.2) \quad \text{the points } P_a, P_b, P_c, \text{ and } P_d \text{ are coplanar.}$$

If (8.2) holds for all quadrilateral tiles in T except one, then it holds for the remaining quadrilateral tile.

While the tiling in Corollary 8.10 is an object of the same kind as the tilings appearing in our master theorem, the geometric constructions associated with these tilings differ between the two contexts. In the master theorem, black vertices correspond to points and white vertices to planes, whereas in Corollary 8.10, all vertices are labeled by points and moreover we associate additional points to the edges of the tiling.

Example 8.11 (*The Möbius configuration*). Tile the torus by four quadrilaterals as shown in Figure 79. Corresponding to the four vertices of this tiling, pick four points A, B, C, D in 3-space. Draw the lines $(AB), (BC), (CD), (DA)$. Corresponding to the eight edges of the tiling, pick eight points $P_5, P_8 \in (AB), P_2, P_3 \in (BC), P_6, P_7 \in (CD), P_1, P_4 \in (AD)$. Corresponding to the four faces of the tiling, we have four instances of condition (8.2). Now state everything in terms of P_1, \dots, P_8 . For example, the existence of the point C means that the lines $(P_2 P_3) = (BC)$ and $(P_6 P_7) = (CD)$ intersect, i.e., the points P_2, P_3, P_6, P_7 are coplanar. Adding four coplanarity conditions corresponding to the points A, B, C, D to the four coplanarity conditions corresponding to the four instances of (8.2), we recover the Möbius configuration (Theorem 5.5).

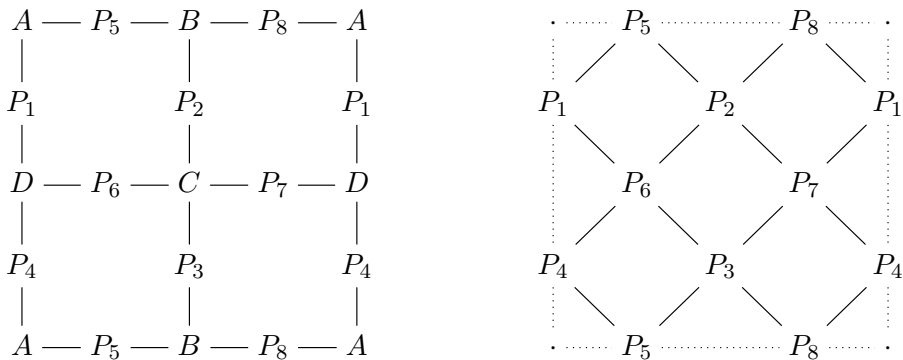


Figure 79: Left: Quadrilateral tiling of the torus that illustrates Corollary 8.10. The opposite sides of the rectangular fundamental domain should be glued to each other. Right: the vertices of each of the eight tiles are coplanar, cf. (5.1).

Remark 8.12. Corollary 8.10 has a generalization to polygonal tilings, similar to the one discussed in Remark 8.6 in the context of 2D incidence geometry.

EDGES IN POLYTOPES

Corollary 8.13. *Let \mathbf{P} be a convex polytope in \mathbb{R}^3 with vertices V_1, \dots, V_n . Pick n distinct points $V'_1, \dots, V'_n \in \mathbb{R}^3$ not lying on the planes containing the faces of \mathbf{P} . For each edge $\{V_i, V_j\}$ of \mathbf{P} , consider the condition*

$$(8.3) \quad \text{the lines } (V_i V_j) \text{ and } (V'_i V'_j) \text{ intersect.}$$

If this condition is satisfied for all edges of \mathbf{P} except one, then it is also satisfied for the remaining edge.

Proof. Once again, we adapt the construction from (the proof of) Proposition 6.2. Viewing \mathbf{P} as a PL-manifold, we tile it by quadrangular tiles as follows. The vertices of the tiling include the vertices of \mathbf{P} plus an additional vertex v_f for each two-dimensional face f of \mathbf{P} . The edges of \mathbf{P} do *not* include the edges of \mathbf{P} . Instead, we connect each vertex v_f with all the vertices V_i lying on the boundary of the face f . The tiles of the resulting tiling of the sphere correspond to the edges of \mathbf{P} .

We now associate points and planes to the vertices of the tiling, as follows. To a vertex of the tiling that comes from a vertex V_i of the polytope \mathbf{P} , we associate the point V'_i . To a vertex v_f of the tiling that comes from a face f of \mathbf{P} , we associate the plane containing the face f . Then the coherence conditions associated to the tiles are precisely the conditions (8.3), and the claim follows. \square

Example 8.14. Let \mathbf{P} be a tetrahedron with vertices P_1, P_2, P_3, P_4 . Corollary 8.13 asserts that given four generic points P'_1, P'_2, P'_3, P'_4 , five of the conditions

$$\text{the lines } (P_i P_j) \text{ and } (P'_i P'_j) \text{ intersect}$$

imply the sixth. We thus recover Theorem 5.1.

Corollary 8.13 straightforwardly generalizes to arbitrary oriented two-dimensional PL-manifolds \mathbf{P} immersed in \mathbb{R}^3 so that each facet of \mathbf{P} is homeomorphic to a disk embedded into \mathbb{R}^3 as a flat polygon (not necessarily convex). Even more generally:

Corollary 8.15. *Consider a tiling of a closed oriented surface by polygons. Associate a point P_v in 3-space to each vertex v . Associate a plane h_f to each polygonal face f . Associate two lines to each edge $u \overset{e}{-} v$ separating two faces f and g :*

- *the line $(P_u P_v)$ connecting the vertices associated with the endpoints of e ;*
- *the line $h_f \cap h_g$ where the planes associated with the faces separated by e meet.*

If these two lines intersect for each edge on the surface except one, then this condition is also satisfied for the remaining edge.

MORE GEOMETRIC REFORMULATIONS

A general correspondence principle established by S. Tabachnikov [58] transforms any incidence theorem in the plane (in particular, any instance of our master theorem) into a theorem about *skewers*, i.e., common perpendiculars to lines in 3-space.

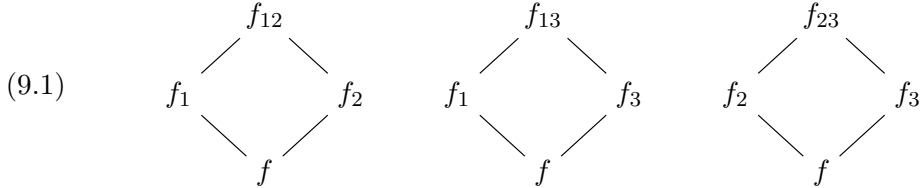
In a similar spirit, *stereographic projection* links incidence theorems about circles in the plane and their counterparts involving circles on a sphere or planes in 3-space. Thus, the cube theorem of Möbius (Theorem 5.5) together with Hesse's associated points theorem yields Wallace's theorem, cf. [18, Section 7] [3, vol. 4, Section 1, 18–20].

9. BOBENKO-SURIS CONSISTENCY OF COHERENT TILINGS

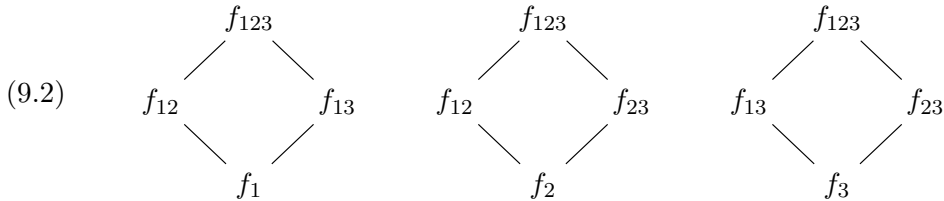
In this section, we discuss the phenomena of 3D and 4D consistency of coherent tilings. They can be viewed as analogues of the notions of 3D and 4D consistency of 2D discrete dynamical systems that play important roles in the context of the “integrability as consistency” paradigm developed by A. Bobenko and Yu. Suris [9].

3D CONSISTENCY FOR POINTS AND LINES IN THE PLANE

Proposition 9.1. *On the real/complex projective plane, let $f, f_{12}, f_{13}, f_{23}$ be four points and let f_1, f_2, f_3 be three lines. Assume that the three tiles*



are coherent and that the seven inputs f, f_i, f_{ij} are generic subject to this condition. Then there exists a unique line f_{123} such that the three tiles



are coherent. The same result holds with the words “point” and “line” interchanged.

To rephrase, if five vertices of a cube are labeled by points and lines so that the three tiles that do not involve the unlabeled vertex are coherent, then the sixth vertex can be labeled, in a unique way, so that the remaining three tiles are coherent as well. See Figure 80.

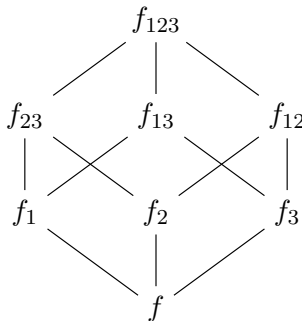


Figure 80: 3D consistency of coherent tilings for points and lines in the plane.

Proof. This statement can be easily seen to be a restatement of Desargues’ theorem, cf. Figure 5. □

3D CONSISTENCY FOR POINTS AND LINES IN 3-SPACE

Definition 9.2. Let A, B (resp., ℓ, m) be distinct points (resp., distinct lines) in the 3-dimensional real/complex projective space. We call the tile with vertices labeled A, ℓ, B, m (see (2.1)) *coherent* if

- neither A nor B is incident to either ℓ or m ;
- the lines ℓ and m intersect at some point P ;
- the line (AB) passes through P .

Remark 9.3. The original coherence property introduced in Definition 2.1 is a codimension 1 condition: it imposes a single equation on the labels of a tile. By contrast, the coherence property in Definition 9.2 is a codimension 3 condition. It can be shown that this condition is equivalent to requiring that for any point O in 3-space, the tile whose vertices are labeled by A, B , and the spans of $\{O, \ell\}$ and $\{O, m\}$ is coherent in the original sense. It follows that if the vertices of a tiling of a closed oriented surface are labeled by points and lines in 3-space so that all tiles but one are coherent (as in Definition 9.2), then the remaining tile is coherent as well.

Proposition 9.4. *In the real/complex projective 3-space, let $f, f_{12}, f_{13}, f_{23}$ be four points in general position. Let f_1, f_2, f_3 be three lines. Assume that the three tiles (9.1) are coherent (cf. Definition 9.2) and the seven inputs f, f_i, f_{ij} are generic subject to the above conditions. (In particular, the three lines f_1, f_2, f_3 lie in one plane h .) Then there exists a unique line f_{123} such that the three tiles (9.2) are coherent. Specifically, $f_{123} = h \cap (f_{12}f_{13}f_{23})$, the “Desargues line” for the perspective triangles $f_{12}f_{13}f_{23}$ and $f_1f_2f_3$.*

Proof. For the tiles (9.2) to be coherent, the line f_{123} must intersect each of the lines f_1, f_2, f_3 , hence lie in the plane h . These conditions also imply that f_{123} intersects each of the lines $(f_{12}f_{13}), (f_{12}f_{23}), (f_{13}f_{23})$, hence lies in the plane $(f_{12}f_{13}f_{23})$. Thus $f_{123} = h \cap (f_{12}f_{13}f_{23})$.

Conversely, let $f_{123} = h \cap (f_{12}f_{13}f_{23})$. Set $f'_{12} = f_1 \cap f_2, f'_{13} = f_1 \cap f_3, f'_{23} = f_2 \cap f_3$. The coherence of the tiles (9.1) means that each triple $\{f, f_{ij}, f'_{ij}\}$ is collinear. Thus the points $f_{12}, f'_{12}, f_{13}, f'_{13}$ are coplanar, so the lines $f_1 = (f'_{12}f'_{13})$ and $(f_{12}f_{13})$ intersect (necessarily at a point lying on $h \cap (f_{12}f_{13}f_{23}) = f_{123}$). We conclude that the first tile in (9.2) is coherent, and so are the other two. \square

Interchanging points and lines in Proposition 9.4 requires a coplanarity assumption:

Proposition 9.5. *In the real/complex projective 3-space, let $f, f_{12}, f_{13}, f_{23}$ be four lines and let f_1, f_2, f_3 be three points. Assume that the lines f_{12}, f_{13}, f_{23} lie in one plane, the three tiles (9.1) are coherent (cf. Definition 9.2), and the seven inputs f, f_i, f_{ij} are generic subject to the above conditions. Then there exists a unique point f_{123} such that the three tiles (9.2) are coherent.*

Proof. Set $f'_1 = f_{12} \cap f_{13}, f'_2 = f_{12} \cap f_{23}, f'_3 = f_{13} \cap f_{23}$. The tiles (9.1) are coherent, so each pair $(f_i f_j), (f'_i f'_j)$ is coplanar. Hence each pair $(f_i f'_i), (f_j f'_j)$ is coplanar. If all three lines $(f_i f'_i)$ are coplanar, then everything lies in a plane and the claim follows by Desargues’ theorem. Otherwise, the three lines $(f_i f'_i)$ are concurrent and the point of their intersection is the unique point f_{123} satisfying the coherence conditions (9.2). \square

4D CONSISTENCY FOR POINTS AND LINES IN 3-SPACE

Theorem 9.6. *In the real/complex projective 3-space, let $f, f_{12}, f_{13}, f_{14}, f_{23}, f_{24}, f_{34}$ be seven points and let f_1, f_2, f_3, f_4 be four lines. Assume that the six tiles*

$$(9.3) \quad \begin{array}{ccc} & f_{ij} & \\ & / \quad \backslash & \\ f_i & & f_j \\ & \backslash \quad / & \\ & f & \end{array}$$

are coherent and the eleven inputs f, f_i, f_{ij} are generic subject to this condition. For each triple $1 \leq i < j < k \leq 4$, let f_{ijk} be the unique line that makes all tiles in

$$(9.4) \quad \begin{array}{ccccc} & & f_{ijk} & & \\ & & / \quad | \quad \backslash & & \\ f_{jk} & & f_{ik} & & f_{ij} \\ & \backslash \quad / & & \backslash \quad / & \\ f_i & & f_j & & f_k \\ & & | & & \\ & & f & & \end{array}$$

coherent, cf. Proposition 9.4. Then there exists a unique point f_{1234} that makes all tiles in Figure 81 coherent.

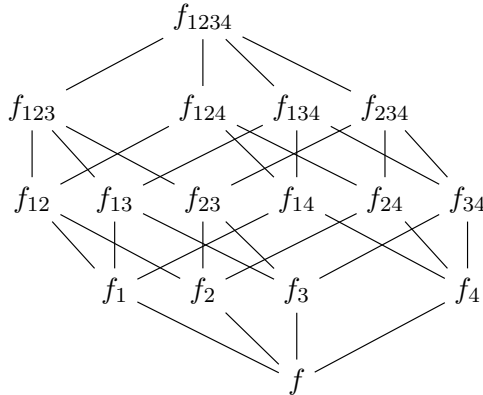


Figure 81: 4D consistency of coherent tilings.

Proof. We will use the notational conventions $f_{ij} = f_{ji}$ and $f_{ijk} = f_{jik} = f_{ikj} = \dots$. The lines (ff_{ij}) and f_i intersect (cf. (9.3)), so the point f_{ij} lies in the plane (ff_i) . Hence each quadruple $\{f, f_{ij}, f_{ik}, f_{il}\}$ is coplanar (all points lie in (ff_i)), so the four planes (f_{ij}, f_{ik}, f_{il}) have a common point f . By the octahedron theorem (or by the cube theorem), the four planes (f_{ij}, f_{ik}, f_{jk}) have a common point f_{1234} .

The coherence of (9.3)–(9.4) and Proposition 9.4 imply that the four lines f_i lie in a common plane h and moreover $f_{ijk} = h \cap (f_{ij}f_{ik}f_{jk})$. Thus the four lines f_{ijk} lie in h and we have $f_{ijk} \cap f_{ij\ell} = h \cap (f_{ij}f_{ik}f_{jk}) \cap (f_{ij}f_{il}f_{j\ell}) = h \cap (f_{ij}f_{1234})$, so the tile with labels $f_{ij}, f_{ijk}, f_{ij\ell}, f_{1234}$ is coherent.

Uniqueness follows by arguing that f_{1234} must lie on the planes (f_{ij}, f_{ik}, f_{jk}) . \square

4D CONSISTENCY FOR POINTS AND LINES IN THE PLANE

Theorem 9.7. *Theorem 9.6 holds verbatim for points and lines in the plane.*

More explicitly, let f be a point on the real/complex plane and let f_1, f_2, f_3, f_4 be four generic lines. For each of the six instances of $1 \leq i < j \leq 4$, pick a point f_{ij} on the line passing through f and $f_i \cap f_j$. For each triple $1 \leq i < j < k \leq 4$, the triangles $f_i f_j f_k$ and f_{ij}, f_{ik}, f_{jk} are in perspective; let f_{ijk} be their Desargues line. Then the six lines obtained by connecting f_{ij} with $f_{ijk} \cap f_{ijl}$ intersect in a point. See Figure 82.

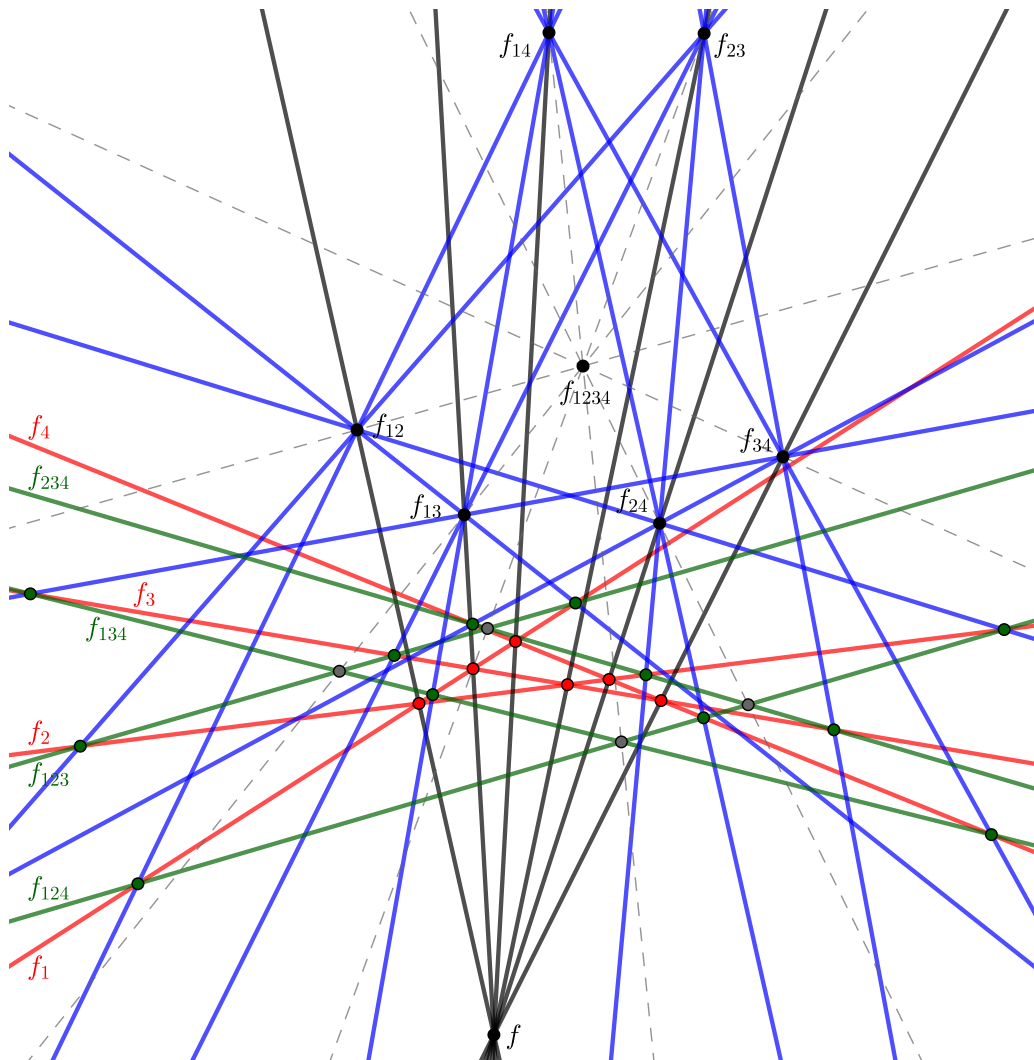


Figure 82: 4D consistency of coherent tilings for points and lines in the plane. Two relevant points, namely $f_{123} \cap f_{124}$ and $f_{134} \cap f_{234}$, are outside the picture frame.

Proof. Lift point f out of the plane h containing the lines f_1, f_2, f_3, f_4 and reproduce the construction of Theorem 9.6. Continuously move f back into h and apply Proposition 9.1 and Theorem 9.6 to obtain the desired result. \square

4D CONSISTENCY FOR POINTS AND PLANES IN 3-SPACE

The phenomenon of 3D consistency, in a version analogous to Proposition 9.1 (cf. [9, Definition 4.1]), does not hold for points and planes in 3-space—not because we cannot complete the 3D cube, but because there are infinitely many ways to do it. Indeed, if a plane f_{123} satisfies two of the three coherence conditions (9.2), then the third condition is automatic by the bundle theorem (Theorem 5.1). Since each condition requires the plane f_{123} to pass through a certain point, the planes satisfying two such conditions form a one-dimensional pencil, so uniqueness of f_{123} fails.

On the other hand, 4D consistency holds for points and planes in 3-space, even without relying on the coherence of the bottom tiles (9.3):

Theorem 9.8. *In the real/complex projective 3-space, let $f_{12}, f_{13}, f_{14}, f_{23}, f_{24}, f_{34}$ be 6 points and let $f_1, f_2, f_3, f_4, f_{123}, f_{124}, f_{134}, f_{234}$ be 8 planes such that the 12 tiles*

$$(9.5) \quad \begin{array}{ccc} & f_{ijk} & \\ & / \quad \backslash & \\ f_{ij} & & f_{ik} \\ & \backslash \quad / & \\ & f_i & \end{array}$$

are coherent and the 14 inputs f_i, f_{ij}, f_{ijk} are generic subject to these conditions. (Here we use the conventions $f_{ij} = f_{ji}$ and $f_{ijk} = f_{jik} = f_{ikj} = \dots$) Then there exist unique points f and f_{1234} that make all tiles in Figure 81 coherent.

Proof. By symmetry, it suffices to show the existence and uniqueness of f_{1234} . Let h_{ij} be the plane through f_{ij} and the line $f_{ijk} \cap f_{ijl}$. We need to show that the six planes h_{ij} have a common point f_{1234} . By the discussion preceding Theorem 9.8, each triple of planes h_{ij}, h_{ik}, h_{il} intersect along a line, so $h_{ij} \cap h_{ik} = h_{ij} \cap h_{ik} \cap h_{il}$. Therefore

$$f_{1234} \stackrel{\text{def}}{=} h_{12} \cap h_{13} \cap h_{23} = h_{12} \cap h_{13} \cap h_{14} \cap h_{23} = \dots = \bigcap h_{ij}. \quad \square$$

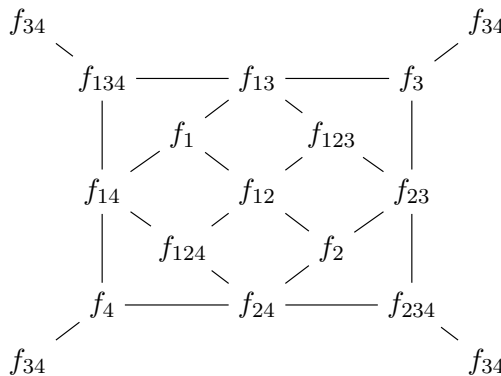


Figure 83: The dependence among conditions (9.5).

Remark 9.9. The 12 coherence conditions (9.5) in Theorem 9.8 are not independent: any 11 among them imply the remaining one, cf. the tiling of the sphere in Figure 83.

Theorem 9.8 can be viewed as a strengthening of a theorem of Cox [9, Exercise 2.28].

THE OCTAGON RELATION FOR DESARGUES FLIPS

Definition 9.10. A *flip* in a tiling is a local transformation that modifies three pairwise-adjacent tiles as shown in Figure 84.

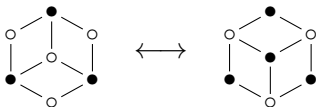


Figure 84: A flip in a tiling. (We can go either left-to-right or right-to-left.)

Remark 9.11. Flips of *zonotopal tilings* play an important role in the combinatorics of symmetric groups, as they correspond to *braid relations* between reduced words. A classical result of J. Tits [60, § 4.3, Proposition 4] describes the syzygies among braid relations. To reformulate it in the language of tilings, fix a centrally symmetric convex polygon \mathbf{P} (a 2-dimensional zonotope) and consider the following graph $G_{\mathbf{P}}$. The vertices of $G_{\mathbf{P}}$ are the tilings of \mathbf{P} by parallelograms (zonotopal tiles). The edges of $G_{\mathbf{P}}$ correspond to flips. Tits' theorem asserts that the cycles in $G_{\mathbf{P}}$ are generated by

- the 4-cycles that correspond to commuting braid moves, together with
- the 8-cycles of the form shown in Figure 85.

These octagonal cycles arise in various fields of mathematics and theoretical physics in the context of the *tetrahedron equation* of A. B. Zamolodchikov [63], see, e.g., [14, 26, 59] and references therein.

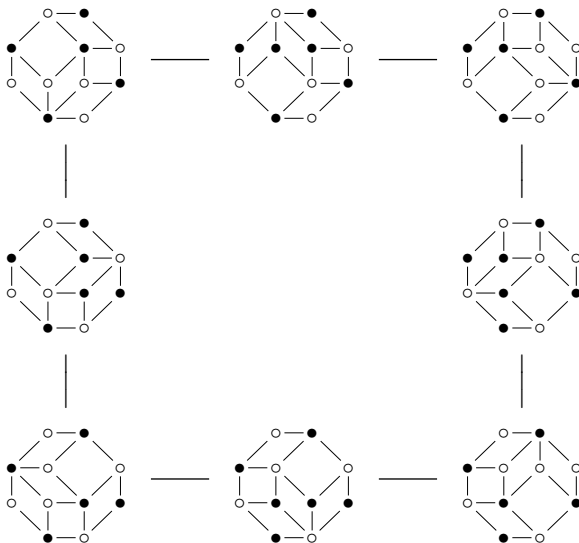


Figure 85: The octagon of flips.

Definition 9.12. Let \mathbf{T} be a tiling of a polygon by coherent tiles. Take three tiles in \mathbf{T} that form a hexagon as in Figure 84. Construct a new tiling \mathbf{T}' by performing a flip and labeling the new vertex so that the tiling remains coherent, cf. Figure 29(ii)–(iii). Under suitable genericity assumptions, Corollary 4.4 ensures that this can be done in a unique way. We then say that \mathbf{T}' is obtained from \mathbf{T} by a *Desargues flip*.

We next show that Desargues flips satisfy the tetrahedron equation:

Theorem 9.13. *Take a zonotopal tiling of an octagon by coherent tiles, cf. Figure 85. Apply a sequence of eight Desargues flips corresponding to going around the perimeter of the octagon. Then the resulting coherent labeling coincides with the original one.*

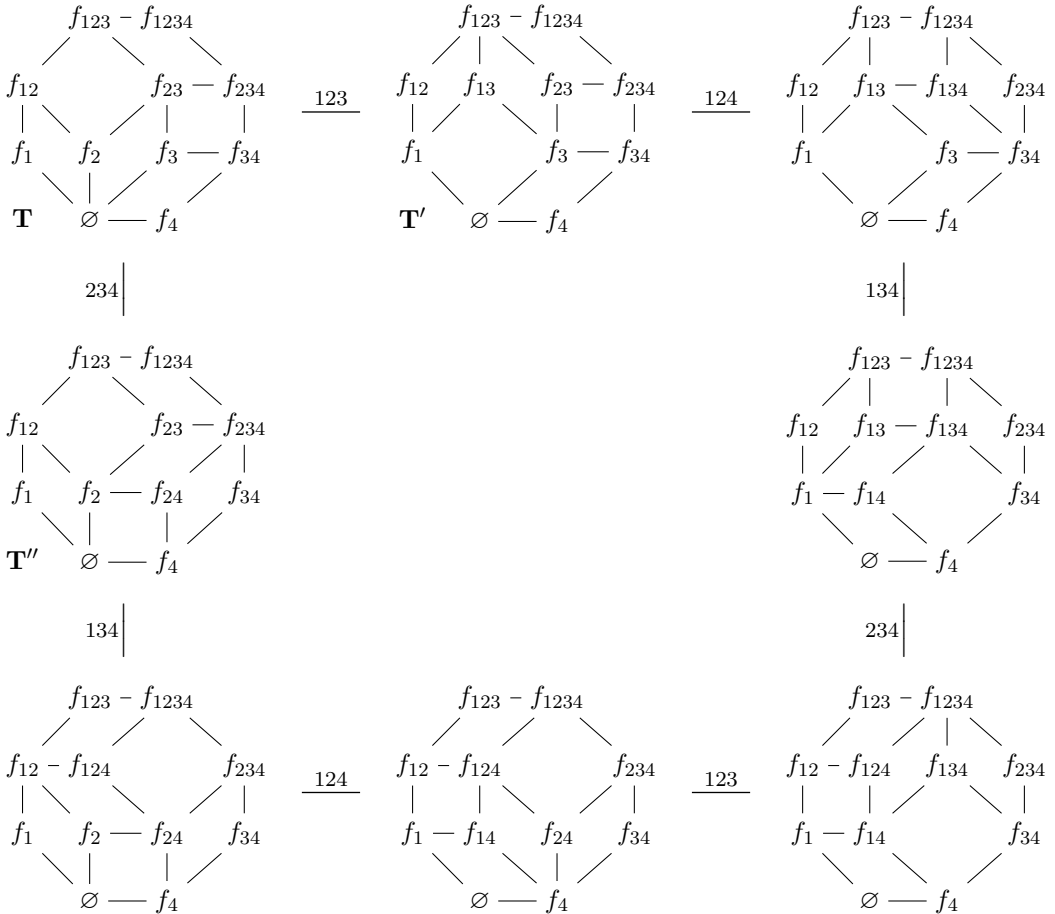


Figure 86: The octagon relation for Desargues flips.

Proof. As we will explain, this result is a consequence of the 4D consistency property discussed above. Let us start with the coherent tiling \mathbf{T} in Figure 86. Our goal is to show that applying Desargues flips along the top and right rims of Figure 86 produces the same outcome as the flips along the left and bottom rims. We note that all the tiles appearing in Figure 86 correspond to 2D faces of the 4D cube, cf. Figure 81.

Apply Desargues flips $\mathbf{T} \rightarrow \mathbf{T}'$ and $\mathbf{T} \rightarrow \mathbf{T}''$ to determine f_{13} and f_{24} . We then get 13 labels, namely f_1, f_4 , and 11 labels in the Hamming ball of radius 2 centered at f_{23} . The latter 11 labels satisfy the conditions in Theorem 9.7 (with suitable re-indexing of the 4D cube). The remaining 5 labels are then uniquely determined by the coherence conditions in the 4D cube, so they must match the original labels f_1, f_4 and the labels f_{124}, f_{134}, f_{14} arising from Desargues flips in Figure 86. \square

10. ANTICOHERENT POLYGONS

Many classical theorems of projective geometry that involve cross-ratios can be obtained using the tiling technique combined with the following notion, which may be viewed as a “negative counterpart” of Definition 4.1.

Definition 10.1. Let $n \geq 2$. Let A_1, \dots, A_n (resp., ℓ_1, \dots, ℓ_n) be an n -tuple of points (resp., lines) on the real/complex projective plane. Assume that each point A_i does not lie on either of the lines ℓ_i and ℓ_{i-1} (with the indexing understood modulo n). Let \mathbf{P} be a $2n$ -gon with vertices labeled $A_1, \ell_1, \dots, A_n, \ell_n$, in this order, see Figure 27. We call \mathbf{P} *anticoherent* if the associated generalized cross-ratio (4.1) is equal to -1 :

$$(A_1, \dots, A_n; \ell_1, \dots, \ell_n) = -1.$$

The anticoherence property is invariant under rotations and reflections of a polygon \mathbf{P} .

We will repeatedly make use of the following simple observation.

Lemma 10.2. *A $2n$ -gon \mathbf{P} with vertex labels $A_1, \ell_1, \dots, A_n, \ell_n$ (cf. Definition 10.1) is anticoherent if and only if \mathbf{P} is not coherent but the $4n$ -gon $\mathbf{P}^{(2)}$ with vertices labeled by $A_1, \ell_1, \dots, A_n, \ell_n, A_1, \ell_1, \dots, A_n, \ell_n$, in this order, is coherent.*

We call the $4n$ -gon $\mathbf{P}^{(2)}$ the *double* of the $2n$ -gon \mathbf{P} .

Proof. This statement is immediate from the identity

$$(A_1, \dots, A_n, A_1, \dots, A_n; \ell_1, \dots, \ell_n, \ell_1, \dots, \ell_n) = (A_1, \dots, A_n; \ell_1, \dots, \ell_n)^2. \quad \square$$

HARMONIC PROPERTY OF A COMPLETE QUADRANGLE

In the case $n = 2$, a quadrilateral tile

$$(10.1) \quad \begin{array}{ccc} P_1 & \text{---} & \ell_1 \\ | & & | \\ \ell_2 & \text{---} & P_2 \end{array}$$

is anticoherent if and only if the quadruple of points $P_1, P_2, (P_1P_2) \cap \ell_1, (P_1P_2) \cap \ell_2$ is *harmonic*. In the language of incidence geometry, this property can be expressed via a classical construction involving a complete quadrangle, which we derive below (in two different versions, see (10.2)) using the tiling method. Cf. also Theorem 3.6.

Theorem 10.3. *Let A_1, A_2, A_3, A_4 be four generic points on the real/complex projective plane. Draw six lines $\ell_{ij} = (A_iA_j)$, $1 \leq i < j \leq 4$. Let $P_{12,34} = \ell_{12} \cap \ell_{34}$ and $P_{14,23} = \ell_{14} \cap \ell_{23}$. Draw the line $\ell_o = (P_{12,34}P_{14,23})$. Set $P_{13} = \ell_{13} \cap \ell_o$ and $P_{24} = \ell_{24} \cap \ell_o$. (See Figure 87.) Then the tiles*

$$(10.2) \quad \begin{array}{ccc} P_{13} & \text{---} & \ell_{14} \\ | & & | \\ \ell_{12} & \text{---} & P_{24} \end{array} \quad \begin{array}{ccc} P_{12,34} & \text{---} & \ell_{13} \\ | & & | \\ \ell_{24} & \text{---} & P_{14,23} \end{array}$$

are anticoherent.

Proof. Apply Lemma 10.2 to the tilings shown in Figures 88–89. □

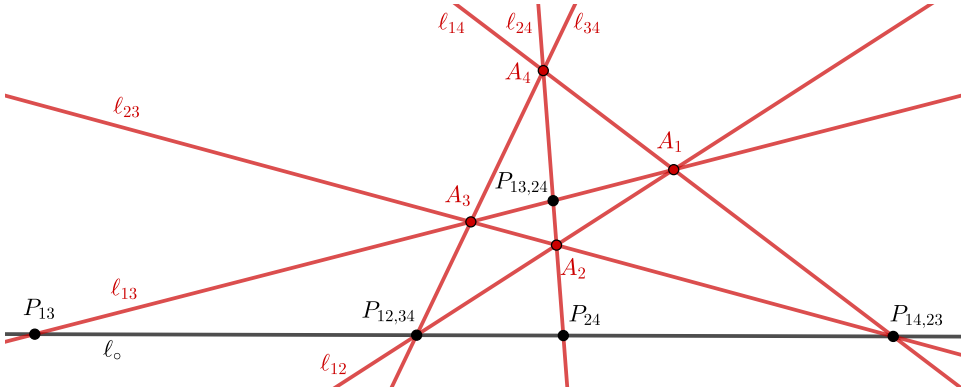


Figure 87: The harmonic property of a complete quadrangle. Here $P_{13,24} = \ell_{13} \cap \ell_{24}$.

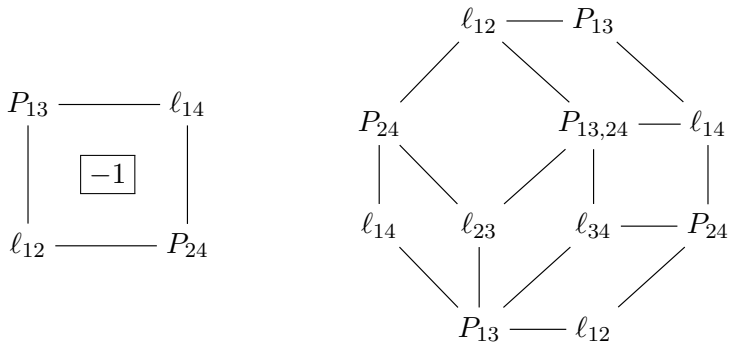


Figure 88: Anticoherent quadrilateral (marked $\boxed{-1}$) and a tiling of its double.

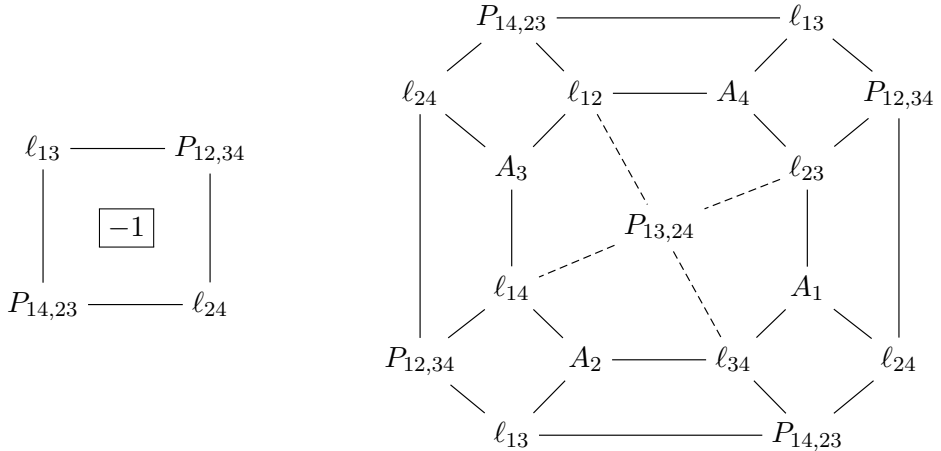


Figure 89: Another anticoherent quadrilateral and a tiling of its double.

Remark 10.4. Over a field of characteristic 2, the notions of coherence and anti-coherence coincide—so the tile shown in Figure 89 on the left is coherent, meaning that the point $P_{13,24}$ where ℓ_{13} and ℓ_{24} intersect lies on the line $(P_{12,34}P_{14,23}) = \ell_0$. Thus in characteristic 2 we have $P_{13} = P_{24} = P_{13,24}$, yielding the *Fano configuration*.

CEVA'S THEOREM

Proposition 10.5. *Let ℓ_1, ℓ_2, ℓ_3 be three concurrent lines on the real/complex plane. Let P_1, P_2, P_3 be points such that $P_1 \in \ell_1, P_2 \in \ell_2, P_3 \in \ell_3$ (but no other incidences). Then the hexagon \mathbf{P} shown in Figure 90 is anticoherent.*

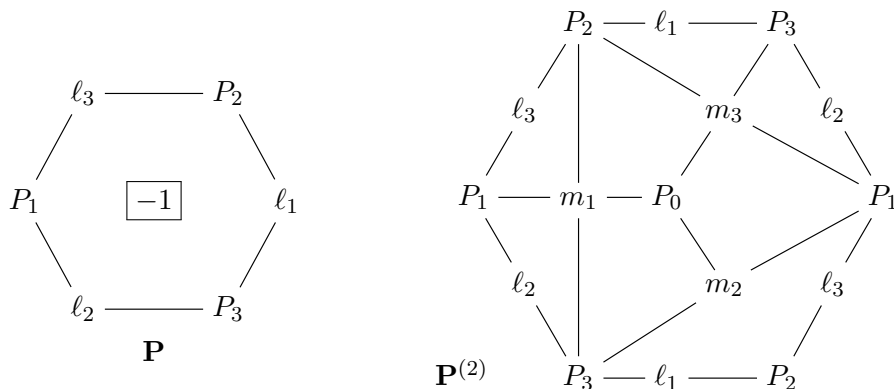


Figure 90: An anticoherent hexagon \mathbf{P} and a tiling of its double $\mathbf{P}^{(2)}$.

Proof. Denote $Q_1 = \ell_1 \cap (P_2P_3)$, $Q_2 = \ell_2 \cap (P_1P_3)$, $Q_3 = \ell_3 \cap (P_1P_2)$, $m_1 = (Q_2Q_3)$, $m_2 = (Q_1Q_3)$, $m_3 = (Q_1Q_2)$. Also let P_0 be the point where ℓ_1, ℓ_2, ℓ_3 meet, see Figure 91. Then the claim follows from the tiling shown in Figure 90. \square

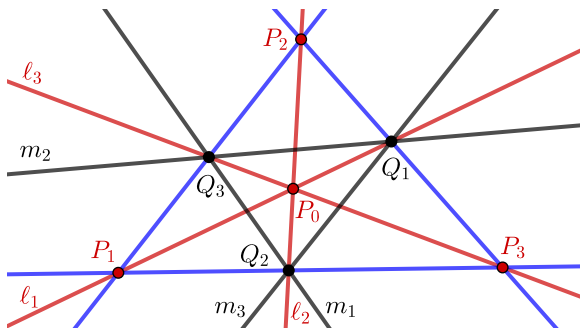


Figure 91: Three concurrent lines, with points on them.

Proposition 10.5 also has a simple algebraic proof, which we omit.

Remark 10.6. Proposition 10.5 is essentially a reformulation of Ceva's theorem (proved by G. Ceva in 1678 and by al-Mu'taman ibn Hūd in the 11th century [25]). Indeed, the mixed cross-ratio associated with the hexagon \mathbf{P} in Figure 90 is equal, up to sign, to the "Ceva ratio" of six Euclidean lengths:

$$(P_1, P_2, P_3; \ell_3, \ell_1, \ell_2) = \frac{\langle \mathbf{P}_1, \ell_3 \rangle \langle \mathbf{P}_2, \ell_1 \rangle \langle \mathbf{P}_3, \ell_2 \rangle}{\langle \mathbf{P}_2, \ell_3 \rangle \langle \mathbf{P}_3, \ell_1 \rangle \langle \mathbf{P}_1, \ell_2 \rangle} = - \frac{|P_1Q_3| \cdot |P_2Q_1| \cdot |P_3Q_2|}{|P_2Q_3| \cdot |P_3Q_1| \cdot |P_1Q_2|}.$$

ANOTHER PROOF OF PROPOSITION 4.9

The use of anticoherent polygons allows us to simplify some of the tiling-based proofs of incidence theorems that appeared earlier in this paper. Instead of tiling an oriented surface with coherent tiles, we can tile it with both coherent and anticoherent polygons, making sure that the number of anticoherent polygons is even. Then any one of these (anti)coherence conditions is implied by the rest.

We illustrate this approach by providing a simpler proof of Proposition 4.9 that avoids using the rather complicated tilings in Figures 34 and 35. By extension, this also simplifies the tiling-based proofs of Theorems 4.10 and 4.15, both of which relied on Proposition 4.9.

Proof of Proposition 4.9. Consider the tiling of a torus by four polygons shown in Figure 92. Two of these polygons (the hexagons marked with $\boxed{-1}$ in the picture) are anticoherent by Proposition 10.5. The octagon at the top of the picture is coherent by Proposition 4.8. It follows that the remaining polygon, which appears at the bottom of the picture, is coherent. This is precisely the decagon from Figure 32. \square

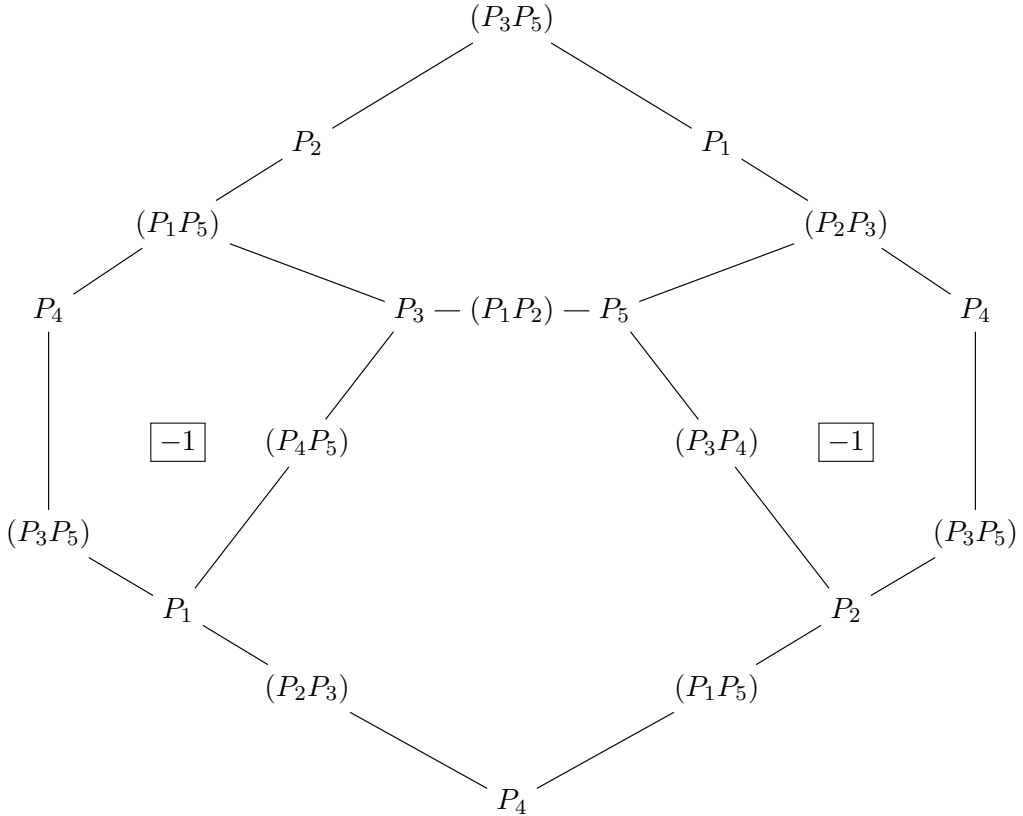


Figure 92: Another proof of Proposition 4.9. The opposite sides of the hexagonal fundamental domain should be glued to each other.

COHERENT ANNULI

Lemma 10.7. *Let P, A, B, C, D be five generic points in the real/complex plane. Then the generalized mixed cross-ratio associated to the annulus*

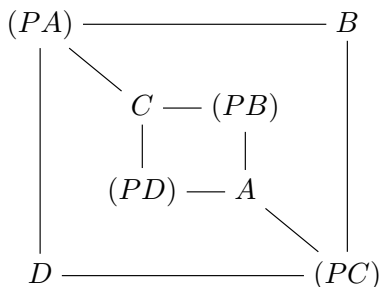
$$(10.3) \quad \begin{array}{ccc} (PA) & \text{-----} & B \\ | & & | \\ & C \text{ --- } (PB) & \\ | & & | \\ (PD) & \text{---} & A \\ | & & | \\ D & \text{-----} & (PC) \end{array}$$

is equal to 1:

$$(B, D; (PC), (PA)) \cdot (A, C; PB, PD) = 1.$$

Proof 1. Applying the definition (4.1) of the generalized mixed cross-ratio, we see that each of the four terms in the numerator cancels out a term in the denominator. \square

Proof 2. Each of the two hexagons in the tiling



of the given annulus is anticoherent by Proposition 10.5. The claim follows. \square

Proof 3. The statement follows from the tiling of the torus shown in Figure 93. \square

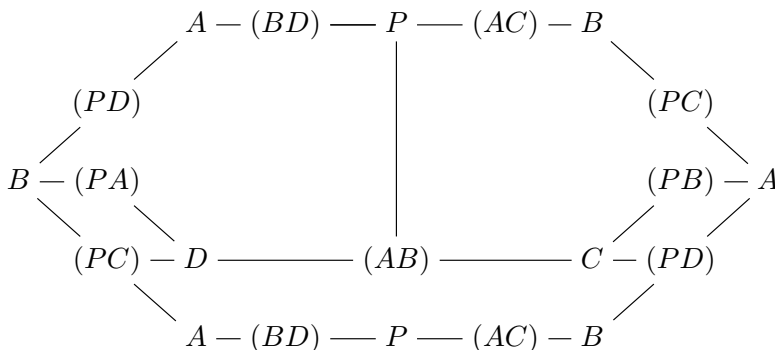


Figure 93: Third proof of Lemma 10.7. Opposite sides of the hexagonal fundamental domain should be glued to each other. Two octagons at the top of the picture and the decagon at the bottom of it are coherent by Propositions 4.8 and 4.9, respectively. The remaining quadrilaterals form the boundary of the annulus in (10.3).

COHERENT 14-GONS AND 16-GONS

Lemma 10.7 can be used to provide a tiling-based proof of the coherence of a $2n$ -gon with boundary labels $P_1 - (P_2P_3) - P_4 - (P_6P_7) - \dots$ for $n \not\equiv 0 \pmod 3$, cf. Remark 4.13. The cases $n = 4$ and $n = 5$ have been treated in Propositions 4.8 and 4.9, respectively. We illustrate the general argument by showing the appropriate tilings for $n = 7$ and $n = 8$ in Figures 94 and 95 below.

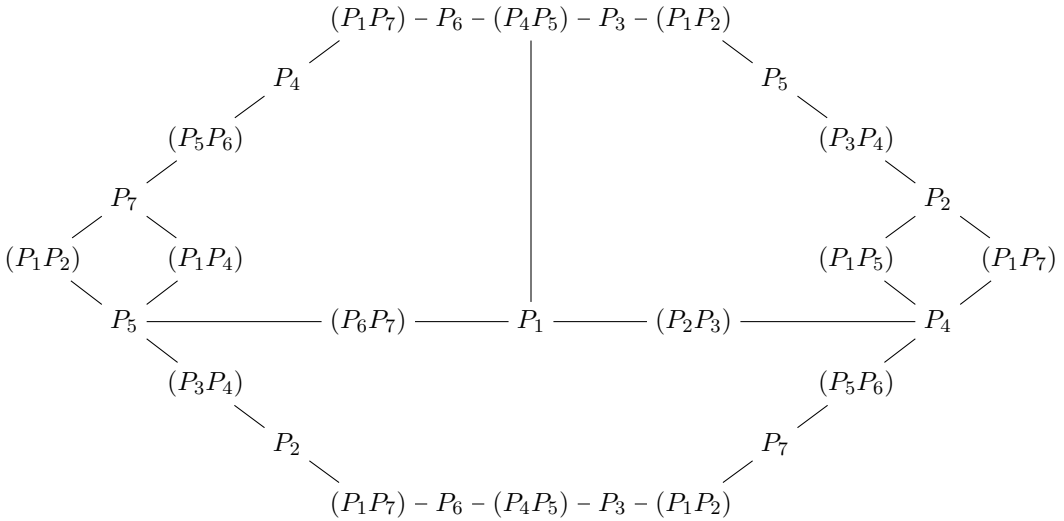


Figure 94: A coherent 14-gon appears of the bottom of the picture. Opposite sides of the hexagonal fundamental domain should be glued to each other. The decagons at the top of the picture are coherent by Proposition 4.9. The two quadrilaterals at the left and right ends form the boundary of the annulus in (10.3).

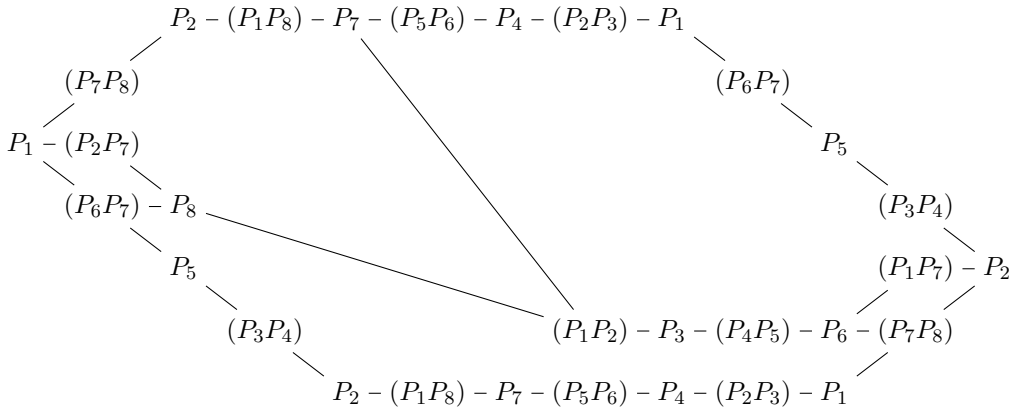


Figure 95: A coherent 16-gon appears of the bottom of the picture. Opposite sides of the hexagonal fundamental domain should be glued to each other. The octagon at the upper-left is coherent by Proposition 4.9. The 14-gon at the upper-right is coherent by Figure 94. The two quadrilaterals at the left and right ends form the boundary of the annulus in (10.3).

11. VARIATIONS OF THE MASTER THEOREM

MASTER THEOREM FOR ARBITRARY DIMENSIONS

The notions of mixed cross-ratio and coherent tile can be naturally extended to involve projective subspaces of arbitrary dimensions, as explained below. This leads to a generalization of our master theorem to tilings labeled by such subspaces.

We continue using the notation from Definition 2.4. In particular, $\mathbb{P} \cong \mathbb{C}\mathbb{P}^d$ is the projectivization of a complex vector space \mathbb{V} of dimension $d + 1$. We fix a skew-symmetric multilinear *volume form* $\text{vol} : \bigwedge^{d+1} \mathbb{V} \rightarrow \mathbb{C}$.

Definition 11.1. A (decomposable) *extensor* of step k in \mathbb{V} is a wedge product

$$\mathbf{e} = e_1 \wedge \cdots \wedge e_k \in \bigwedge^k \mathbb{V}$$

of k linearly independent vectors $e_1, \dots, e_k \in \mathbb{V}$. The projectivization of \mathbf{e} is uniquely determined by the k -dimensional subspace $E = \text{span}(e_1, \dots, e_k)$. That is, the extensor \mathbf{e} does not depend on the choice of a basis e_1, \dots, e_k in E , up to a scalar factor.

Let \mathbf{e} and \mathbf{f} be extensors of steps k and ℓ , respectively, with $k + \ell = \dim \mathbb{V} = d + 1$. We then denote by $\langle \mathbf{e}, \mathbf{f} \rangle = \text{vol}(\mathbf{e} \wedge \mathbf{f})$ the natural pairing of \mathbf{e} and \mathbf{f} ,

Definition 11.2. Let r and s be positive integers such that $r + s = d - 1$. Let a_1, a_2, a_3, a_4 be projective subspaces of $\mathbb{P} \cong \mathbb{C}\mathbb{P}^d$ of dimensions r, s, r, s , respectively. Let $\mathbf{A}_1, \mathbf{A}_2, \mathbf{A}_3, \mathbf{A}_4$ be arbitrary choices of extensors associated with a_1, a_2, a_3, a_4 , respectively, cf. Definition 11.1. Assume that all four intersections

$$a_1 \cap a_2, a_2 \cap a_3, a_3 \cap a_4, a_4 \cap a_1$$

are empty; equivalently, all four pairings

$$\langle \mathbf{A}_1, \mathbf{A}_2 \rangle, \langle \mathbf{A}_2, \mathbf{A}_3 \rangle, \langle \mathbf{A}_3, \mathbf{A}_4 \rangle, \langle \mathbf{A}_4, \mathbf{A}_1 \rangle$$

are nonzero. The (generalized) *mixed cross-ratio* $(a_1, a_3; a_2, a_4)$ is defined by

$$(11.1) \quad (a_1, a_3; a_2, a_4) = \frac{\langle \mathbf{A}_1, \mathbf{A}_2 \rangle \langle \mathbf{A}_3, \mathbf{A}_4 \rangle}{\langle \mathbf{A}_3, \mathbf{A}_2 \rangle \langle \mathbf{A}_1, \mathbf{A}_4 \rangle}.$$

As in Definition 2.4, the mixed cross-ratio $(a_1, a_3; a_2, a_4)$ does not depend on the choice of extensors \mathbf{A}_i representing the subspaces a_i .

Generalizing Definition 2.1/Proposition 2.5, we say that the tile

$$(11.2) \quad \begin{array}{ccc} a_1 & \text{---} & a_2 \\ | & & | \\ a_4 & \text{---} & a_3 \end{array}$$

is *coherent* if and only if

$$(11.3) \quad (a_1, a_3; a_2, a_4) = 1.$$

Our master theorem (Theorem 2.6) generalizes—practically verbatim and with the same proof—to the setting of Definition 11.2. We label the black (resp., white) vertices of a tiling by projective subspaces of dimension r (resp., s) such that adjacent vertices are labeled by disjoint subspaces. Then, if all tiles but one are coherent, then the remaining tile is coherent as well.

GEOMETRY OF GENERALIZED MIXED CROSS-RATIOS

The geometric interpretation of the generalized mixed cross-ratio $(a_1, a_3; a_2, a_4)$ is more complicated than the original case of vectors and covectors (cf. (2.3)) might suggest. These complications ultimately stem from the following fact.

Lemma 11.3. *Let \mathbb{P} be a d -dimensional complex projective space. Let a_1, a_2, a_3, a_4 be generic subspaces of \mathbb{P} of dimensions r, s, r, s , respectively, where $r + s = d - 1$. Then there are exactly $d - \max(r, s)$ lines that pierce all four subspaces a_1, a_2, a_3, a_4 .*

Proof. This is an exercise in Schubert Calculus, see, e.g., [16, 33]. We need to count 2-dimensional subspaces of $\mathbb{V} \cong \mathbb{C}^{d+1}$ that nontrivially intersect given generic subspaces of dimensions $r+1, s+1, r+1, s+1$. This translates into computing the product of the corresponding special Schubert classes in the cohomology ring $H^*(\text{Gr}_{2,d+1}(\mathbb{C}))$. To be specific, the intersection number in question is equal to the coefficient of $s_{(d-1,d-1)}$ in the Schur function expansion of the product $(s_{(d-r-1)}s_{(d-s-1)})^2$. Assuming that $r \leq s$ and using the Pieri rule, we see that the above number is the number of semistandard Young tableaux of shape $(d-1, d-1)$ and content $(d-r-1, d-s-1, d-s-1, d-r-1)$. This number is easily seen to be equal to $d-s$. \square

The simplest instance of the above setting that provides new examples not covered before is the case $d=3, r=s=1$. In that case, Lemma 11.3 asserts that four generic lines in \mathbb{CP}^3 can be pierced by exactly two lines, cf. Remark 5.9. For each of these lines, the corresponding quadruple of points of intersection gives rise to a cross-ratio. The product of these cross-ratios yields the mixed cross-ratio of the original four lines:

Proposition 11.4. *Let b and c be two distinct lines in \mathbb{P} piercing four generic lines a_1, a_2, a_3, a_4 . For $i = 1, 2, 3, 4$, let $B_i = b \cap a_i$ and $C_i = c \cap a_i$. We then have*

$$(11.4) \quad (a_1, a_3; a_2, a_4) = (B_1, B_3; B_2, B_4) \cdot (C_1, C_3; C_2, C_4).$$

Consequently, the tile (11.2) is coherent if and only if the quadruples (B_1, B_2, B_3, B_4) and (C_2, C_3, C_4, C_1) are projectively equivalent.

Proof. We will use the shorthand $\langle \mathbf{a}, \mathbf{b}, \mathbf{c}, \mathbf{d} \rangle \stackrel{\text{def}}{=} \text{vol}(\mathbf{a} \wedge \mathbf{b} \wedge \mathbf{c} \wedge \mathbf{d})$. Let \mathbf{b}_i (resp., \mathbf{c}_i) be a vector in \mathbb{V} representing the point B_i (resp., C_i). Since the points B_1, \dots, B_4 lie on the line b , the vectors $\mathbf{b}_1, \dots, \mathbf{b}_4$ belong to a 2-dimensional subspace of V . We can therefore rescale these four vectors so that their endpoints lie on a line. In other words, we may assume that all the vectors $\mathbf{b}_i - \mathbf{b}_j$ are collinear. We may similarly assume that all the vectors $\mathbf{c}_i - \mathbf{c}_j$ are collinear. It follows that

$$\begin{aligned} (a_1, a_3; a_2, a_4) &= \frac{\langle \mathbf{b}_1 \wedge \mathbf{c}_1, \mathbf{b}_2 \wedge \mathbf{c}_2 \rangle \langle \mathbf{b}_3 \wedge \mathbf{c}_3, \mathbf{b}_4 \wedge \mathbf{c}_4 \rangle}{\langle \mathbf{b}_2 \wedge \mathbf{c}_2, \mathbf{b}_3 \wedge \mathbf{c}_3 \rangle \langle \mathbf{b}_4 \wedge \mathbf{c}_4, \mathbf{b}_1 \wedge \mathbf{c}_1 \rangle} \\ &= \frac{\langle \mathbf{b}_1, \mathbf{c}_1, \mathbf{b}_2, \mathbf{c}_2 \rangle \langle \mathbf{b}_3, \mathbf{c}_3, \mathbf{b}_4, \mathbf{c}_4 \rangle}{\langle \mathbf{b}_2, \mathbf{c}_2, \mathbf{b}_3, \mathbf{c}_3 \rangle \langle \mathbf{b}_4, \mathbf{c}_4, \mathbf{b}_1, \mathbf{c}_1 \rangle} \\ &= \frac{\langle \mathbf{b}_1, \mathbf{c}_1, \mathbf{b}_2 - \mathbf{b}_1, \mathbf{c}_2 - \mathbf{c}_1 \rangle \langle \mathbf{b}_3, \mathbf{c}_3, \mathbf{b}_4 - \mathbf{b}_3, \mathbf{c}_4 - \mathbf{c}_3 \rangle}{\langle \mathbf{b}_2, \mathbf{c}_2, \mathbf{b}_3 - \mathbf{b}_2, \mathbf{c}_3 - \mathbf{c}_2 \rangle \langle \mathbf{b}_4, \mathbf{c}_4, \mathbf{b}_1 - \mathbf{b}_4, \mathbf{c}_1 - \mathbf{c}_4 \rangle} \\ &= \frac{\langle \mathbf{b}_1, \mathbf{c}_1, \mathbf{b}_2 - \mathbf{b}_1, \mathbf{c}_2 - \mathbf{c}_1 \rangle \langle \mathbf{b}_1, \mathbf{c}_1, \mathbf{b}_4 - \mathbf{b}_3, \mathbf{c}_4 - \mathbf{c}_3 \rangle}{\langle \mathbf{b}_1, \mathbf{c}_1, \mathbf{b}_3 - \mathbf{b}_2, \mathbf{c}_3 - \mathbf{c}_2 \rangle \langle \mathbf{b}_1, \mathbf{c}_1, \mathbf{b}_1 - \mathbf{b}_4, \mathbf{c}_1 - \mathbf{c}_4 \rangle} \\ &= (B_1, B_3; B_2, B_4) \cdot (C_1, C_3; C_2, C_4). \end{aligned}$$

\square

REAL CROSS-RATIOS

Yet another variation of the master theorem arises from the following beautiful observation, see, e.g., [54, §5, Theorem A] [9, Exercise 3.2].

Proposition 11.5. *Identify the real plane \mathbb{R}^2 with the field of complex numbers \mathbb{C} in the usual way. Then four distinct points in \mathbb{R}^2 lie on a circle if and only if their cross-ratio is real.*

We note that the order among the four points in Proposition 11.5 does not matter since all possible cross-ratios are related to each other by rational transformations that preserve reality.

Corollary 11.6. *Consider a tiling of a closed oriented surface by quadrilateral tiles. Associate to the vertices in the tiling distinct points on the Euclidean plane. Suppose that for all tiles but one, the four points associated with the vertices of the tile lie on a circle. Then the same property holds for the remaining tile.*

Proof. This corollary is a direct consequence of Proposition 11.5. The product of mixed cross-ratios associated with individual tiles is equal to 1. If all of these cross-ratios, with the exception of one, are real, then the remaining cross-ratio must be real as well. \square

Remark 11.7. Corollary 11.6 immediately extends to the *Möbius plane* $\mathbb{R}^2 \cup \{\infty\}$, a one-point compactification of the Euclidean plane. (This can be seen by applying an inversion transformation.) On the Möbius plane, straight lines are viewed as circles passing through ∞ . If we label one of the vertices of the tiling by ∞ , then the condition associated with a tile with labels A, B, C, ∞ will simply say that the points A, B, C are collinear.

In the special case of the tiling of the sphere by six quadrilaterals (cf. Figure 43), Corollary 11.6 yields *Miquel's theorem* reproduced below, see, e.g., [9, Theorem 9.21] [49, Theorem 18.5].

Corollary 11.8. *Let P_1, \dots, P_6 be distinct points on the Euclidean plane. If five of the six quadruples*

$$(11.5) \quad \begin{aligned} &\{P_1, P_2, P_7, P_8\}, \{P_1, P_2, P_5, P_6\}, \{P_1, P_4, P_5, P_8\}, \\ &\{P_2, P_3, P_6, P_7\}, \{P_3, P_4, P_7, P_8\}, \{P_3, P_4, P_5, P_6\} \end{aligned}$$

are concyclic (i.e., lie on a circle), then the remaining quadruple is also concyclic. See Figure 96.

While the proof of Miquel's theorem based on Proposition 11.5 is by no means new, applications of Corollary 11.6 that are based on other tilings can produce new results about configurations of circles and lines.

As we just saw, Miquel's theorem comes from the tiling of the sphere that was used to prove the Desargues theorem. Using instead a tiling of the torus that gave rise to the Pappus theorem, we obtain the following statement, cf. Figure 97.

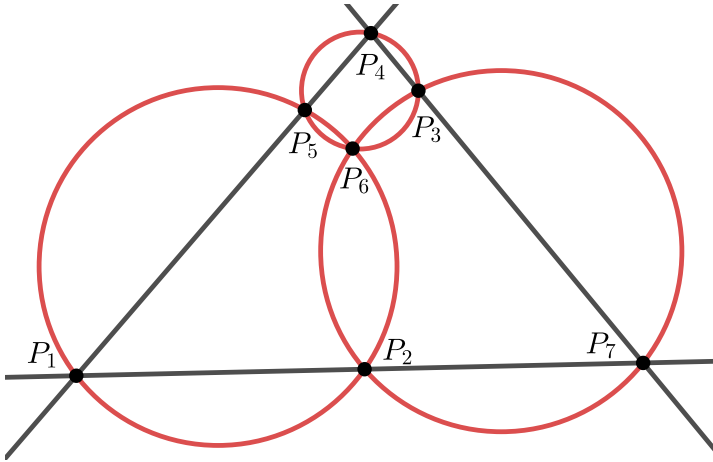


Figure 96: Miquel's theorem. Here $P_8 = \infty$.

Theorem 11.9. Consider two circles on the plane passing through points a and b . Draw a straight line through a and denote by P_1, P_2 the points (other than a) where this line intersects the two circles. Draw a straight line through b and denote by P_4, P_5 the points (other than b) where this line intersects the two circles. Set $P_3 = (AP_4) \cap (BP_2)$ and $P_6 = (AP_5) \cap (bP_1)$. Then the points a, P_3, P_6, b are concyclic.

Proof. This result is obtained by applying Corollary 11.6 to the tiling in Figure 9, where we set $c = \infty$. □

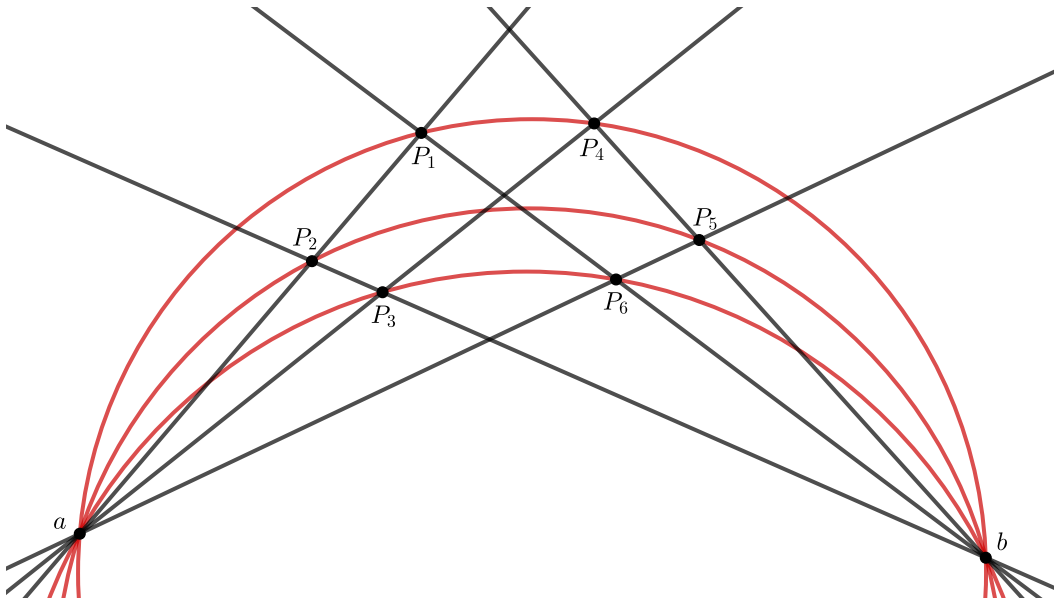


Figure 97: The configuration of circles and lines in Theorem 11.9.

REFERENCES

- [1] S. A. Amitsur, Polynomial identities. *Israel J. Math.* **19** (1974), 183–199.
- [2] E. Artin, *Geometric algebra*, John Wiley & Sons, Inc., 1988.
- [3] H. F. Baker, *Principles of geometry, vol. 1-6*, Reprint of the 1922 original, Cambridge Univ. Press, 2010.
- [4] J. A. Bondy and U. S. R. Murty, *Graph theory*, Springer, 2008.
- [5] C. Baltus, *Collineations and conic sections—an introduction to projective geometry in its history*, Springer, 2020.
- [6] M. K. Bennett, K. Bogart, and J. E. Bonin, The geometry of Dowling lattices, *Adv. Math.* **103** (1994), 131–161.
- [7] A. Björner, M. Las Vergnas, B. Sturmfels, N. White, and G. Ziegler, *Oriented matroids*, 2nd edition, Cambridge Univ. Press, 1999.
- [8] A. I. Bobenko and Yu. B. Suris, Integrable systems on quad-graphs, *Int. Math. Res. Not.* **2002**, no. 11, 573–611.
- [9] A. I. Bobenko and Yu. B. Suris, *Discrete differential geometry. Integrable structure*, Amer. Math. Soc., 2008.
- [10] E. Casas-Alvero, *Analytic projective geometry*, Europ. Math. Soc. (EMS), 2014.
- [11] S.-C. Chou, X. S. Gao, and J. Z. Zhang, *Machine proofs in geometry*, World Scientific, 1994.
- [12] H. S. M. Coxeter, *Non-Euclidean geometry*, 6th edition, MAA, 1998.
- [13] H. S. M. Coxeter, *Projective geometry*, Springer-Verlag, 1994.
- [14] A. Dimakis and F. Müller-Hoissen, Simplex and polygon equations, *SIGMA Symmetry Integrability Geom. Methods Appl.* **11** (2015), Paper 042, 49 pp.
- [15] S. Faghihi, *A history of configurations from Möbius to Coxeter*, Ph.D. Thesis (Dr. rer. nat.)—Universität in Mainz (Germany), 2021, 121 pp.
- [16] W. Fulton, *Young tableaux*, Cambridge Univ. Press, 1997.
- [17] D. G. Glynn, A rabbit hole between topology and geometry, *ISRN Geom.* **2013**, Art. ID 379074, 9 pp.
- [18] D. G. Glynn, A note on N_K configurations and theorems in projective space, *Bull. Austral. Math. Soc.* **76** (2007), 15–31.
- [19] D. G. Glynn, Theorems of points and planes in three-dimensional projective space, *J. Aust. Math. Soc.* **88** (2010), 75–92.
- [20] J. E. Goodman and R. Pollack, On the combinatorial classification of nondegenerate configurations in the plane, *J. Combin. Theory Ser. A* **29** (1980), 220–235.
- [21] G. Hessenberg, Beweis des Desarguesschen Satzes aus dem Pascalschen, *Math. Ann.* **61** (1905), 161–172.
- [22] A. Heyting, *Axiomatic projective geometry*, 2nd edition, North-Holland, 1980.
- [23] D. Hilbert, *The foundations of geometry*, Authorized translation by E. J. Townsend (Open Court Publishing Co., 1902), Project Gutenberg, 2005.
- [24] D. Hilbert and S. Cohn-Vossen, *Geometry and the imagination*, Chelsea Publishing Co., 1952.
- [25] J. P. Hogendijk, al-Mu'taman ibn Hūd, 11th century king of Saragossa and brilliant mathematician, *Historia Math.* **22** (1995), 1–18.
- [26] M. M. Kapranov and V. A. Voevodsky, 2-categories and Zamolodchikov tetrahedra equations, Proc. Sympos. Pure Math., **56**, Part 2, Amer. Math. Soc., 1994, 177–259.
- [27] J. Kahn, Locally projective-planar lattices which satisfy the bundle theorem, *Math. Z.* **175** (1980), 219–247.
- [28] D. E. Knuth, Foreword to: M. Petkovšek, H. Wilf, and D. Zeilberger, $A = B$, A K Peters, 1996.
- [29] S. K. Lando and A. K. Zvonkin, *Graphs on surfaces and their applications*, Springer, 2004.
- [30] A. Leykin and F. Sottile, Galois groups of Schubert problems via homotopy computation, *Math. Comp.* **78** (2009), no. 267, 1749–1765.
- [31] H. Li, *Invariant algebras and geometric reasoning*, World Scientific, 2008.
- [32] H. Li and Y. Wu, Automated theorem proving in incidence geometry—a bracket algebra based elimination method, in: Automated deduction in geometry (Zurich, 2000), 199–227, *Lecture Notes in Comput. Sci.* **2061**, Springer, 2001.

- [33] L. Manivel, *Symmetric functions, Schubert polynomials and degeneracy loci*, AMS/SMF, 2001.
- [34] E. A. Marchisotto, The theorem of Pappus: a bridge between algebra and geometry, *Amer. Math. Monthly* **109** (2002), no. 6, 497–516.
- [35] D. Mayhew, G. Whittle, and M. Newman, Is the missing axiom of matroid theory lost forever? *Q. J. Math.* **65** (2014), 1397–1415.
- [36] N. E. Mnëv, Varieties of combinatorial types of projective configurations and convex polyhedra, *Soviet Math. Dokl.* **32**, no. 1, 335–337. Russian original: *Dokl. Akad. Nauk SSSR* **283** (1985), no. 6, 1312–1314.
- [37] A. F. Moebius, Kann von zwei dreiseitigen Pyramiden eine jede in Bezug auf die andere um- und eingeschrieben zugleich heissen?, *J. Reine Angew. Math.* **3** (1828), 273–278.
- [38] R. Moufang, *Foundations of geometry* (notes “Grundlagen der Geometrie” at the University of Frankfurt, 1948), translated into English by J. Stillwell, [arXiv:2012.05809](https://arxiv.org/abs/2012.05809).
- [39] O. Nehring, Zyklische Projektionen im Dreieck, *J. Reine Angew. Math.* **184** (1942), 129–137.
- [40] A. Nixon, B. Schulze, and W. Whiteley, Rigidity through a projective lens, *Appl. Sci.* **2021**, 11, 11946.
- [41] J. Oxley, *Matroid theory*, 2nd edition, Oxford University Press, Oxford, 2011.
- [42] V. Pambuccian, Early examples of resource-consciousness, *Studia Logica* **77** (2004), 81–86.
- [43] V. Pambuccian and C. Schacht, The axiomatic destiny of the theorems of Pappus and Desargues, in: *Geometry in history*, 355–399, Springer, 2019.
- [44] G. Pickert, *Projektive Ebenen*, 2nd edition, Springer-Verlag, 1975.
- [45] T. Pisanski and B. Servatius, *Configurations from a graphical viewpoint*, Birkhäuser/Springer, 2013.
- [46] J. Richter-Gebert, Mechanical theorem proving in projective geometry, *Ann. Math. Artificial Intelligence* **13** (1995), 139–172.
- [47] J. Richter-Gebert and U. Kortenkamp, *The interactive geometry software Cinderella*, Springer-Verlag, Berlin, 1999.
- [48] J. Richter-Gebert, Meditations on Ceva’s theorem, *The Coxeter legacy*, 227–254, Amer. Math. Soc., 2006.
- [49] J. Richter-Gebert, *Perspectives on projective geometry*, Springer, 2011.
- [50] A. Saam, Ein neuer Schließungssatz für projektive Ebenen, *J. Geom.* **29** (1987), 36–42.
- [51] A. Saam, Schließungssätze als Eigenschaften von Projektivitäten, *J. Geom.* **32** (1988), 86–130.
- [52] A. Seidenberg, Pappus implies Desargues, *Amer. Math. Monthly* **83** (1976), no. 3, 190–192.
- [53] A. Seidenberg, *Lectures in projective geometry*, D. Van Nostrand, 1962.
- [54] H. Schwerdtfeger, *Geometry of complex numbers*, Dover Publ., 1979.
- [55] B. Sturmfels, Computational algebraic geometry of projective configurations, *J. Symbolic Comput.* **11** (1991), 595–618.
- [56] B. Sturmfels, On the decidability of Diophantine problems in combinatorial geometry, *Bull. Amer. Math. Soc. (N.S.)* **17** (1987), 121–124.
- [57] B. Sturmfels, *Algorithms in invariant theory*, 2nd edition, Springer, 2008.
- [58] S. Tabachnikov, Skewers, *Arnold Math. J.* **2** (2016), 171–193.
- [59] D. V. Talalaev, Tetrahedron equation: algebra, topology, and integrability, *Russian Math. Surveys* **76** (2021), 685–721.
- [60] J. Tits, A local approach to buildings, *The geometric vein*, pp. 519–547, Springer, 1981.
- [61] P. Vámos, The missing axiom of matroid theory is lost forever. *J. London Math. Soc. (2)* **18** (1978), 403–408.
- [62] B. L. van der Waerden, *Science awakening*, 2nd edition, Oxford Univ. Press, 1961.
- [63] A. B. Zamolodchikov, Tetrahedra equations and integrable systems in three-dimensional space, *Soviet Phys. JETP* **52** (2) (1980), 325–336.

DEPARTMENT OF MATHEMATICS, UNIVERSITY OF MICHIGAN, ANN ARBOR, MI 48109, USA

Email address: fomin@umich.edu

DEPARTMENT OF MATHEMATICS, UNIVERSITY OF MINNESOTA, MINNEAPOLIS, MN 55414, USA

Email address: pplyavs@umn.edu